The Surprising X-ray Properties of τ Sco and HD 191612

David Cohen
Swarthmore College

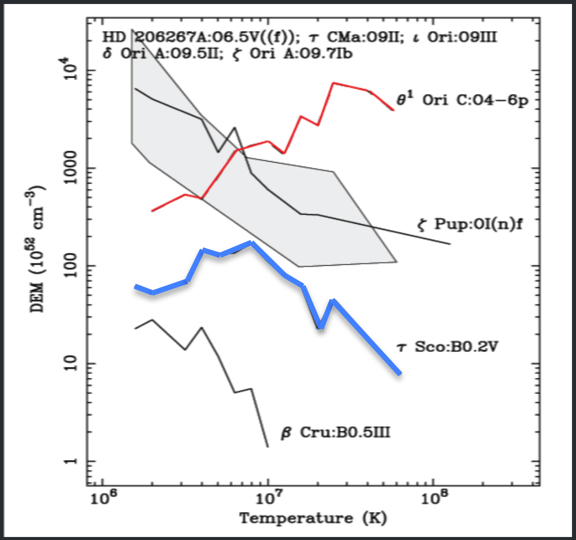

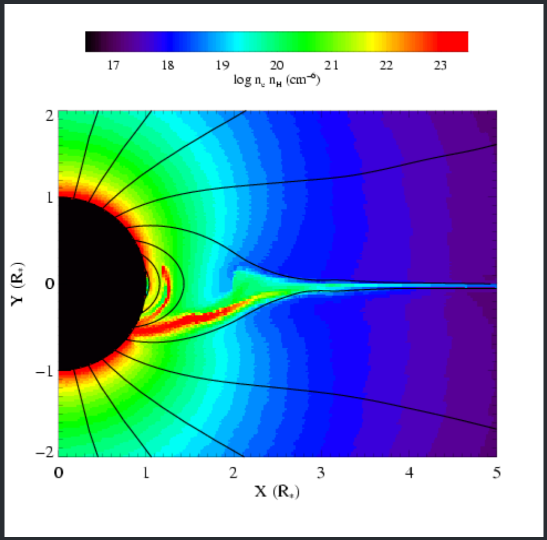

Initial focus on the prototype θ^1 Ori C

The Astrophysical Journal, 628:986–1005, 2005 August 1

CHANDRA HETGS MULTIPHASE SPECTROSCOPY OF THE YOUNG MAGNETIC O STAR θ^1 ORIONIS C

Marc Gagné,[1] Mary E. Oksala,[1,2] David H. Cohen,[3] Stephanie K. Tonnesen,[3,4] Asif ud-Doula,[5] Stanley P. Owocki,[6] Richard H. D. Townsend,[6] and Joseph J. MacFarlane[7]
Received 2004 November 1; accepted 2005 April 11

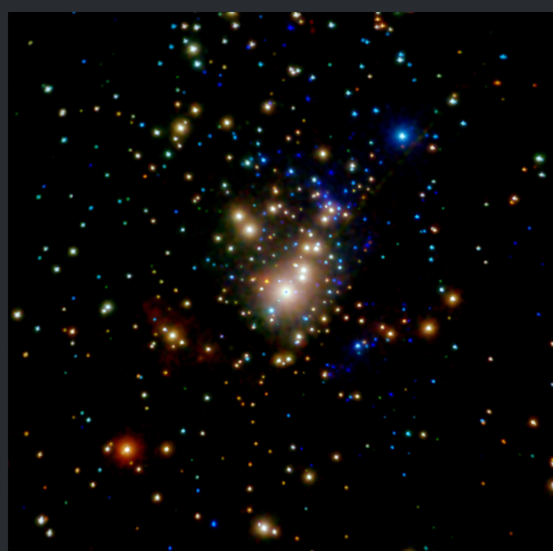

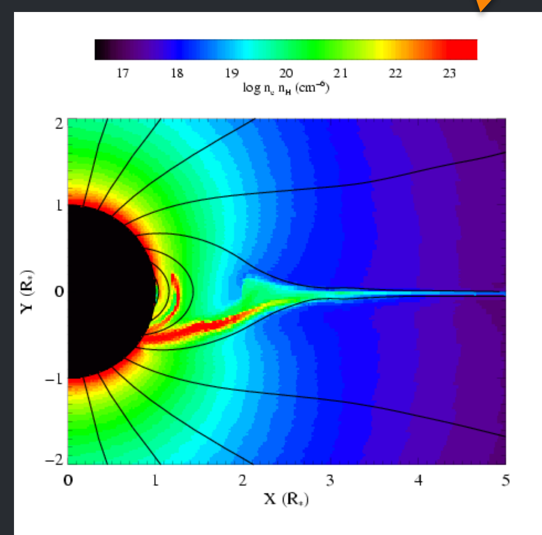

Orion Nebula Cluster: *Chandra*

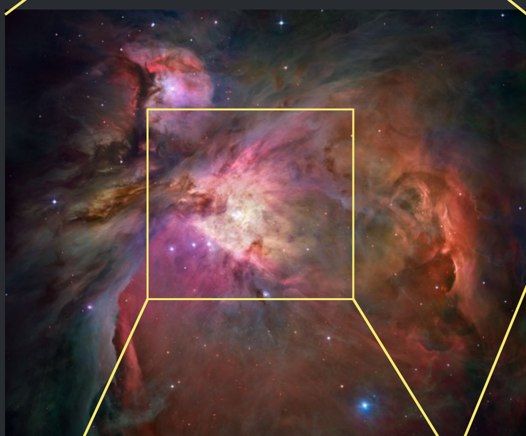

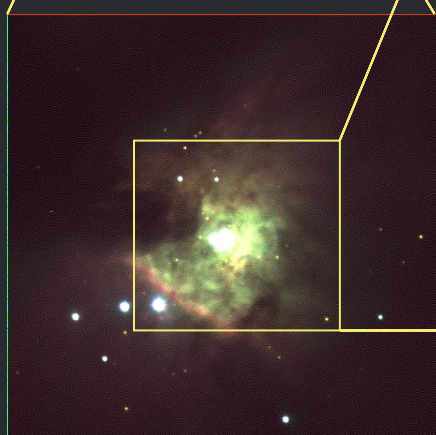

Chandra ~10^6 seconds, COUP (Penn. St.)

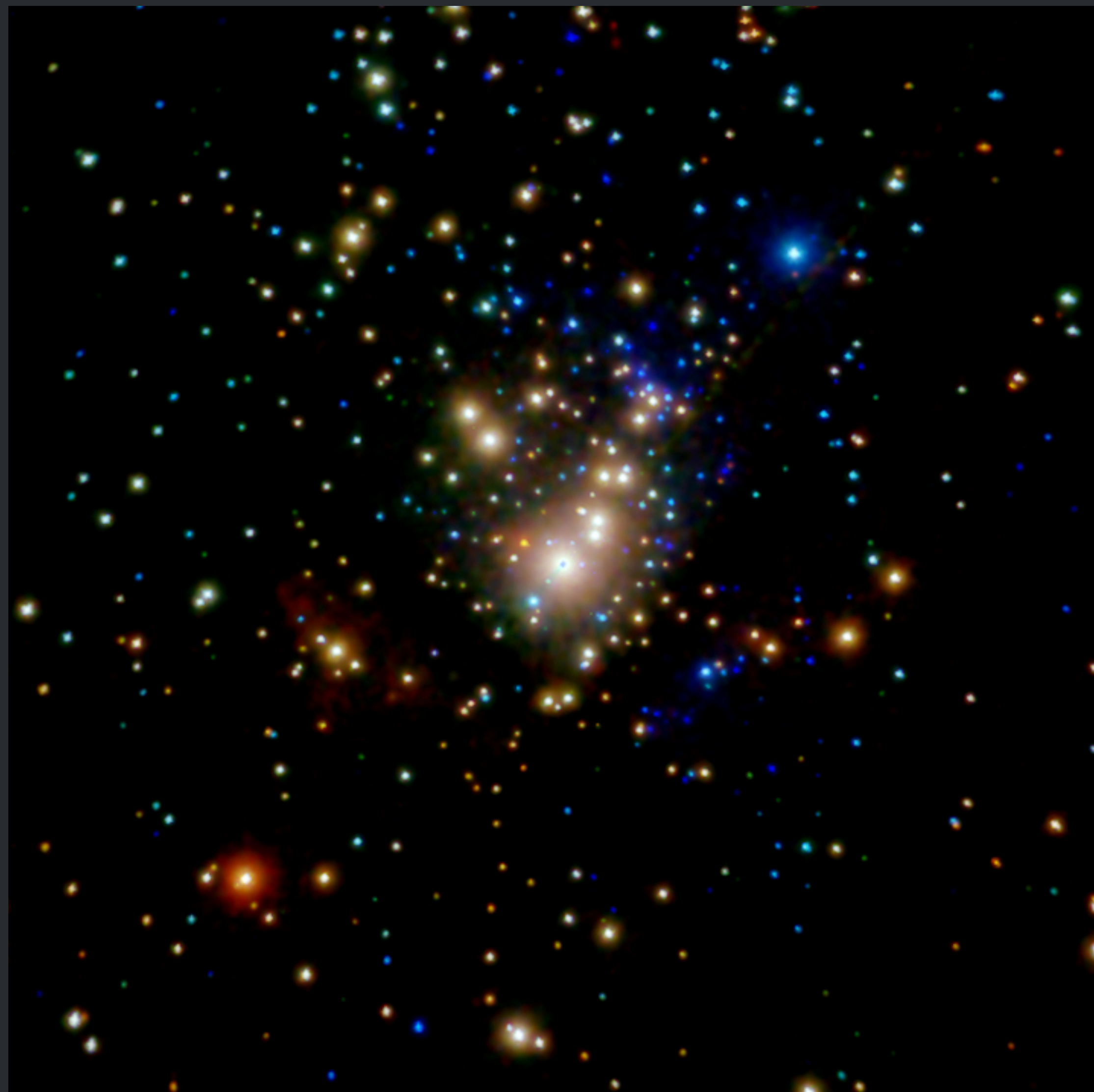

Color coding of x-ray energy: <1keV, 1keV < E < 2.5keV, >2.5keV

Color coding of x-ray energy: <1keV, 1keV < E < 2.5keV, >2.5keV

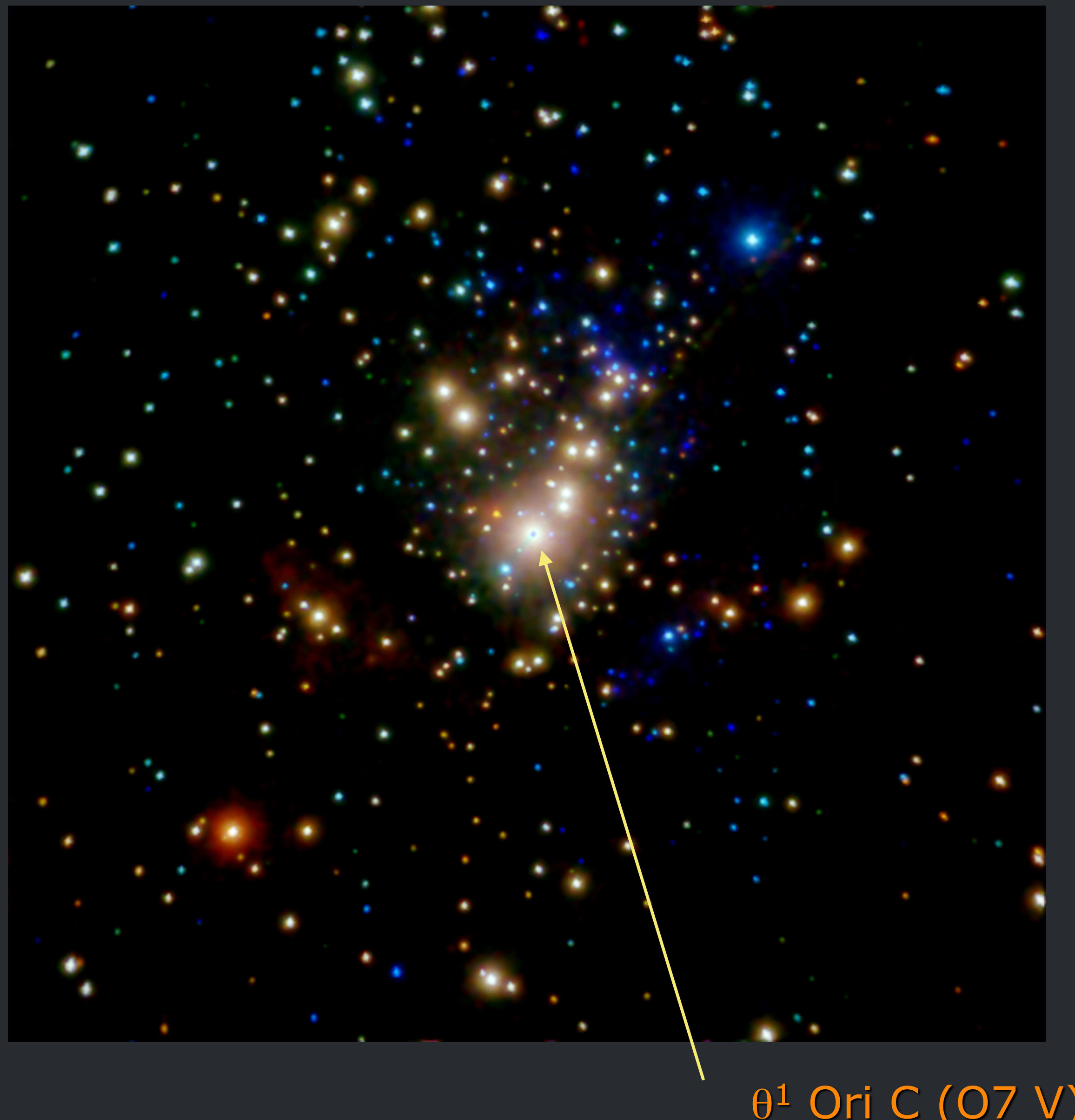

Color coding of x-ray energy: <1keV, 1keV < E < 2.5keV, >2.5keV

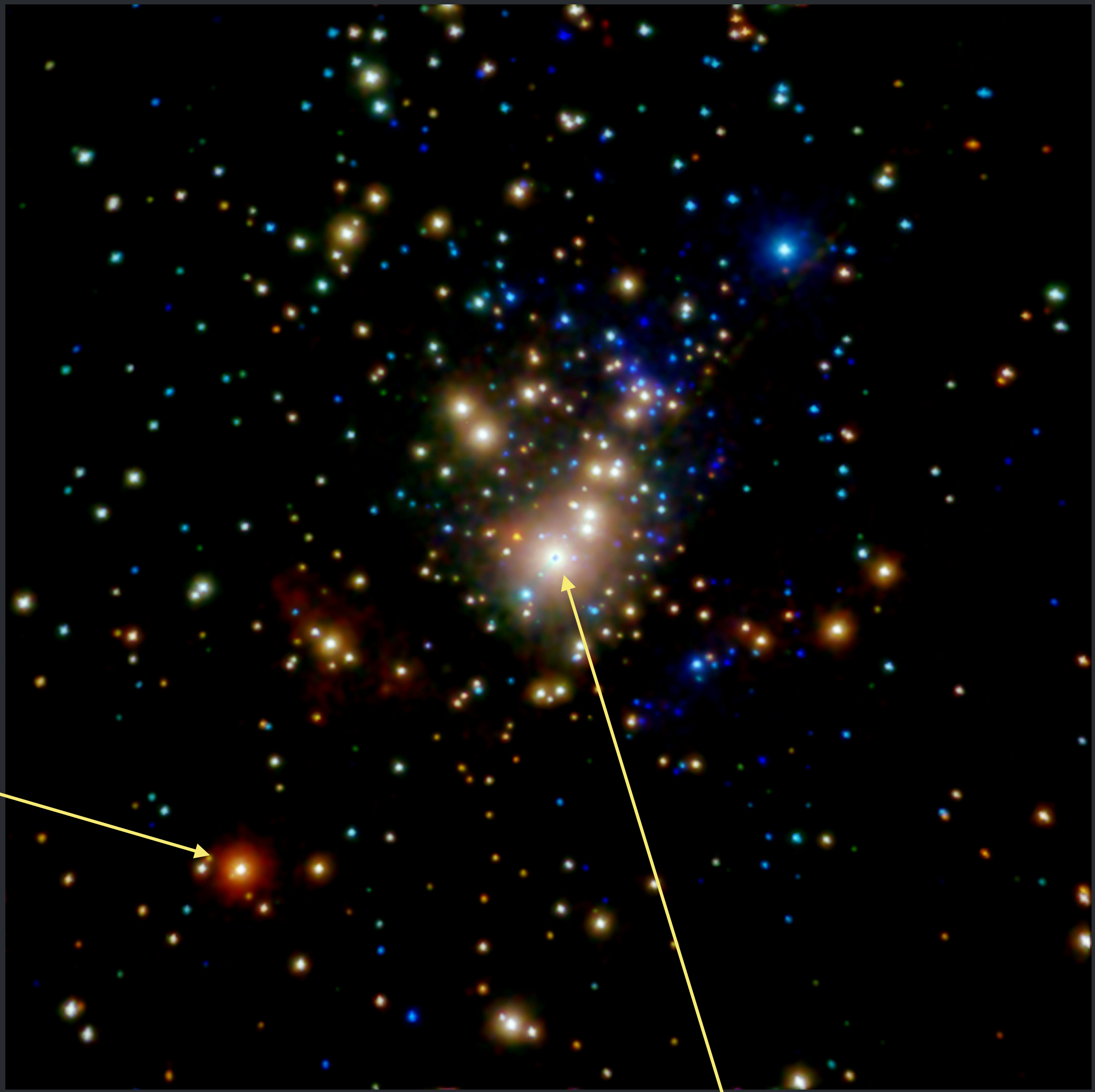

θ^2 Ori A (O9.5 V)

non-magnetic

θ^1 Ori C (O7 V)

Initial assumption:

Magnetic massive stars have distinct and universal X-ray properties: **High** X-ray **luminosities** and **high temperatures** due to channeling (strong shocks) and confinement (high density, or efficiency)

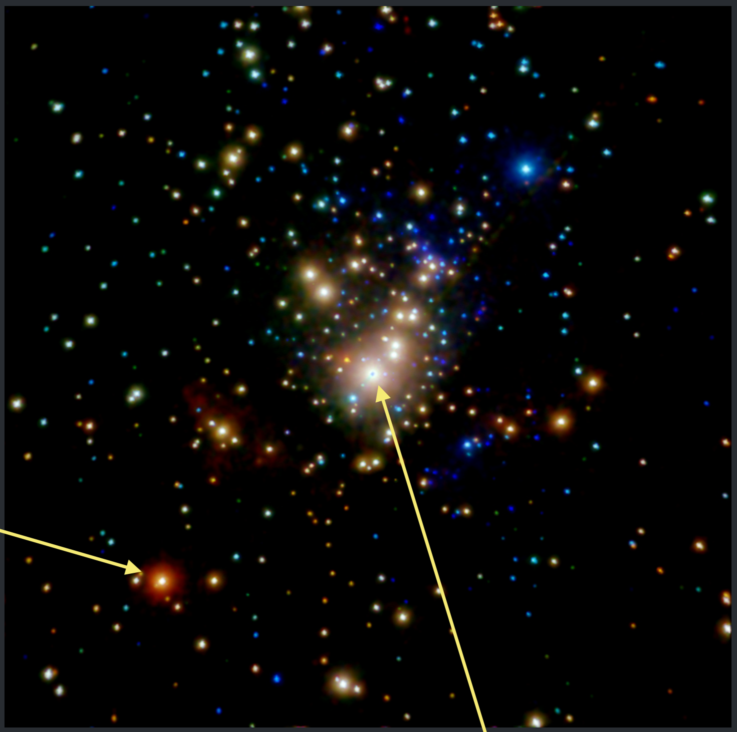

Initial assumption:

Magnetic massive stars have distinct and universal X-ray properties: **High** X-ray **luminosities** and **high temperatures** due to channeling (strong shocks) and confinement (high density, or efficiency)

$L_X = 1.0 \times 10^{33}$ erg/s

$L_X = 10^{-6} L_{Bol}$

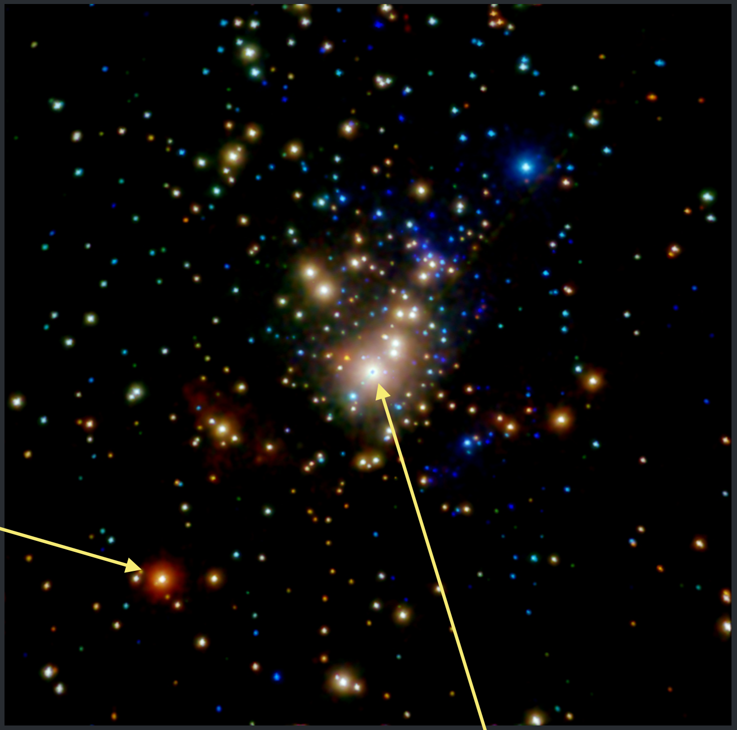

Chandra HETGS

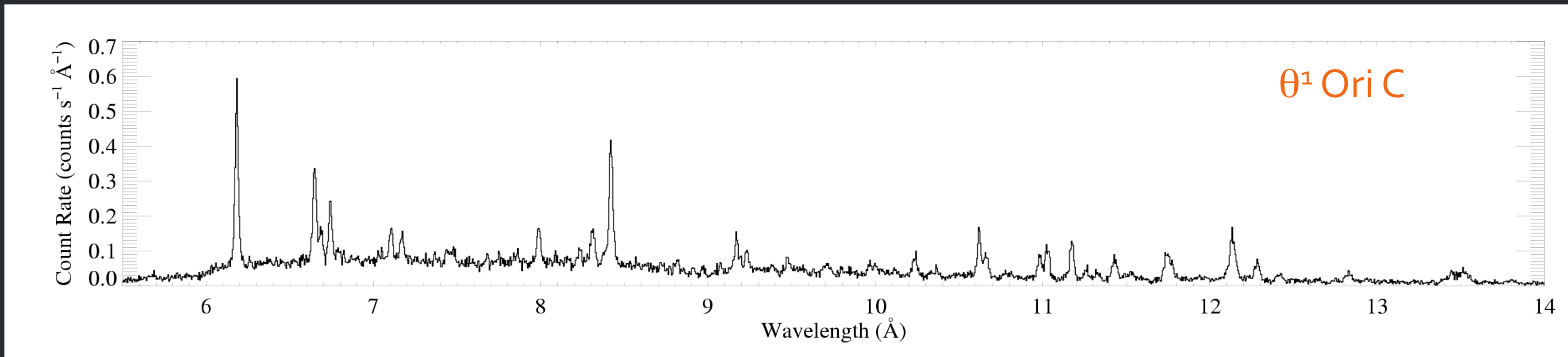

θ¹ Ori C: hotter plasma, narrower emission lines

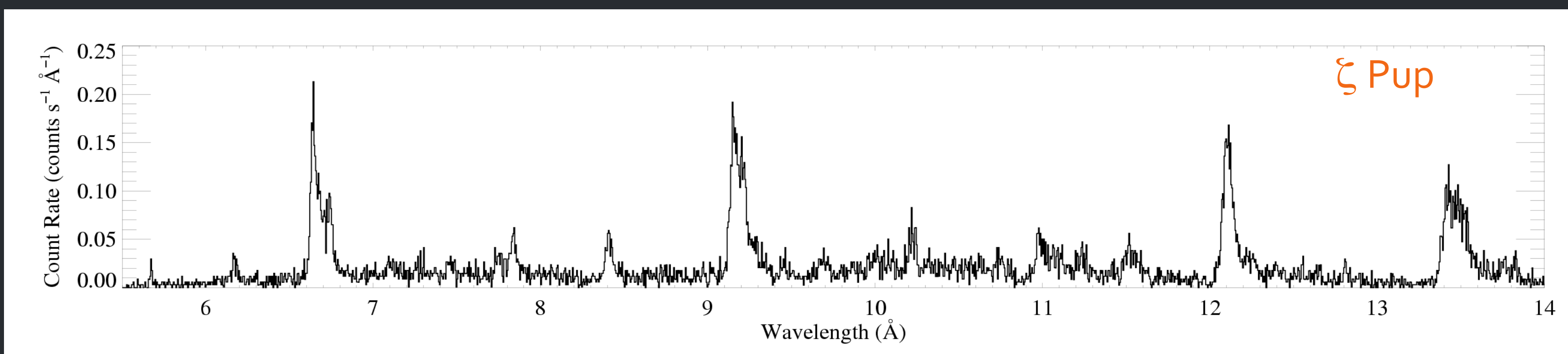

ζ Pup (O4 I): cooler plasma, broad emission lines

H-like/He-like ratio is temperature sensitive

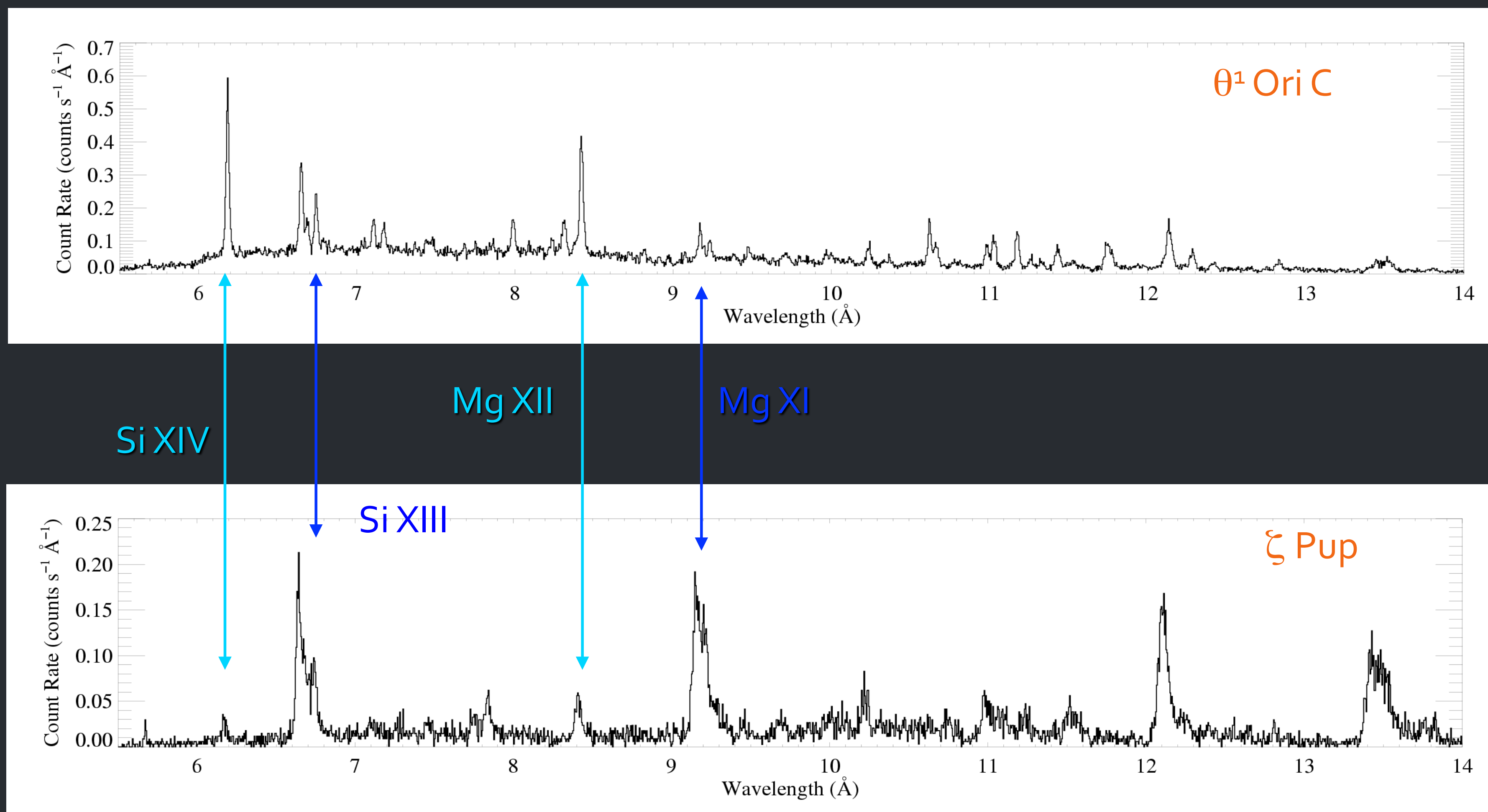

Differential emission measure
(temperature distribution)

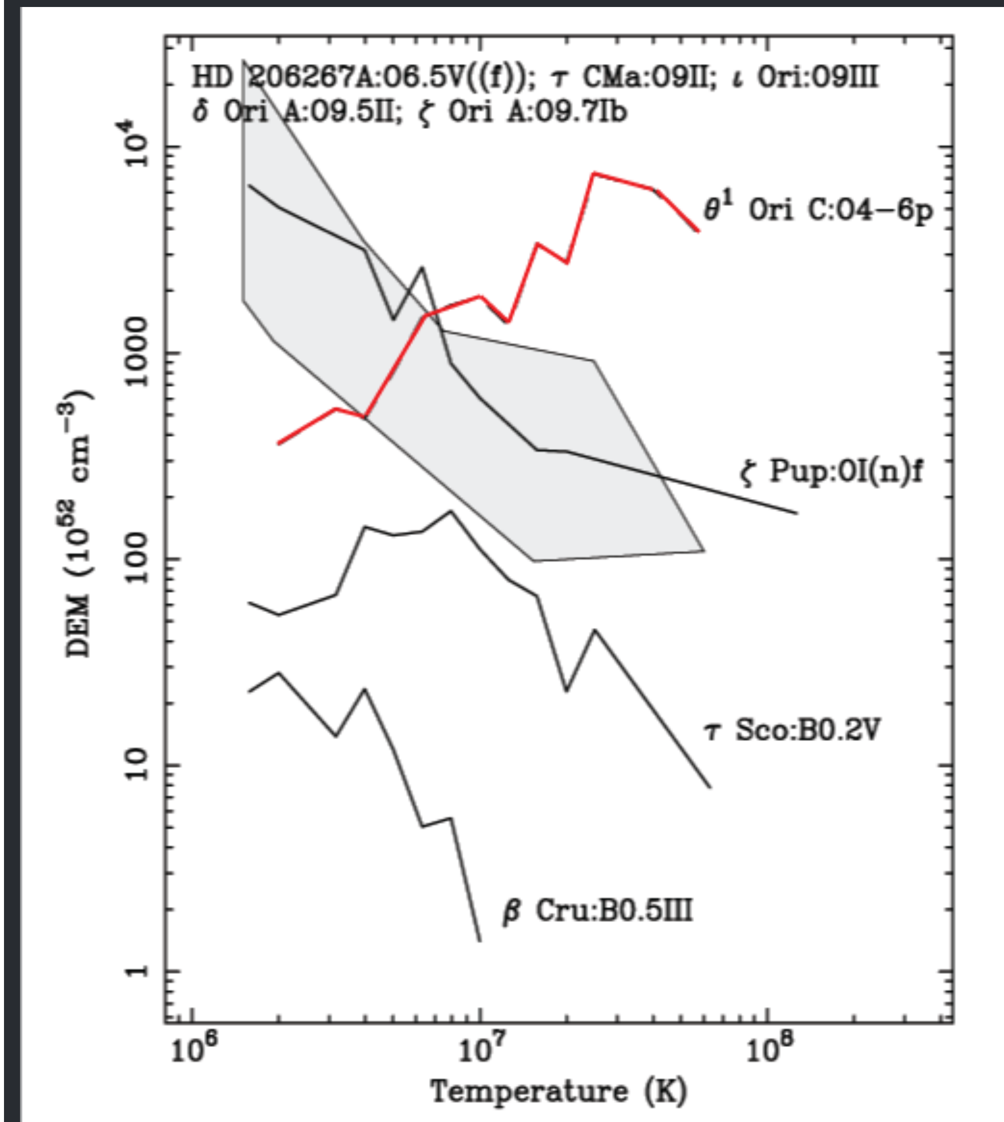

Wojdowski & Schulz (2005)

θ^1 Ori C:

peak near 30 million K

Non-magnetic O stars,
peak at a few million K

Differential emission measure
(temperature distribution)

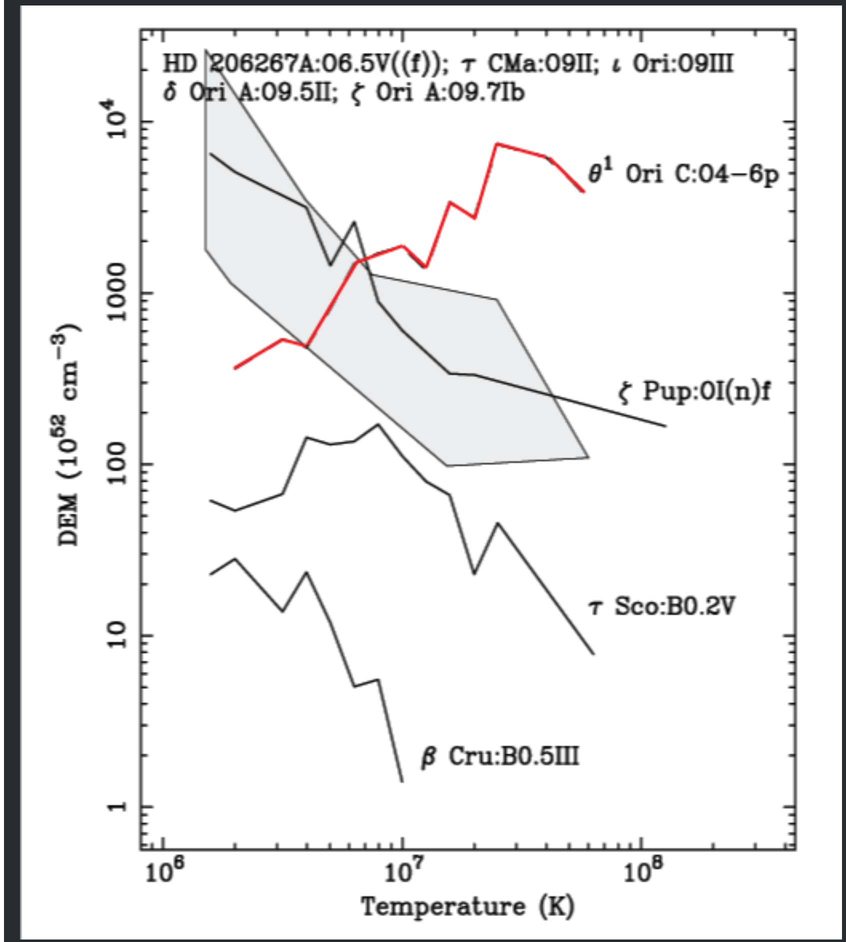

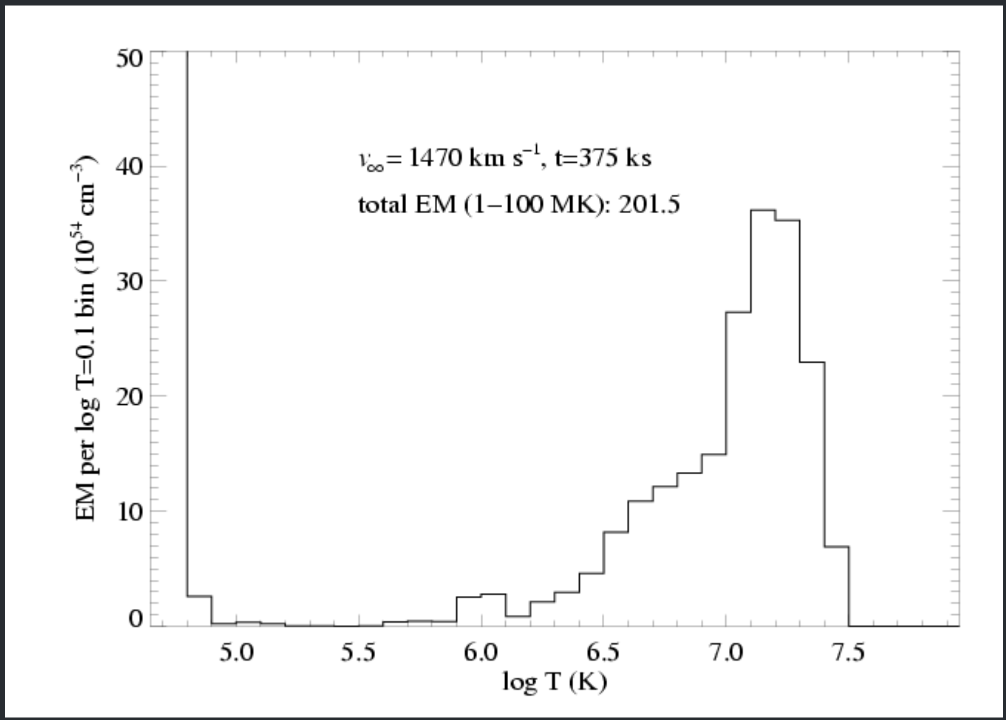

MHD simulation of θ¹ Ori C reproduces the observed differential emission measure

Dipole magnetic field (> 1 kG) measured on θ^1 Ori C

$i \sim 45°, \beta \sim 45°$

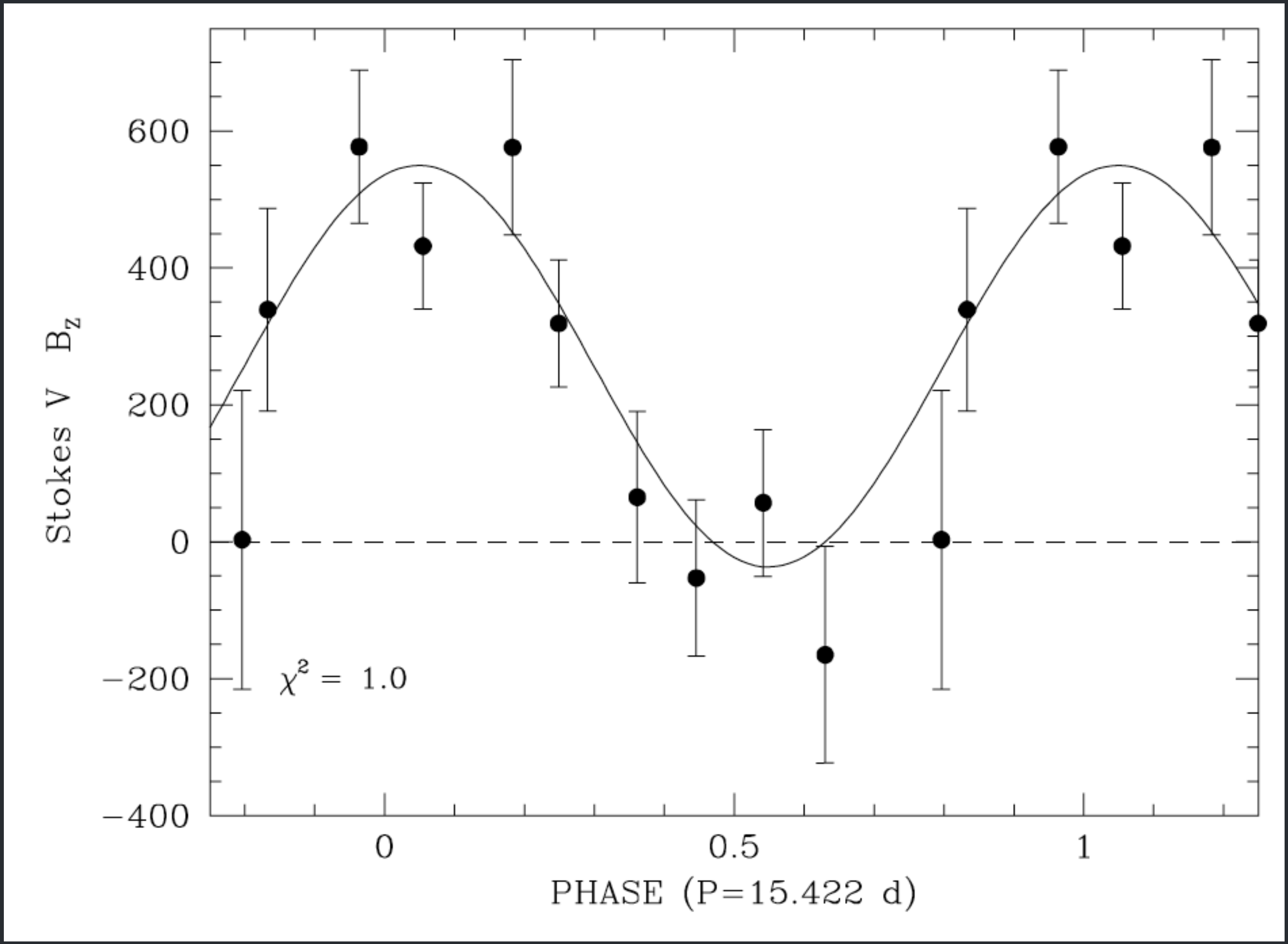

Wade et al. (2006)

MHD simulations of magnetically channeled wind

temperature

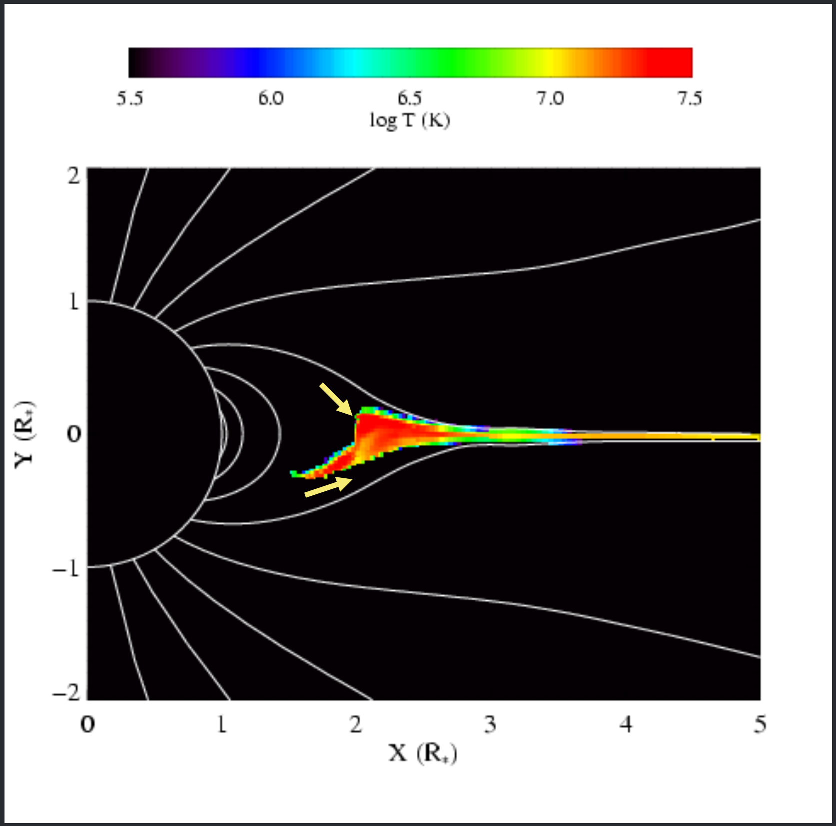

emission measure

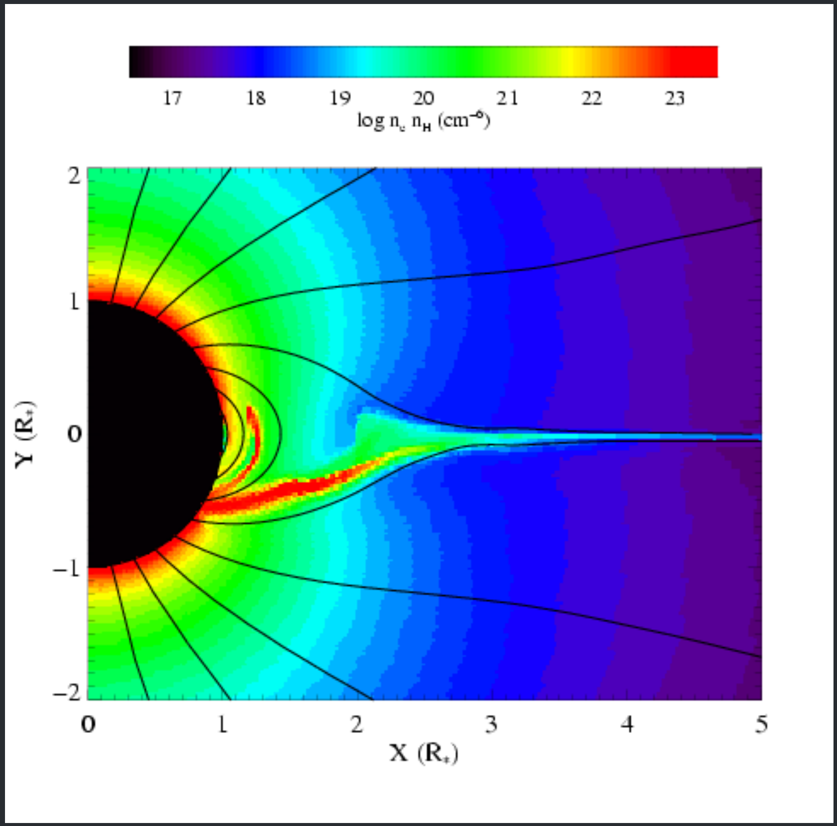

simulations by A. ud-Doula; Gagné et al. (2005)

Channeled collision is close to head-on – at 1000+ km s^{-1} : $T = 10^7$+ K

Differential emission measure

(temperature distribution)

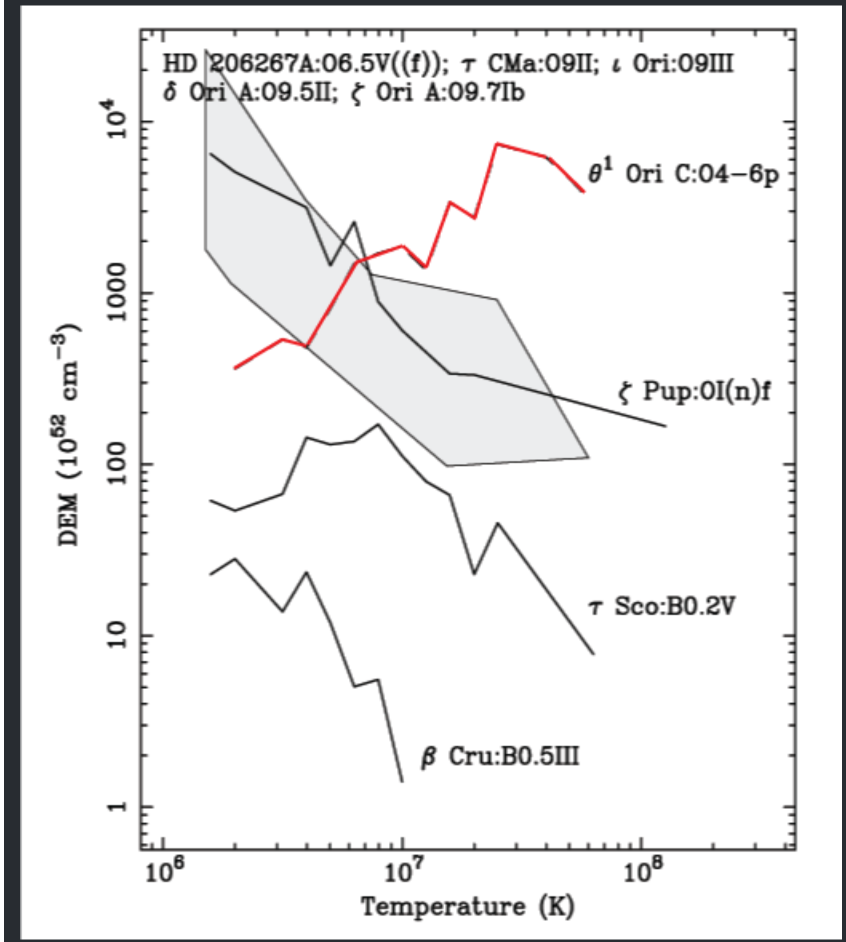

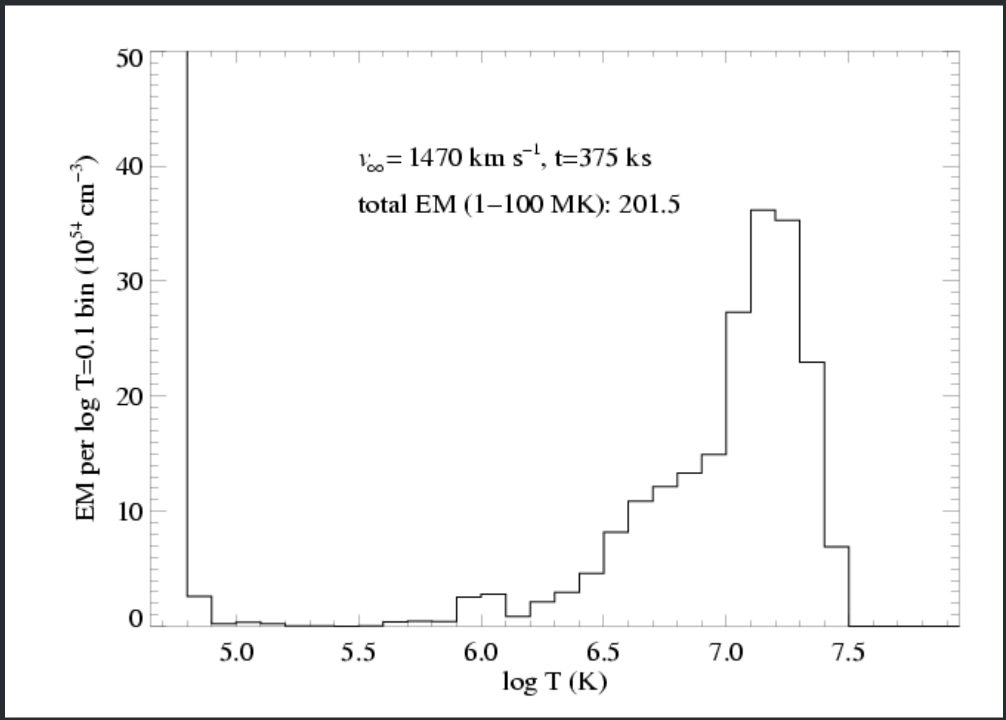

MHD simulation of θ¹ Ori C reproduces the observed differential emission measure

Inclination, *i* ~ 45 deg; magnetic obliquity, β ~ 45 deg

*so we see a full range of viewing angles with respect to the magnetic field over the course of a rotation period

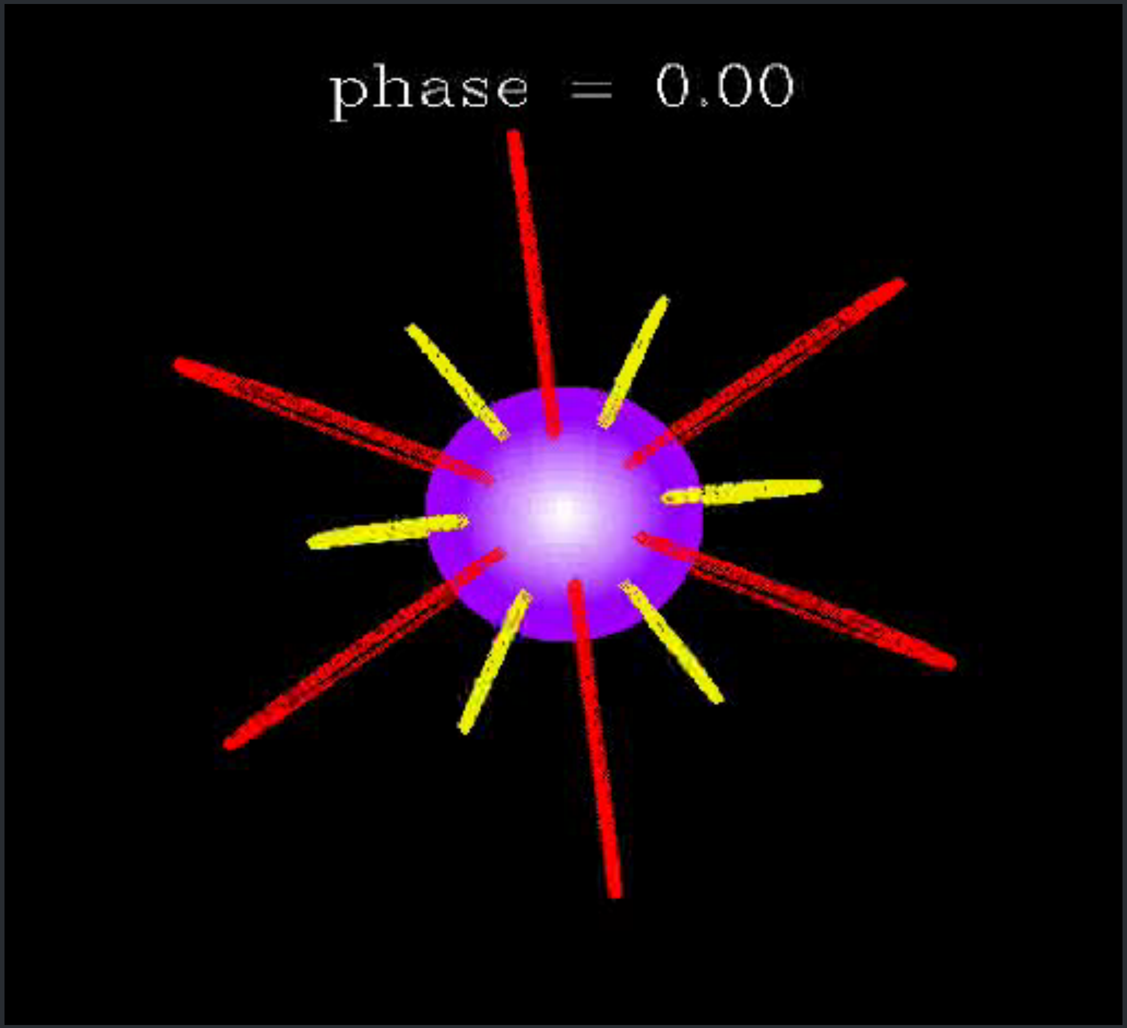

Chandra broadband count rate vs. rotational phase

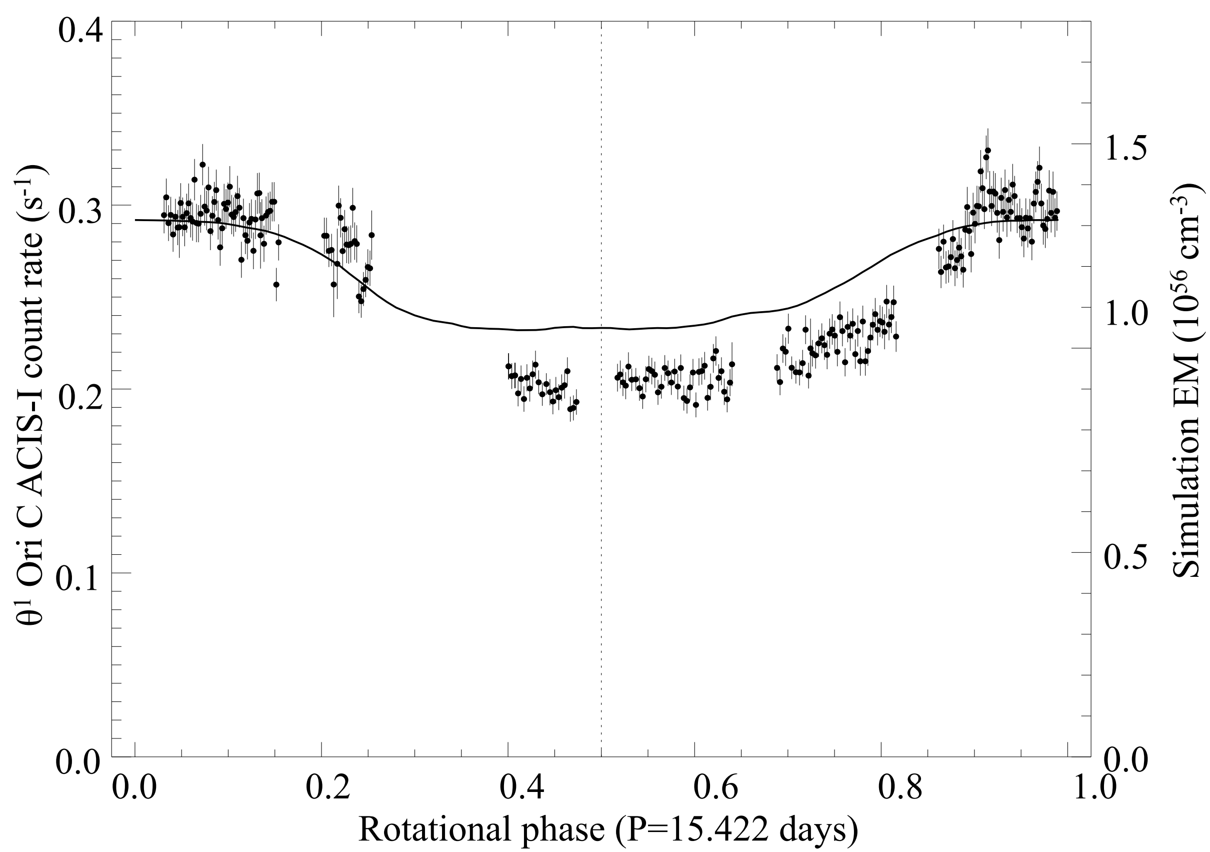

Model from MHD simulation

Chandra broadband count rate vs. rotational phase

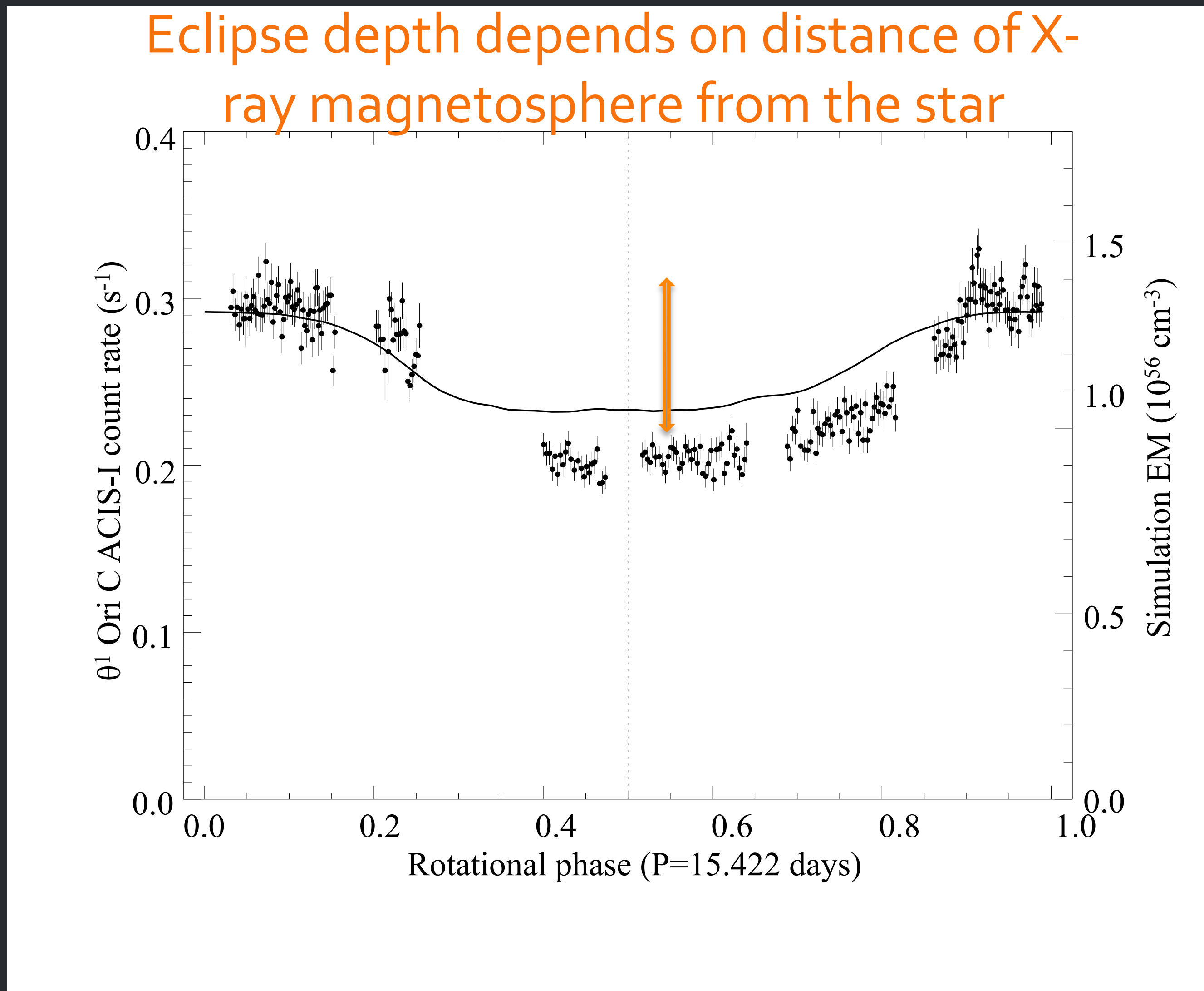

Model from MHD simulation

Chandra broadband count rate vs. rotational phase

Eclipse depth depends on distance of X-ray magnetosphere from the star

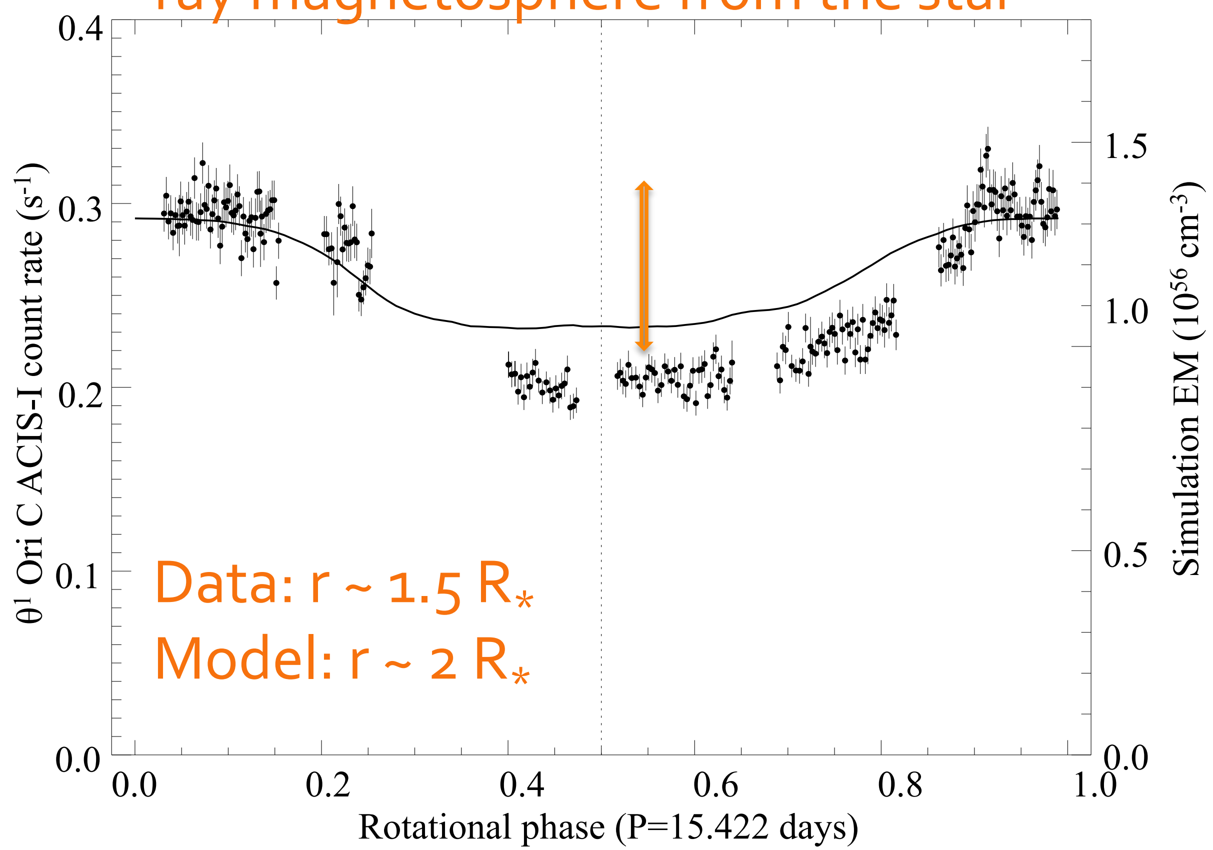

Model from MHD simulation

Unified picture

B-field

wind
absorption

X-rays

H-alpha

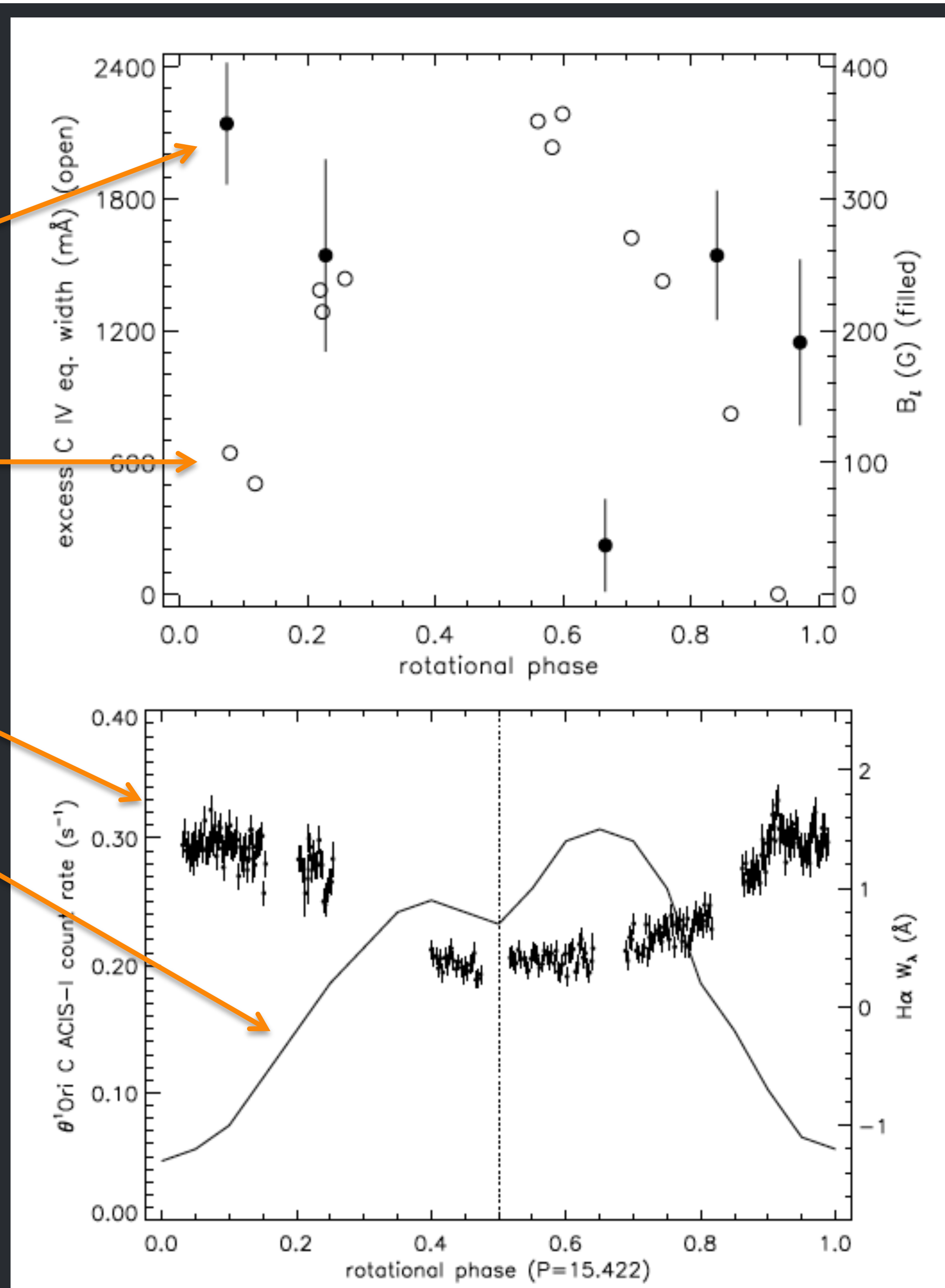

Fig. 4.—Phase-folded light curves of θ^1 Ori C. *Top:* Open circles indicate the excess C IV equivalent width (left axis) taken from Walborn & Nichols (1994) and phased to the ephemeris of Stahl et al. (1996): period $P = 15.422$ days and epoch $\mathrm{MJD}_0 = 48832.50$. Maximum C IV absorption occurs near phase 0.5 ($\alpha = 3°$) as a result of outflowing plasma in the magnetic equatorial plane. Note that Walborn & Nichols (1994) calculate W_λ by subtracting the *IUE* spectrum at a given phase from the *IUE* spectrum with the shallowest line profile, then calculating the equivalent width of the line in the difference spectrum. Filled circles show the longitudinal magnetic field strength, B_l (right axis), as measured by Donati et al. (2002) using the same ephemeris. Note that Walborn & Nichols (1994) and Donati et al. (2002) used different period estimates. The B_l is maximum near phase 0.0 when the magnetic pole is in the line of sight. *Bottom:* Hα equivalent width (*solid curve*) from Stahl et al. (1996). The data points with error bars represent the ACIS-I count rate from the 850 ks *Chandra* Orion Ultra-Deep Project. X-ray and Hα maxima occur at low viewing angles when the entire X-ray torus is visible; the minima occur when part of the X-ray torus is occulted by the star.

Additional constraints from the high-resolution X-ray spectra

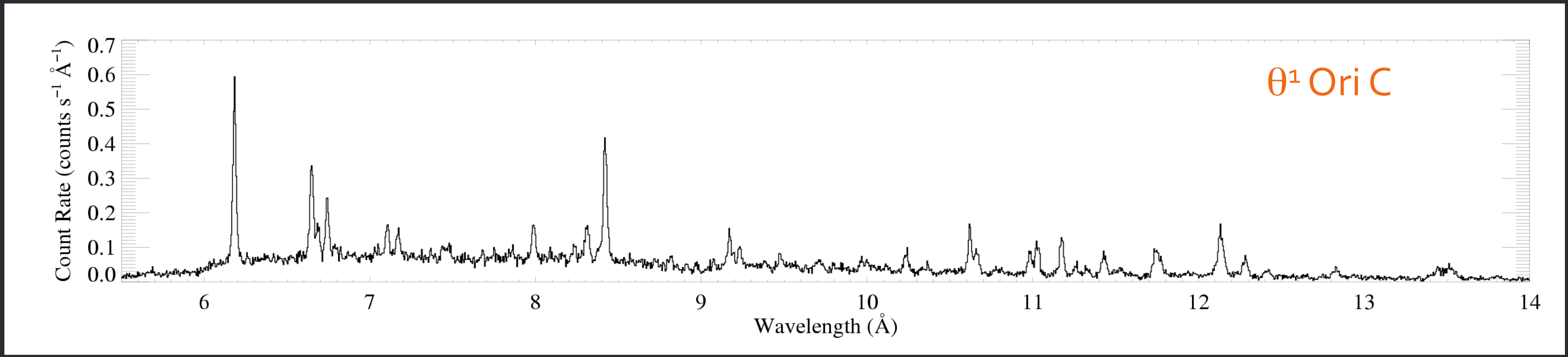

Emission measure

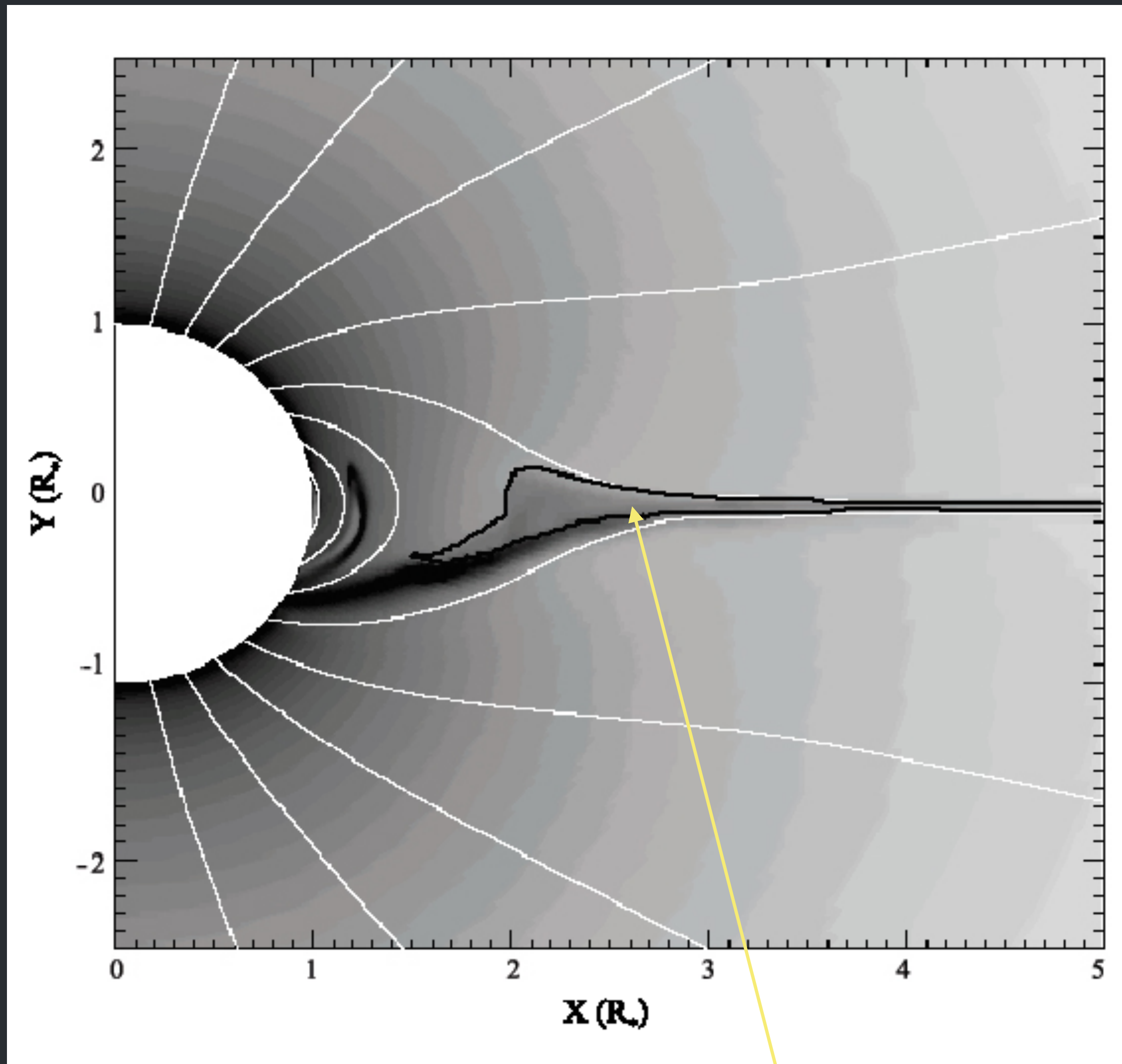

contour encloses T > 10^6 K

MHD simulations show multi-10^6 K plasma, moving slowly, ~$1R_*$ above photosphere

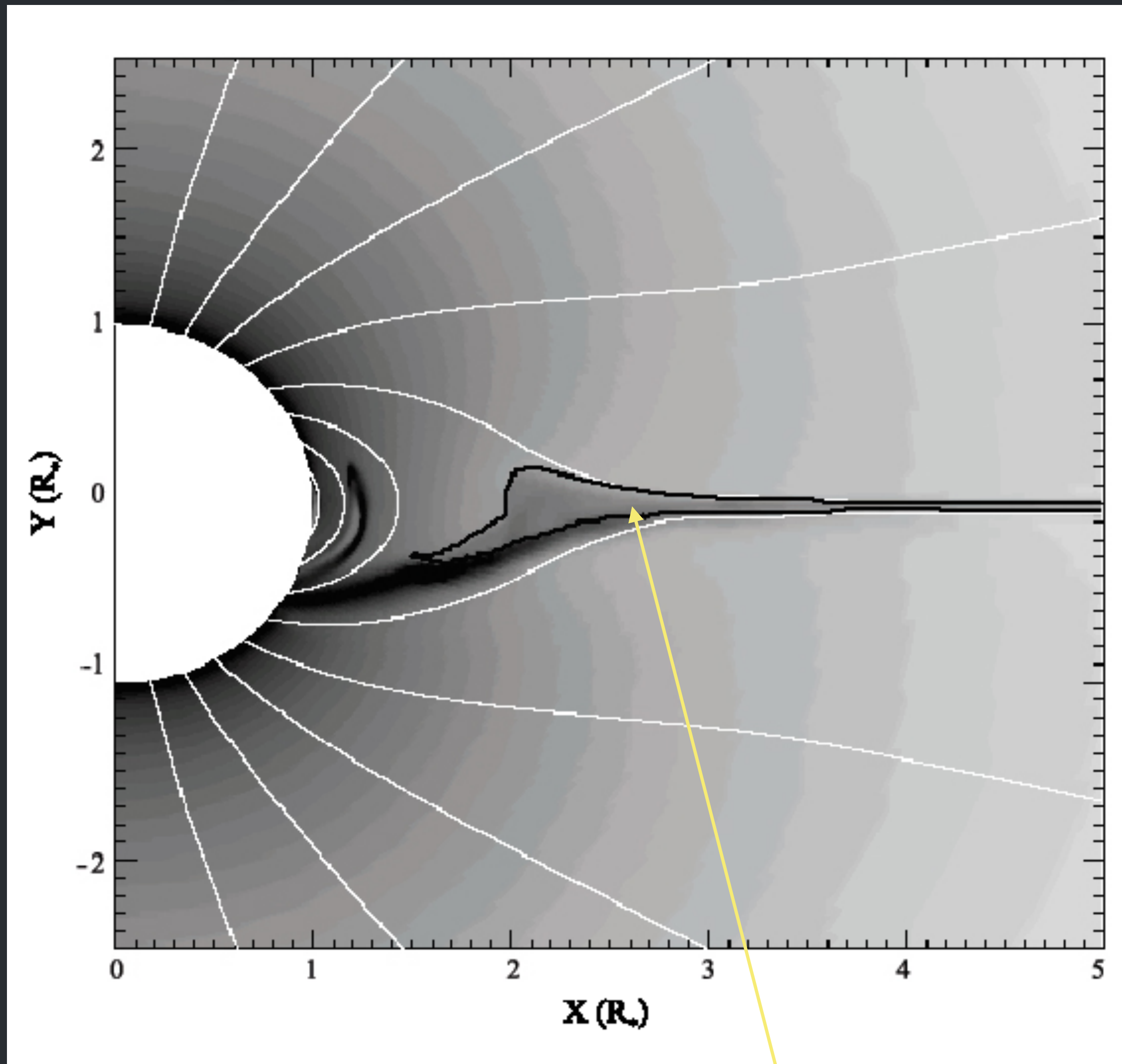

contour encloses T > 10^6 K

Helium-like ions (e.g. O^{+6}, Ne^{+8}, Mg^{+10}, Si^{+12}, S^{+14}) – schematic energy level diagram

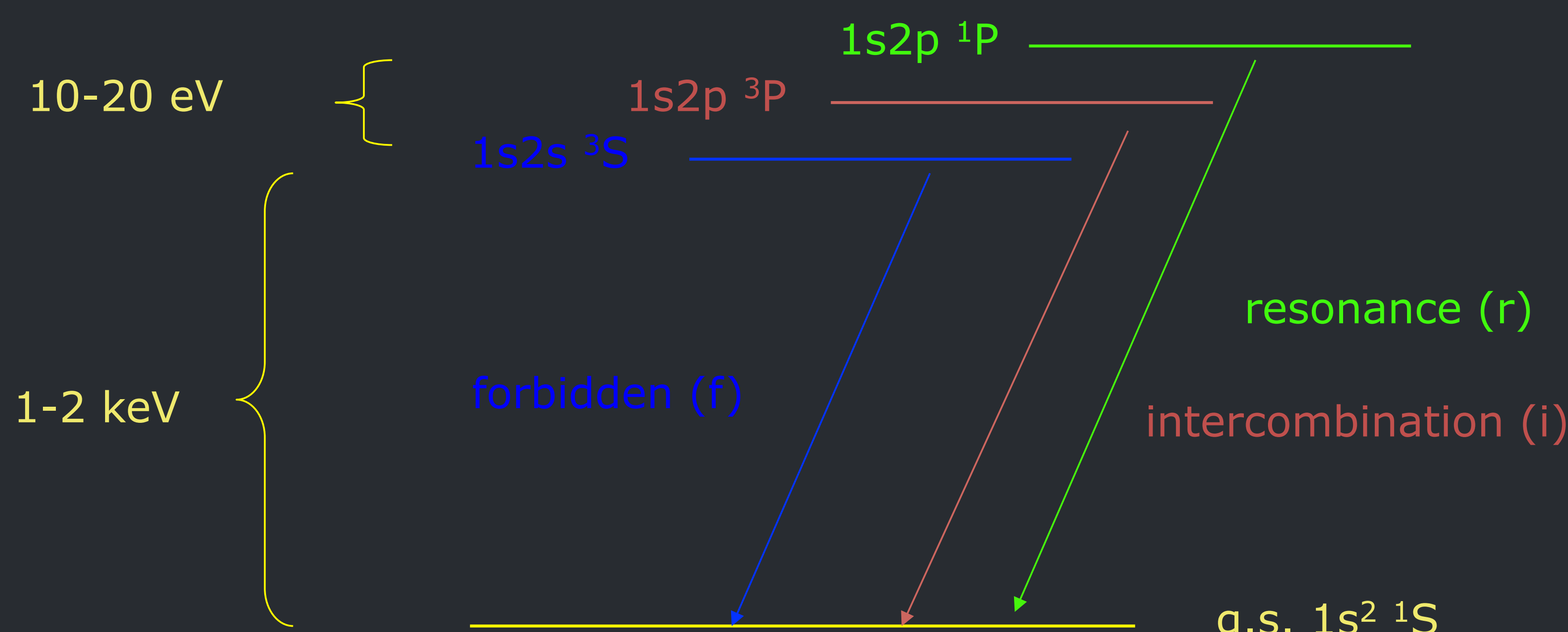

The *f*/*i* ratio is thus a diagnostic of the strength of the local UV radiation field.

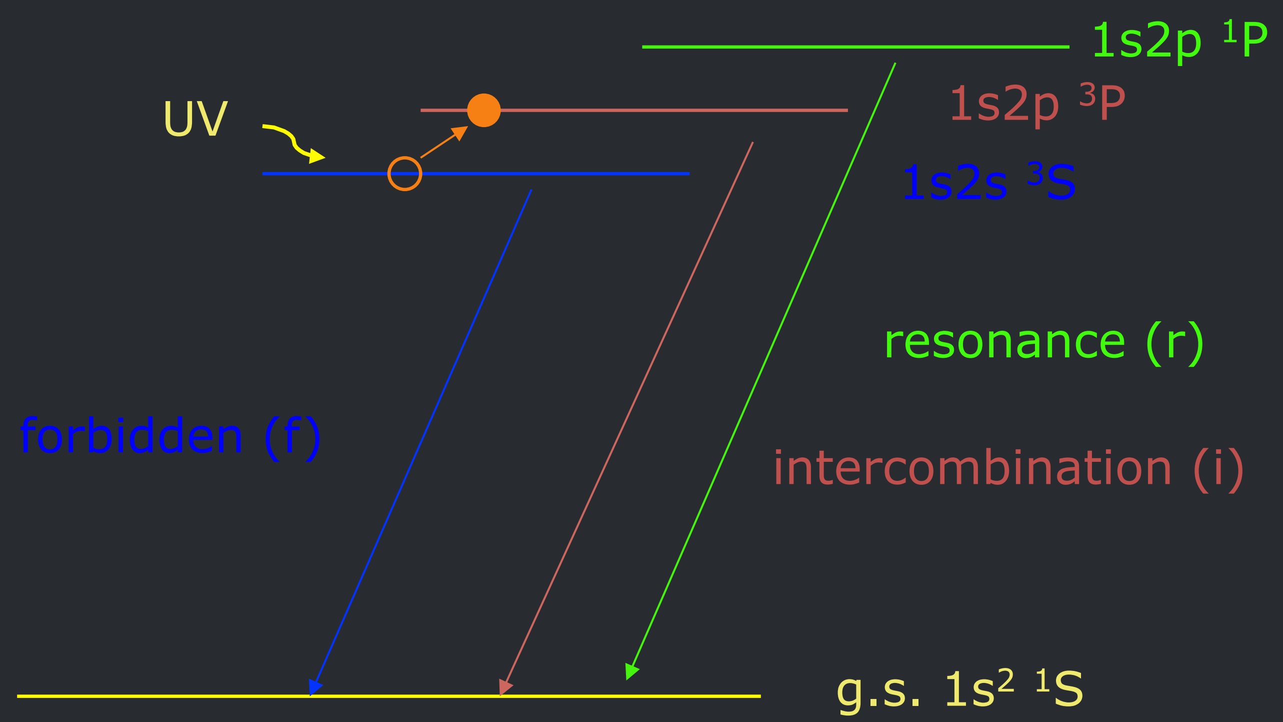

If you know the UV intensity emitted from the star's surface, it thus becomes a diagnostic of the distance that the x-ray emitting plasma is from the star's surface.

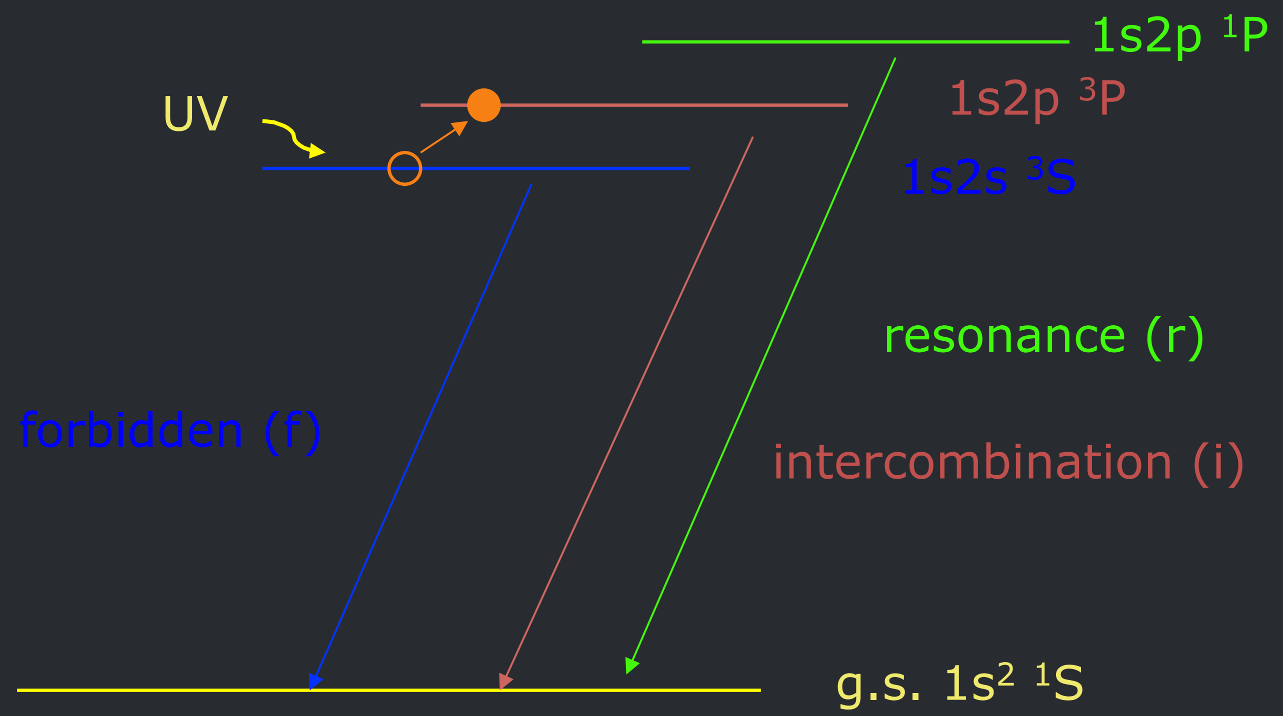

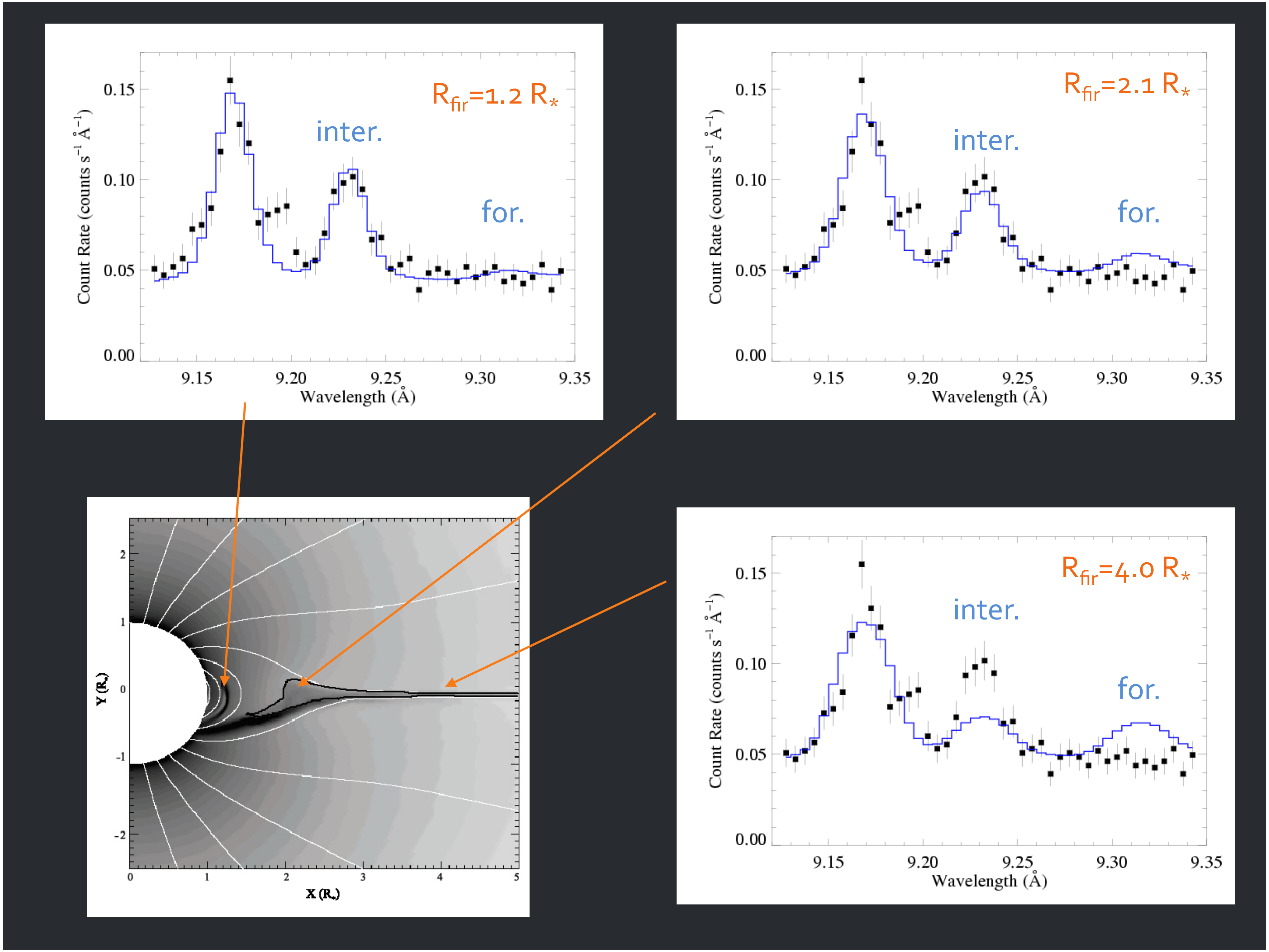

Count Rate (counts s^{-1} Å^{-1})
0.15
0.10
0.05
0.00
9.15
9.20
9.25
9.30
9.35
Wavelength (Å)
R_{fir}=1.2 R_*
inter.
for.
R_{fir}=2.1 R_*
inter.
for.
R_{fir}=4.0 R_*
inter.
for.
Y (R_*)
X (R_*)

X-ray lightcurve and f/i ratios both indicate X-ray plasma is just a few tenths R_* from the photosphere

MHD simulations are generally in agreement, but the bulk of the X-ray plasma is a bit further from the photosphere (height ~ 1 R_*)

X-ray emission lines are quite narrow

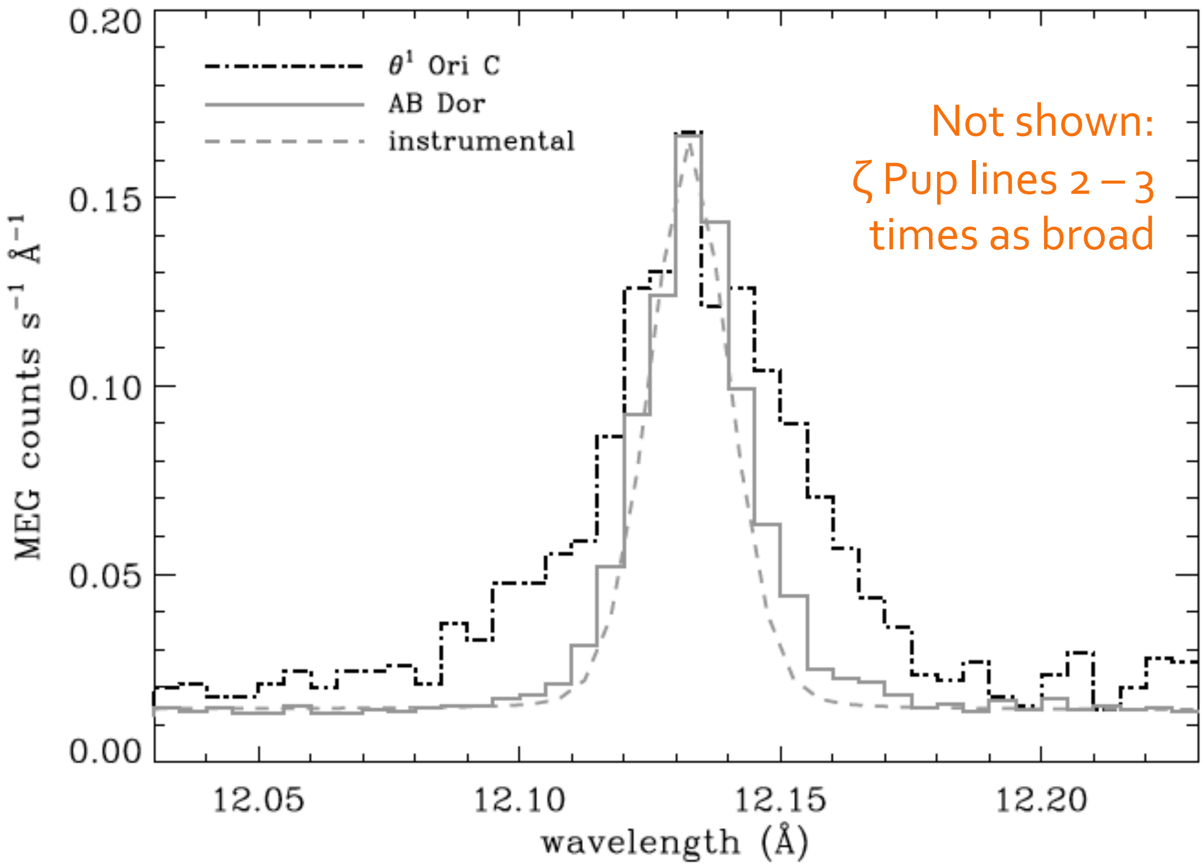

FIG. 8.—Ne Lyα line in the combined *Chandra* MEG spectrum from all four observations of θ^1 Ori C (*solid histogram*) compared to the same line seen in the MEG spectrum of the active young K-type dwarf, AB Doradus (*dash-dotted histogram*). A delta function convolved with the MEG instrumental response (*dashed line*) is also shown for comparison. The θ^1 Ori C line is clearly broader than both the narrow line or the AB Dor line.

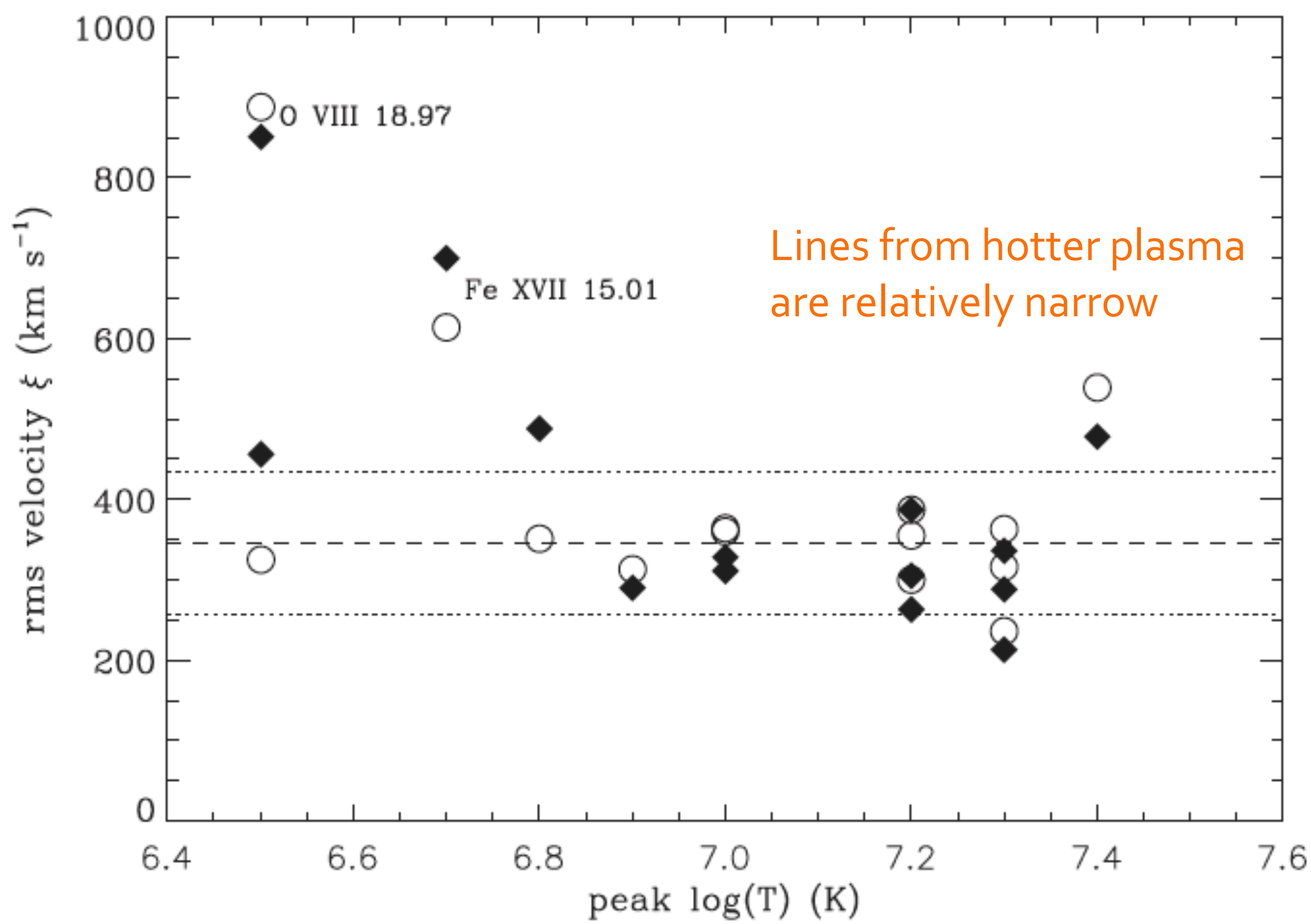

FIG. 9.—Line widths for the strongest lines in the *Chandra* spectra plotted against the temperature of peak line emissivity, taken from APED. The open circles represent the Doppler width as measured by SHERPA. The filled diamonds represent the rms velocity as measured by ISIS. The mean rms velocity and standard deviations of these lines are indicated by the horizontal lines. Note that two of the lines formed in the coolest plasma are significantly broader than the mean, but most of the lines have nonthermal line widths of a 250–450 km s^{-1}.

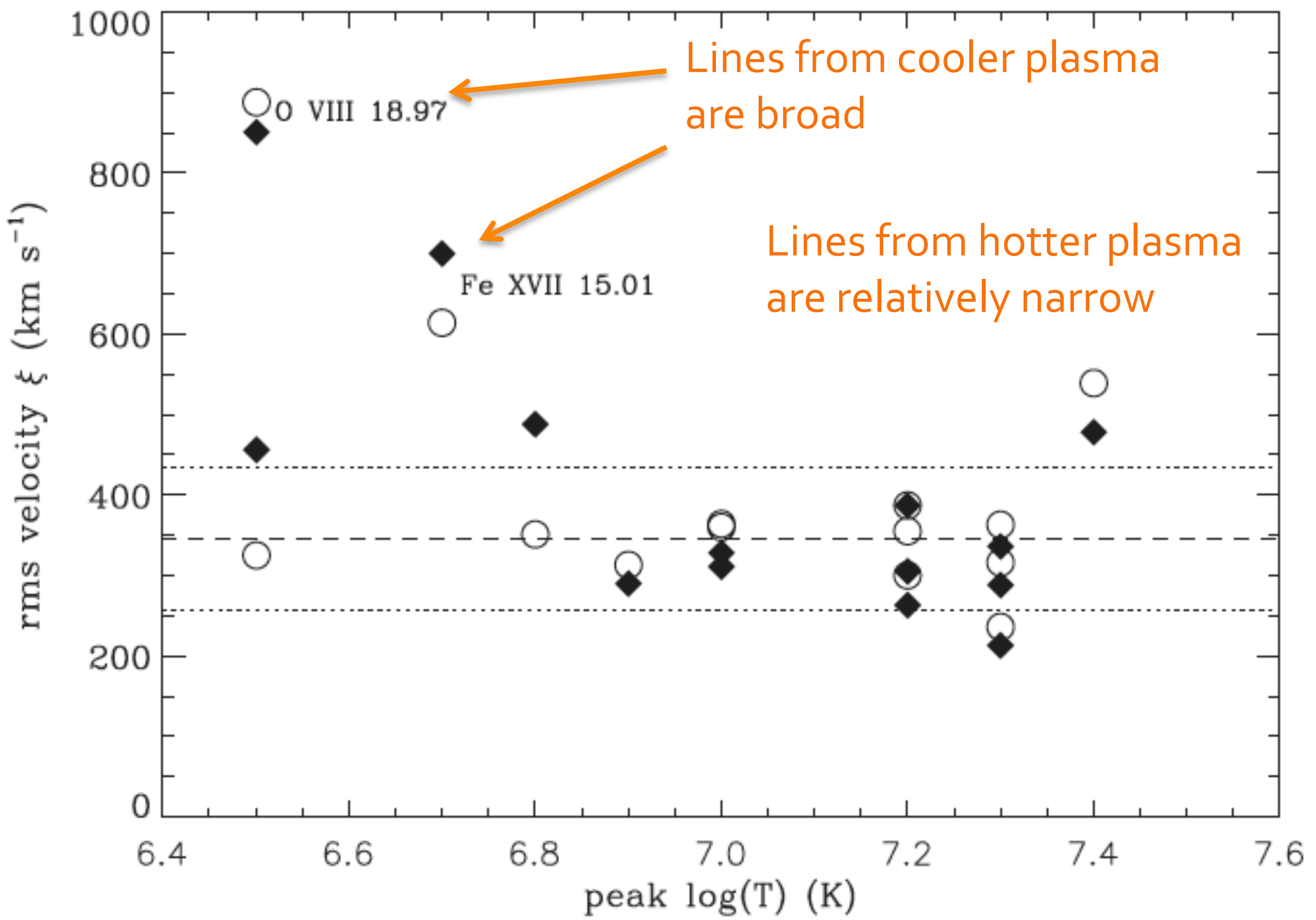

FIG. 9.—Line widths for the strongest lines in the *Chandra* spectra plotted against the temperature of peak line emissivity, taken from APED. The open circles represent the Doppler width as measured by SHERPA. The filled diamonds represent the rms velocity as measured by ISIS. The mean rms velocity and standard deviations of these lines are indicated by the horizontal lines. Note that two of the lines formed in the coolest plasma are significantly broader than the mean, but most of the lines have nonthermal line widths of a 250–450 km s^{-1}.

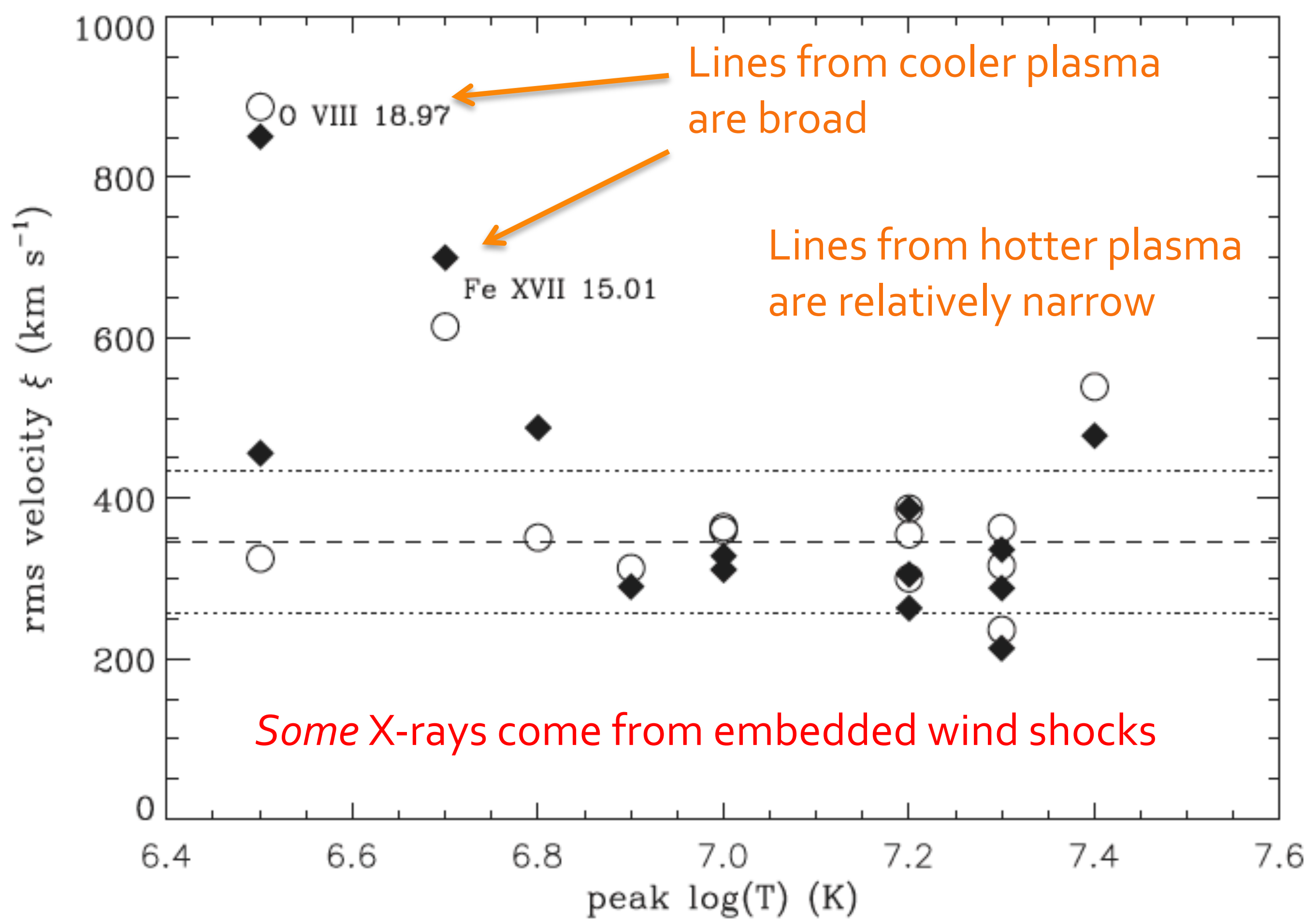

FIG. 9.—Line widths for the strongest lines in the *Chandra* spectra plotted against the temperature of peak line emissivity, taken from APED. The open circles represent the Doppler width as measured by SHERPA. The filled diamonds represent the rms velocity as measured by ISIS. The mean rms velocity and standard deviations of these lines are indicated by the horizontal lines. Note that two of the lines formed in the coolest plasma are significantly broader than the mean, but most of the lines have nonthermal line widths of a 250–450 km s^{-1}.

2D Model of θ^1 Ori C

log(density) Log(T)

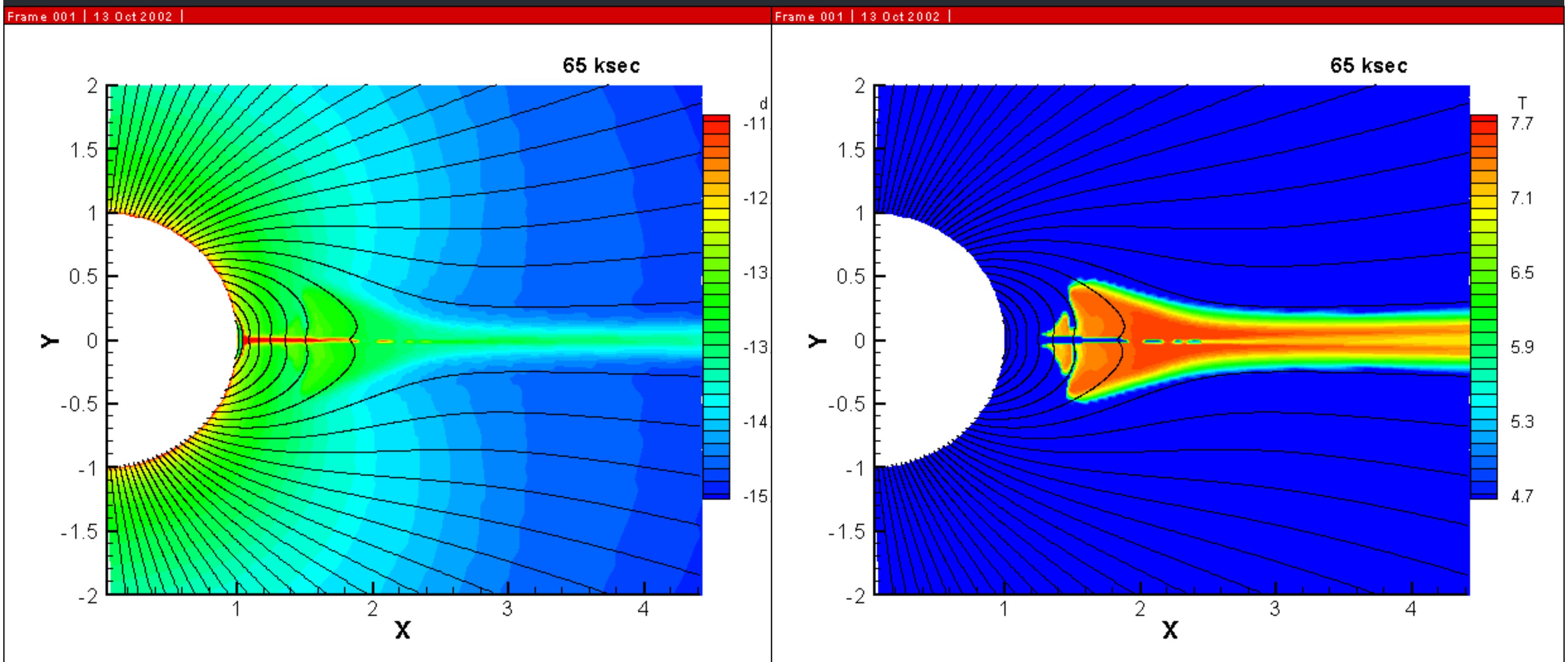

3D Model of θ¹ Ori C

Basic Top view

log(density) **Log(T)**

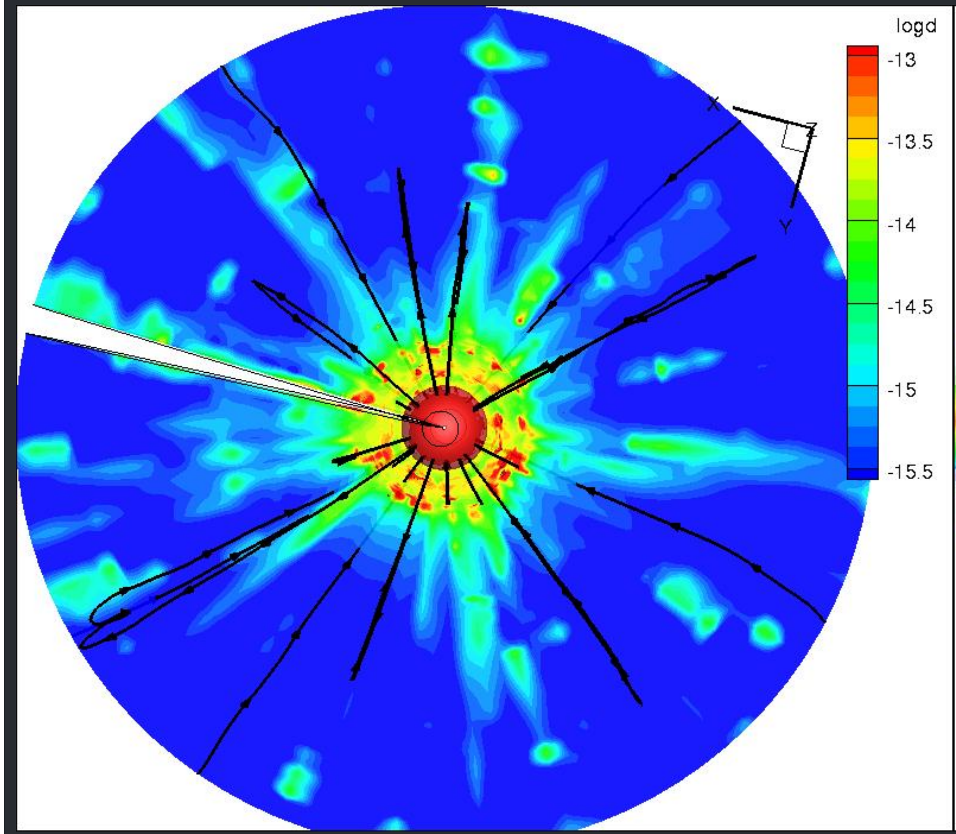

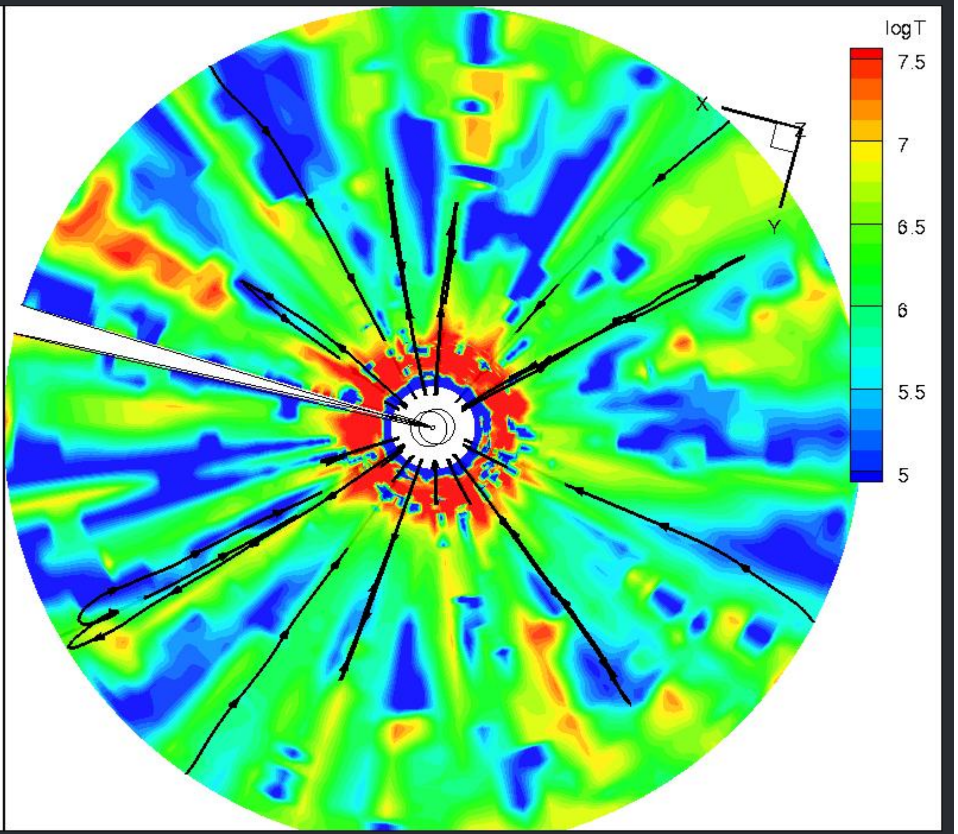

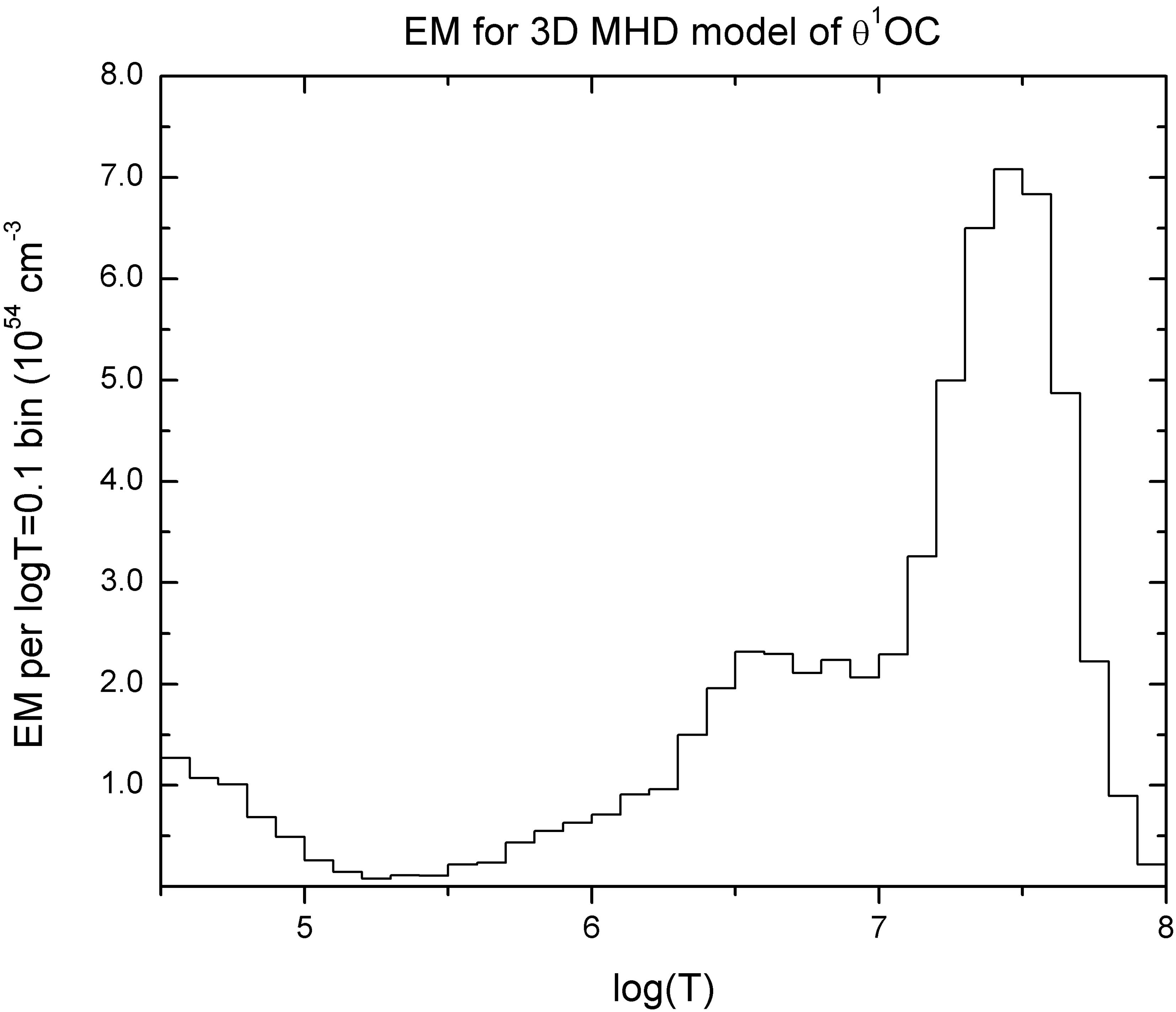

EM for 3D MHD model of θ¹OC
8.0
7.0
6.0
5.0
4.0
3.0
2.0
1.0
EM per logT=0.1 bin (10^54 cm^-3
5
6
7
8
log(T)

Magnetically Channeled Wind Shock (MCWS) scenario – as shown by MHD simulations – looks very good

Can we apply this paradigm to other magnetic massive stars?

What characterizes X-ray emission from Magnetically Channeled Wind Shocks (MCWS) in O Stars?

High X-ray luminosity

Hard X-ray spectrum

Narrow X-ray lines

θ^1 Ori C: *Chandra*

This should be true for all magnetic OB stars with large-scale fields, strong confinement, and significant wind mass-loss rates

What characterizes X-ray emission from Magnetically Channeled Wind Shocks (MCWS) in O Stars?

High X-ray luminosity

$L_X \sim 10^{-6}\ L_{Bol}$

Hard X-ray spectrum

Narrow X-ray lines

This should be true for all magnetic OB stars with large-scale fields, strong confinement, and significant wind mass-loss rates

What characterizes X-ray emission from Magnetically Channeled Wind Shocks (MCWS) in O Stars?

High X-ray luminosity

Hard X-ray spectrum

Narrow X-ray lines

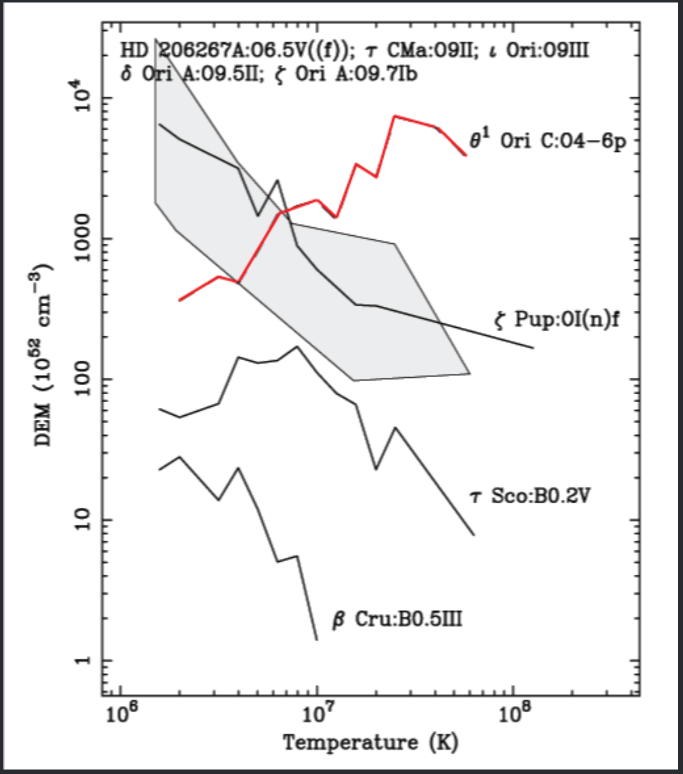

This should be true for all magnetic OB stars with large-scale fields, strong confinement, and significant wind mass-loss rates

What characterizes X-ray emission from Magnetically Channeled Wind Shocks (MCWS) in O Stars?

High X-ray luminosity

Hard X-ray spectrum

Narrow X-ray lines

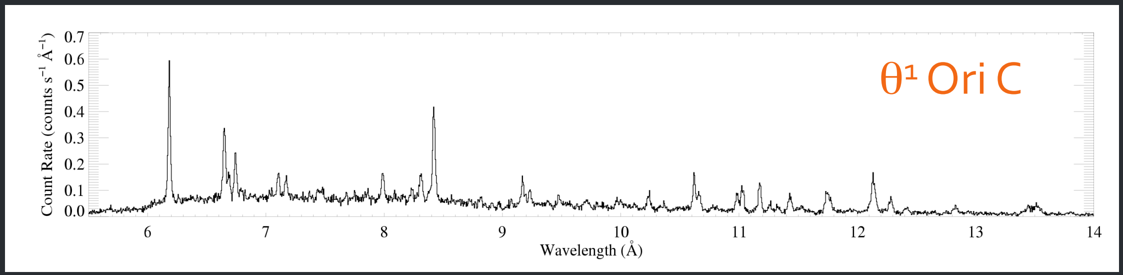

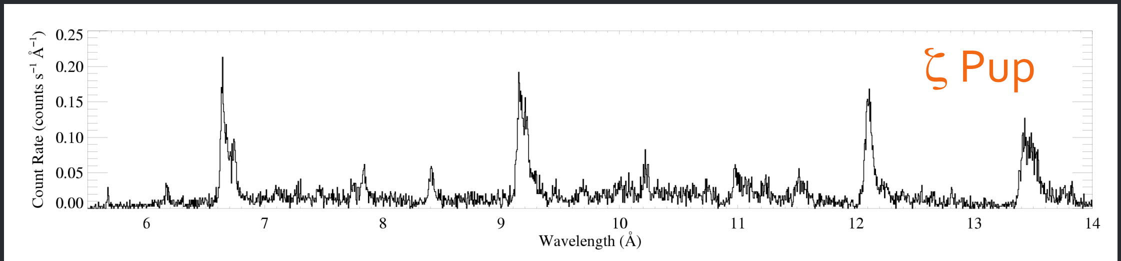

This should be true for all magnetic OB stars with large-scale fields, strong confinement, and significant wind mass-loss rates

τ Sco physical and magnetic properties

B0 V
young
slow rotator (41^d period)
V_∞ = 1500 km/s
Mdot < 10^{-8} M_{sun}/yr
O VI (Copernicus) shows
redshifted absorption (!)

Strong B-field, not a dipole: more highly structured

Mon. Not. R. Astron. Soc. **370**, 629–644 (2006) doi:10.1111/j.1365-2966.2006.

The surprising magnetic topology of τ Sco: fossil remnant or dynamo output?⋆

J.-F. Donati,[1]† I.D. Howarth,[2]† M. M. Jardine,[3]† P. Petit,[1]† C. Catala,[4]†
J. D. Landstreet,[5]† J.-C. Bouret,[6]† E. Alecian,[4]† J. R. Barnes,[3]† T. Forveille,[7]†
F. Paletou[1]† and N. Manset[7]†

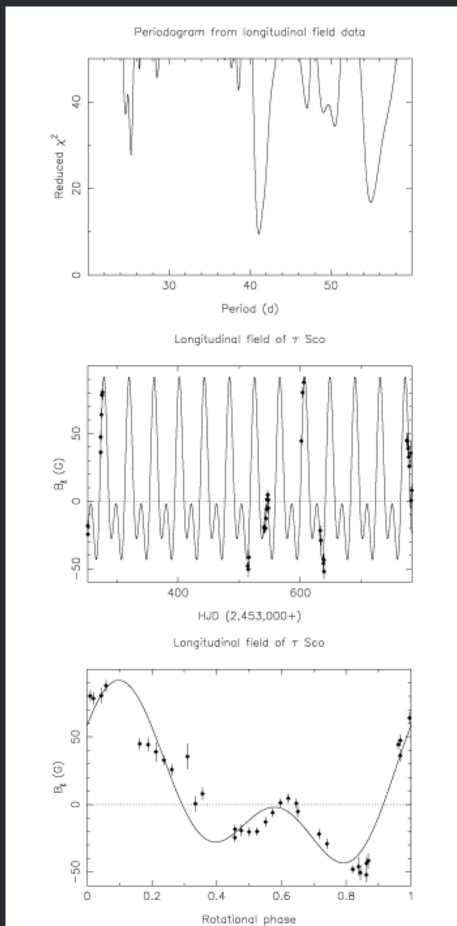

Figure 2. Periodogram resulting from a double sine-wave fit to the longitudinal-field data of τ Sco. Top panel: χ^2_ν as a function of the period of the main sine wave. A clear minimum is obtained for a period of about 41 d. Middle panel: temporal fluctuations of the longitudinal field of τ Sco (full dots, with 1σ error bars) along with the model fit (full line) for the adopted period of 41.033 d, as a function of heliocentric Julian date (HJD). Bottom panel: as for the middle panel, but as a function of rotation phase, computed using the ephemeris of equation (1).

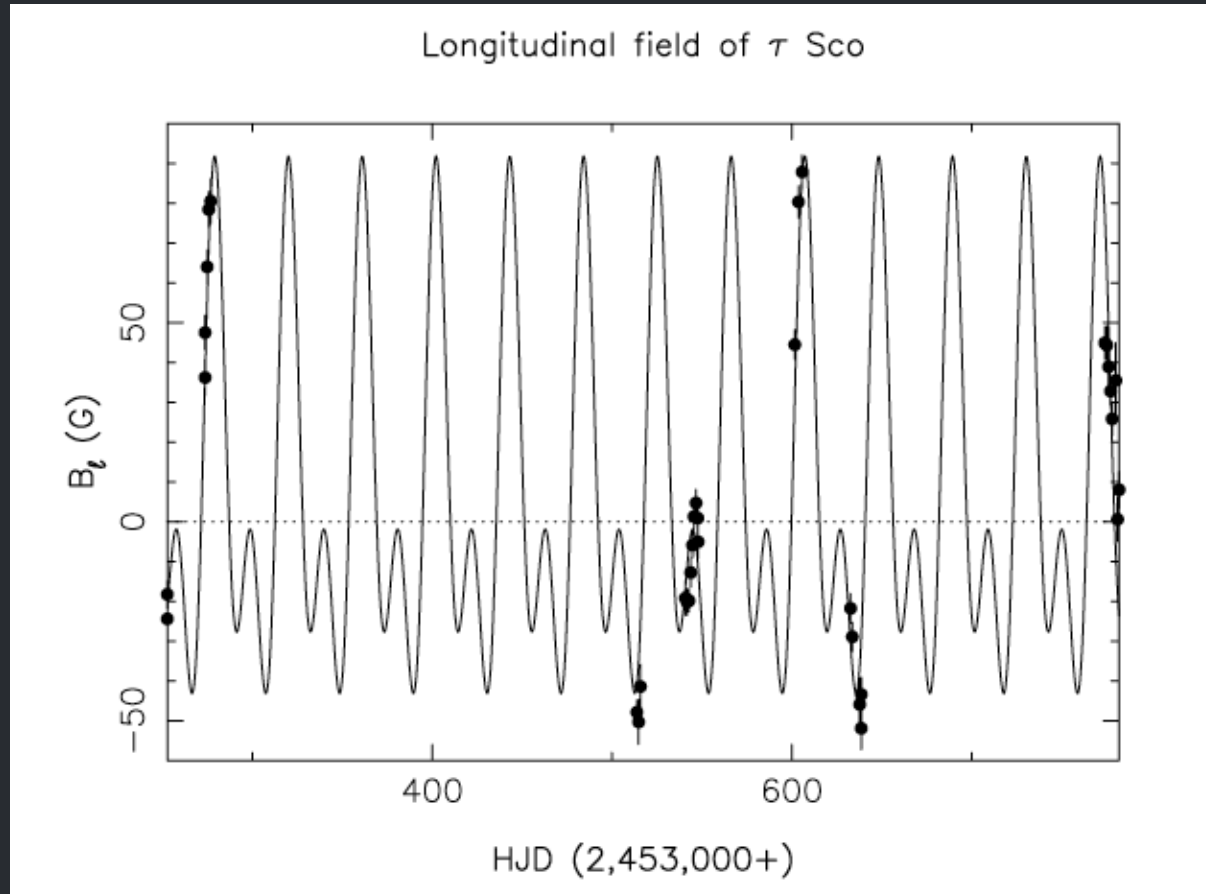

Figure 2. Periodogram resulting from a double sine-wave fit to the longitudinal-field data of τ Sco. Top panel: χ^2_ν as a function of the period of the main sine wave. A clear minimum is obtained for a period of about 41 d. Middle panel: temporal fluctuations of the longitudinal field of τ Sco (full dots, with 1σ error bars) along with the model fit (full line) for the adopted period of 41.033 d, as a function of heliocentric Julian date (HJD). Bottom panel: as for the middle panel, but as a function of rotation phase, computed using the ephemeris of equation (1).

Donati et al., 2006, *MNRAS*, 370, 629

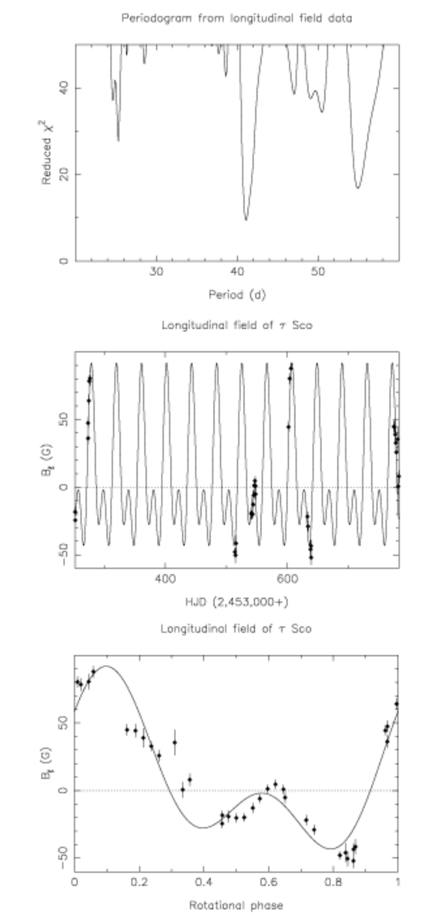

Figure 2. Periodogram resulting from a double sine-wave fit to the longitudinal-field data of τ Sco. Top panel: χ^2_ν as a function of the period of the main sine wave. A clear minimum is obtained for a period of about 41 d. Middle panel: temporal fluctuations of the longitudinal field of τ Sco (full dots, with 1σ error bars) along with the model fit (full line) for the adopted period of 41.033 d, as a function of heliocentric Julian date (HJD). Bottom panel: as for the middle panel, but as a function of rotation phase, computed using the ephemeris of equation (1).

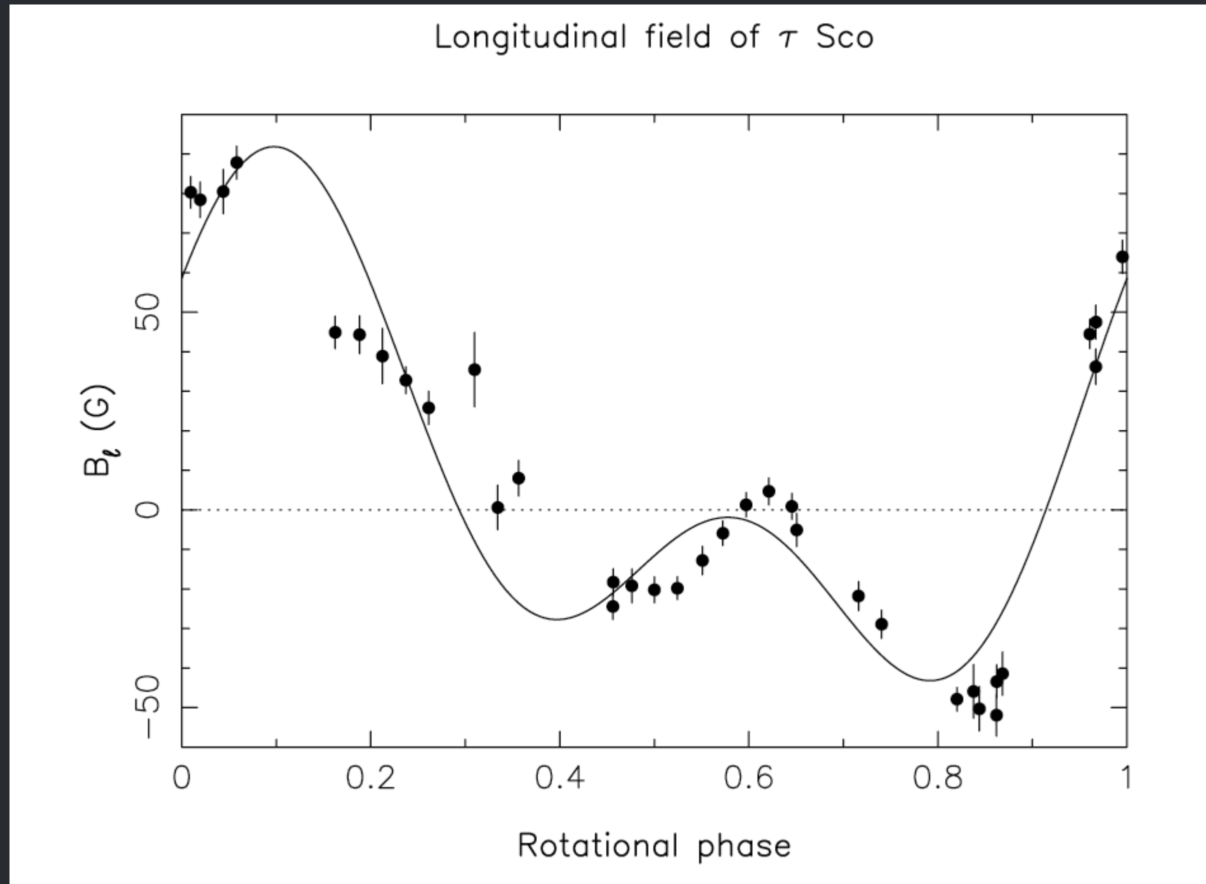

Figure 2. Periodogram resulting from a double sine-wave fit to the longitudinal-field data of τ Sco. Top panel: χ^2_ν as a function of the period of the main sine wave. A clear minimum is obtained for a period of about 41 d. Middle panel: temporal fluctuations of the longitudinal field of τ Sco (full dots, with 1σ error bars) along with the model fit (full line) for the adopted period of 41.033 d, as a function of heliocentric Julian date (HJD). Bottom panel: as for the middle panel, but as a function of rotation phase, computed using the ephemeris of equation (1).

Donati et al., 2006, *MNRAS*, 370, 629

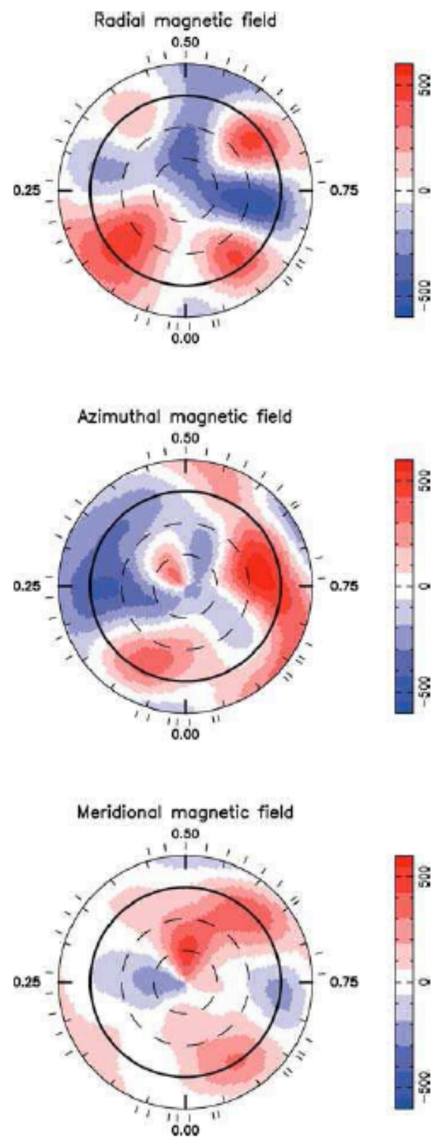

Figure 8. Maximum-entropy reconstructions of the magnetic topology of τ Sco, assuming that the global field can be expressed as the sum of a potential field and a toroidal field. The three components of the field are displayed from top to bottom panel (flux values labelled in G). The top image (radial field component) is described through the set of complex coefficients $\alpha_{\ell,m}$ (see Section 5). The star is shown in flattened polar projection down to latitudes of $-30°$, with the equator depicted as a bold circle and parallels as dashed circles. Radial ticks around each plot indicate phases of observations.

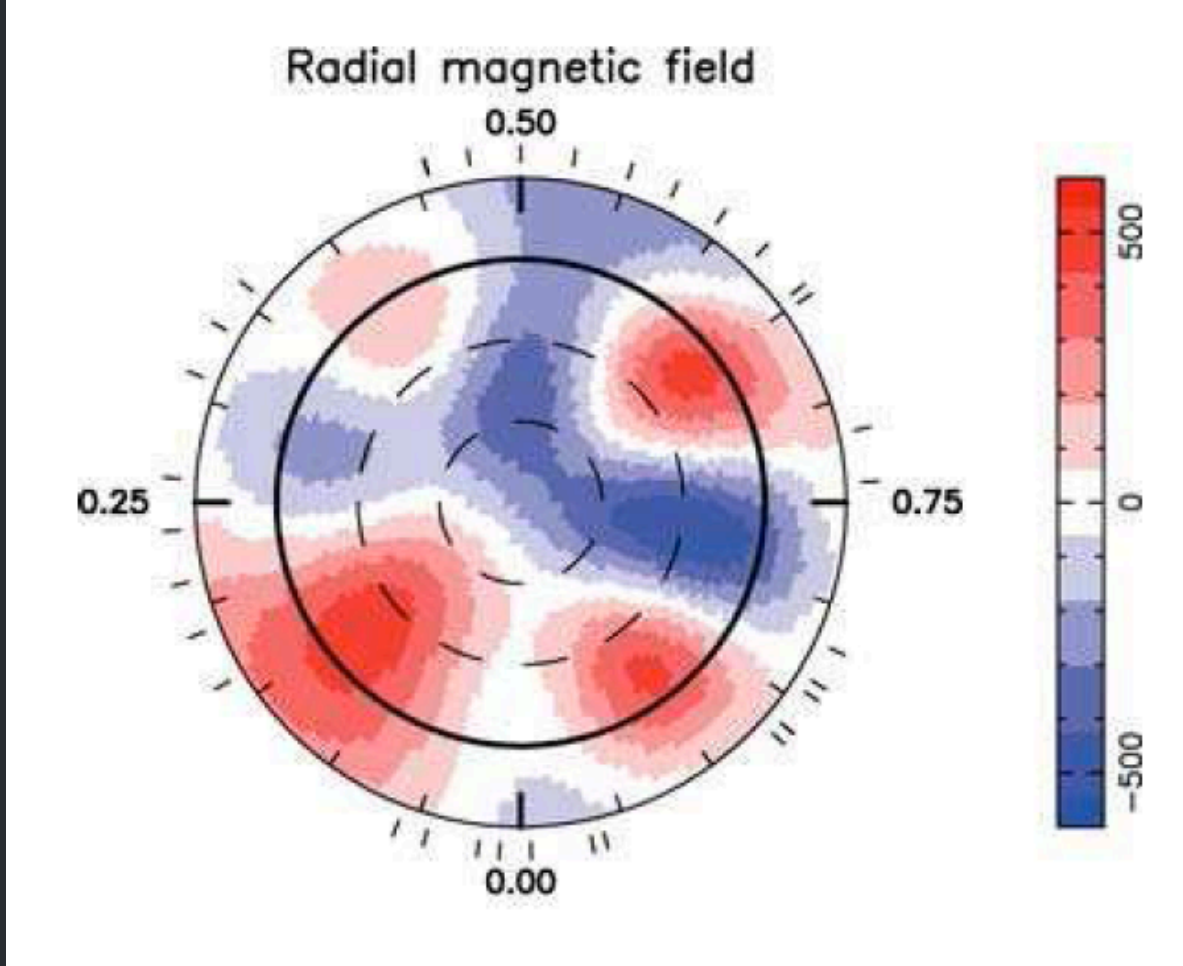

Figure 8. Maximum-entropy reconstructions of the magnetic topology of τ Sco, assuming that the global field can be expressed as the sum of a potential field and a toroidal field. The three components of the field are displayed from top to bottom panel (flux values labelled in G). The top image (radial field component) is described through the set of complex coefficients $\alpha_{\ell,m}$ (see Section 5). The star is shown in flattened polar projection down to latitudes of $-30°$, with the equator depicted as a bold circle and parallels as dashed circles. Radial ticks around each plot indicate phases of observations.

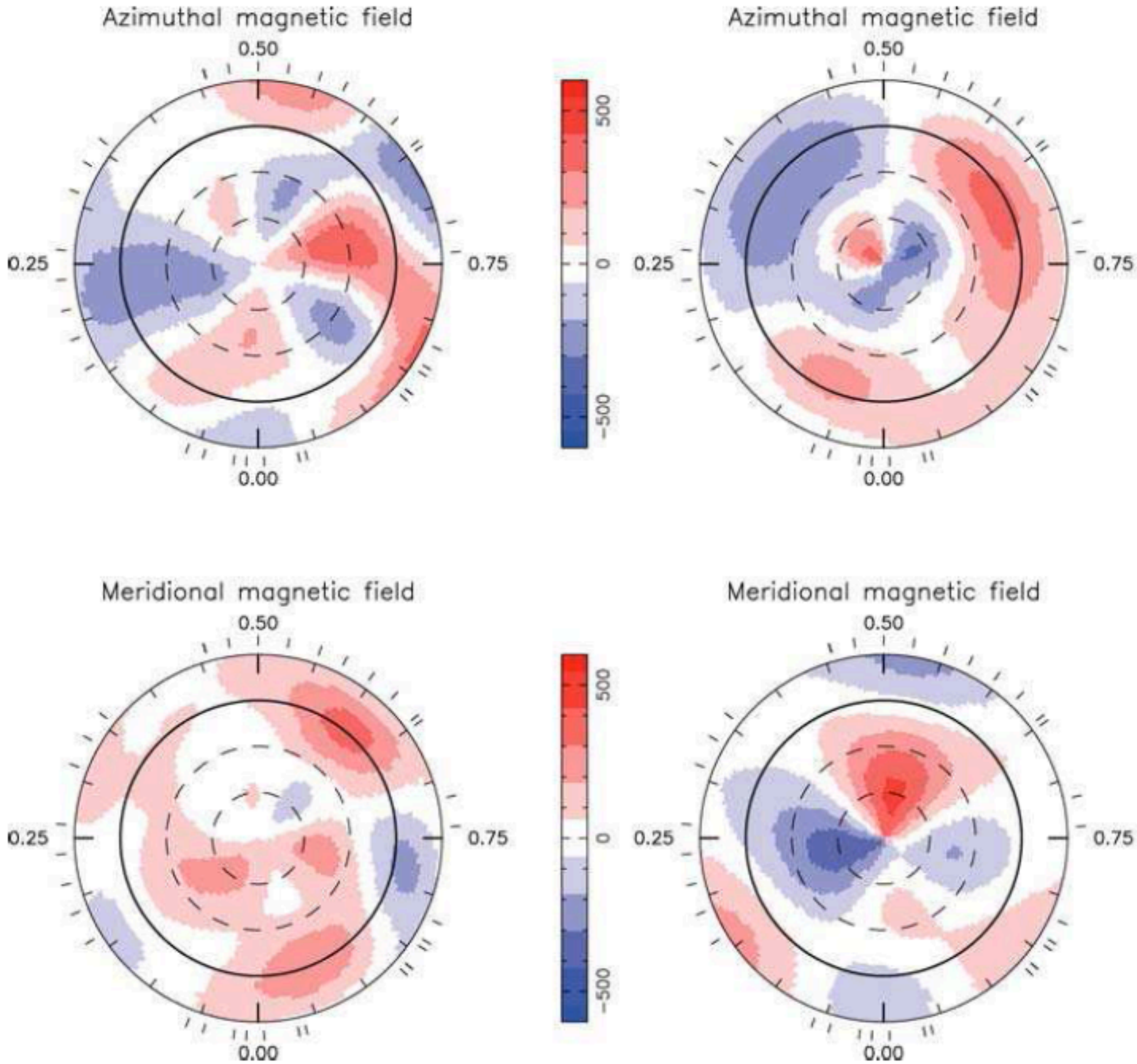

Figure 9. Azimuthal and meridional components of the reconstructed potential (left-hand column) and toroidal (right-hand column) field structures. Adding both yields the azimuthal and meridional field components shown in Fig. 8. The image on the left-hand side is described through the set of complex coefficients $\beta_{\ell,m}$, while that on the right-hand side is obtained through the coefficients $\gamma_{\ell,m}$ (see Section 5).

642 *J.-F. Donati et al.*

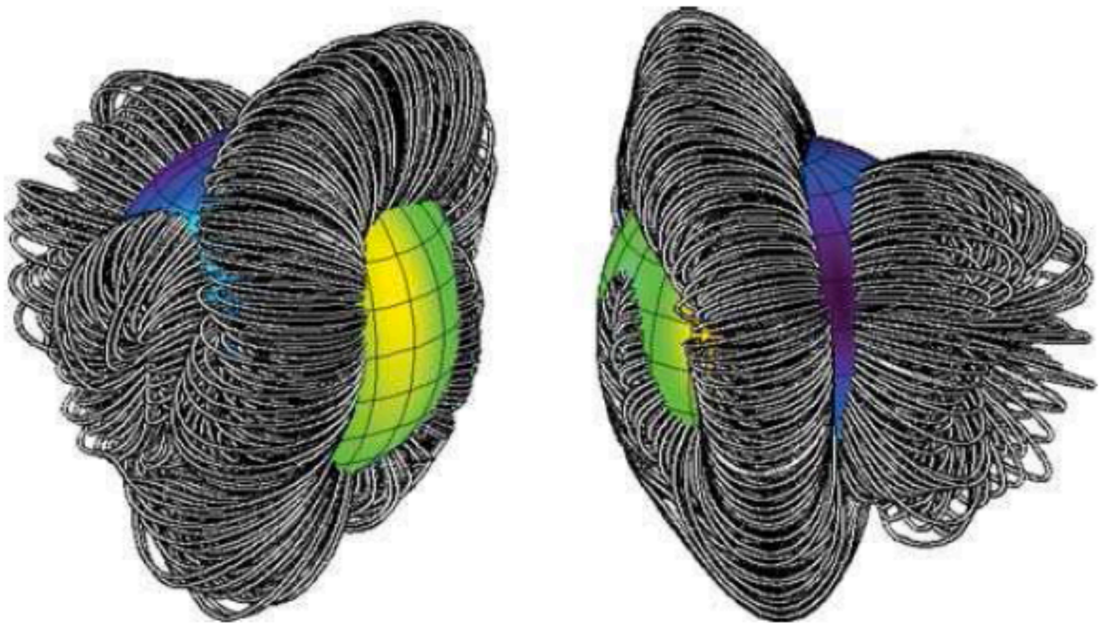

Figure 11. Closed magnetic field lines of the extended magnetic configuration of τ Sco, extrapolated from the photospheric map of Fig. 8. The star is shown at phases 0.25 (left-hand panel) and 0.83 (right-hand panel). Note the warp of the magnetic equator and the additional networks of closed loops around phase 0.65 (mostly visible on the right-hand side of the right-hand panel).

This model is not unique…and does it account for the effects of the wind realistically?

τ Sco X-ray properties

Higher X-ray luminosity

Harder spectrum than most OB stars; not as hard as θ^1 Ori C, though

Lines resolved by *Chandra*, but narrow

τ Sco X-ray properties requiring more interpretation

Forbidden-to-intercombination line ratios in He-like ion states put hot plasma off of the photosphere ($r > 2R_{star}$)

There is no rotational modulation of the overall X-ray flux as would be expected if the X-rays arise in the closed magnetic loops shown in Donati et al. Fig. 11

High X-ray Luminosity

$$L_x = 4.4 \times 10^{31} \text{ erg s}^{-1}$$

$$L_x/L_{bol} = 10^{-6.5}$$

For a mass-loss rate of $10^{-8}\ M_{sun}\ yr^{-1}$, an emission measure filling factor approaching unity is required

Note: Oskinova et al. (2011) find Mdot ~ $10^{-9}\ M_{sun}\ yr^{-1}$

THE ASTROPHYSICAL JOURNAL, 586:495–505, 2003 March 20

HIGH-RESOLUTION *CHANDRA* SPECTROSCOPY OF τ SCORPII: A NARROW-LINE X-RAY SPECTRUM FROM A HOT STAR

DAVID H. COHEN AND GENEVIÈVE E. DE MESSIÈRES
Department of Physics and Astronomy, Swarthmore College, Swarthmore, PA 19081;
cohen@astro.swarthmore.edu, gdemess1@swarthmore.edu

JOSEPH J. MACFARLANE
Prism Computational Sciences, 455 Science Drive, Madison, WI 53711; jjm@prism-cs.com

NATHAN A. MILLER
Department of Physics and Astronomy, 105 Garfield Avenue, University of Wisconsin, Eau Claire, WI 54702;
millerna@uwec.edu

JOSEPH P. CASSINELLI
Department of Astronomy, 475 North Charter Street, University of Wisconsin, Madison, WI 53706;
cassinelli@astro.wisc.edu

STANLEY P. OWOCKI
Bartol Research Institute, University of Delaware, Newark, DE 19716; owocki@bartol.udel.edu

AND

DUANE A. LIEDAHL
Lawrence Livermore National Laboratory, Livermore, CA 94550; liedahl1@llnl.gov
Received 2002 August 16; accepted 2002 November 25

τ Sco: *Chandra* HETGS

Medium Energy Grating (MEG)

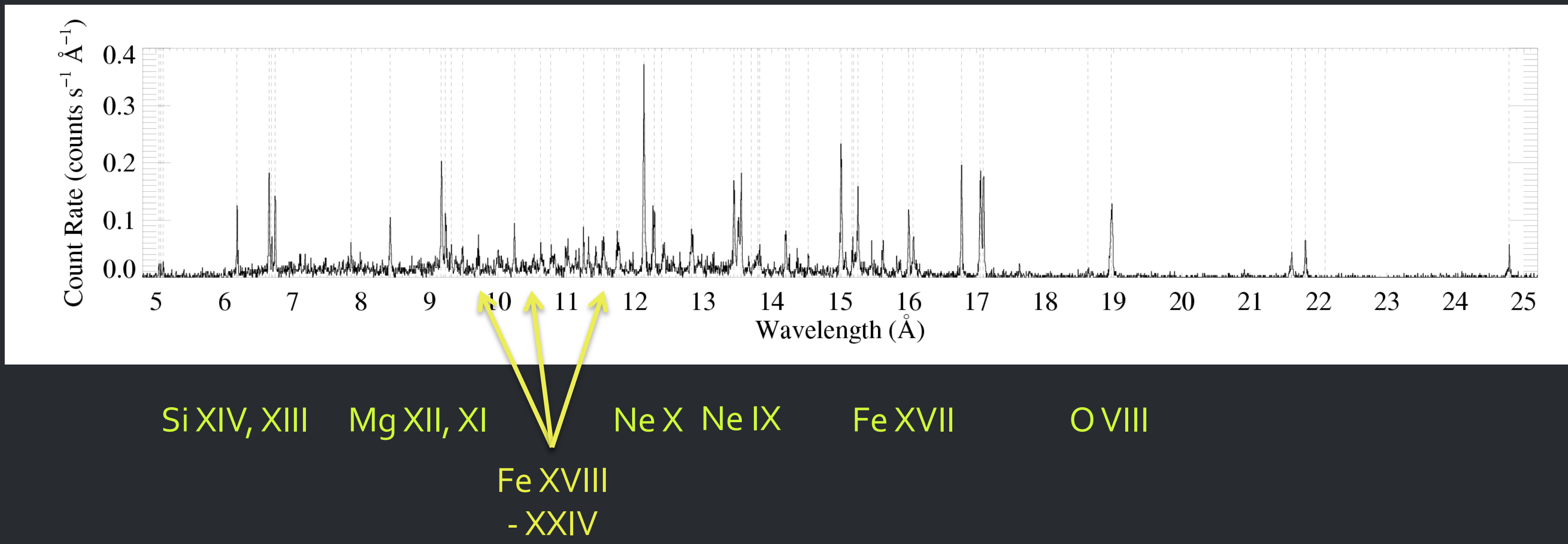

These lines arise in plasma with **T > 10^{7} K**, and are *not* seen in normal O stars

H-like/He-like ratio is temperature sensitive

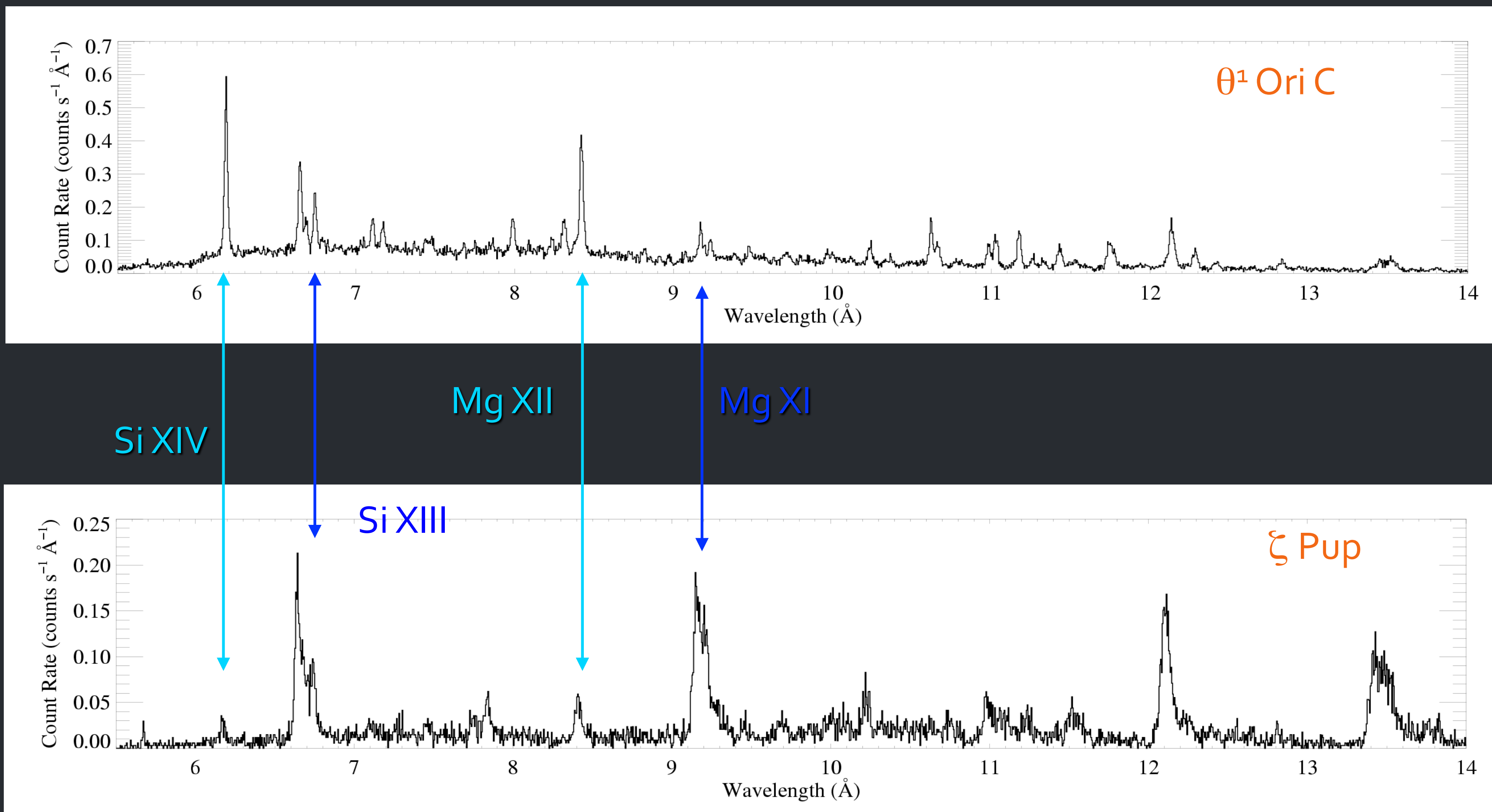

τ Sco: *Chandra* HETGS

Medium Energy Grating (MEG)

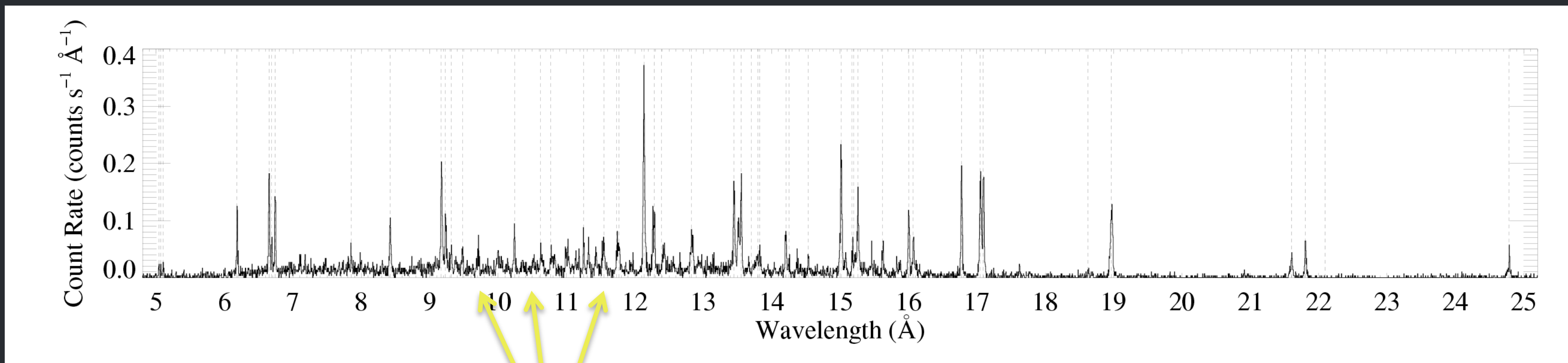

Si XIV, XIII   Mg XII, XI   Ne X   Ne IX   Fe XVII   O VIII

Fe XVIII
- XXIV

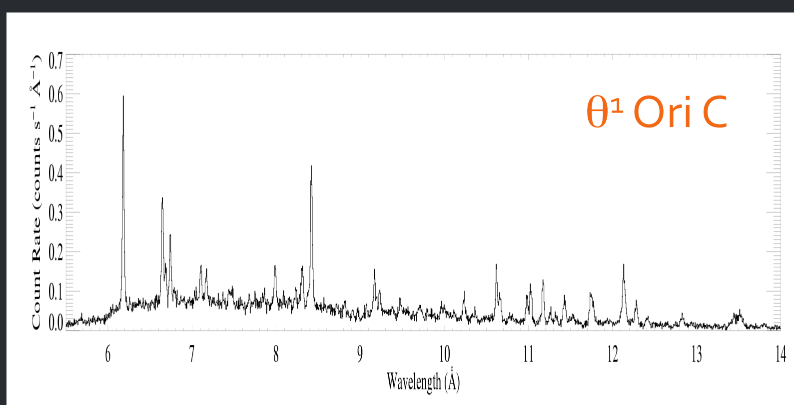

τ Sco: *Chandra* HETGS

H-like/He-like ratio is temperature sensitive

Medium Energy Grating (MEG)

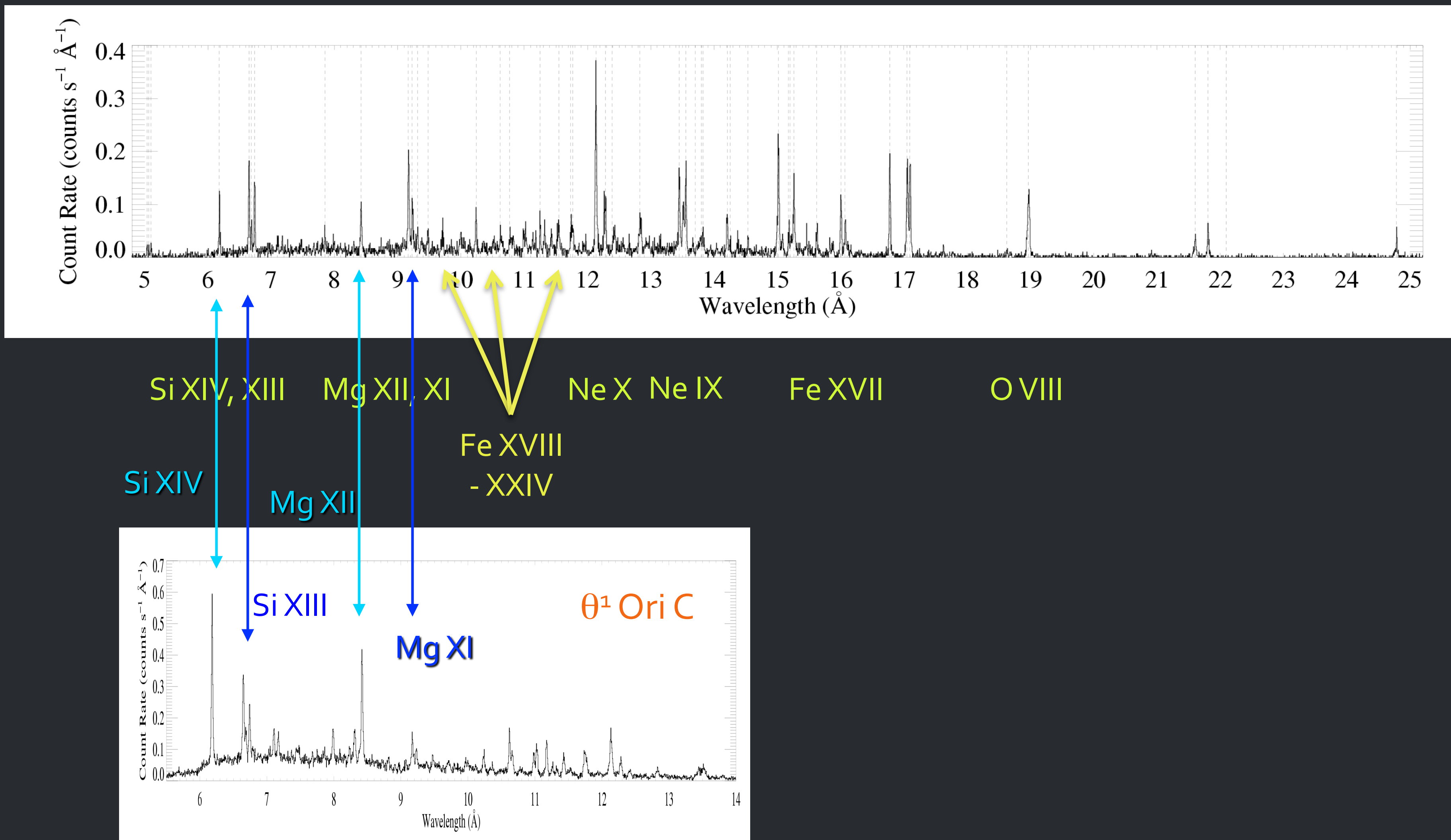

Differential emission measure

(temperature distribution)

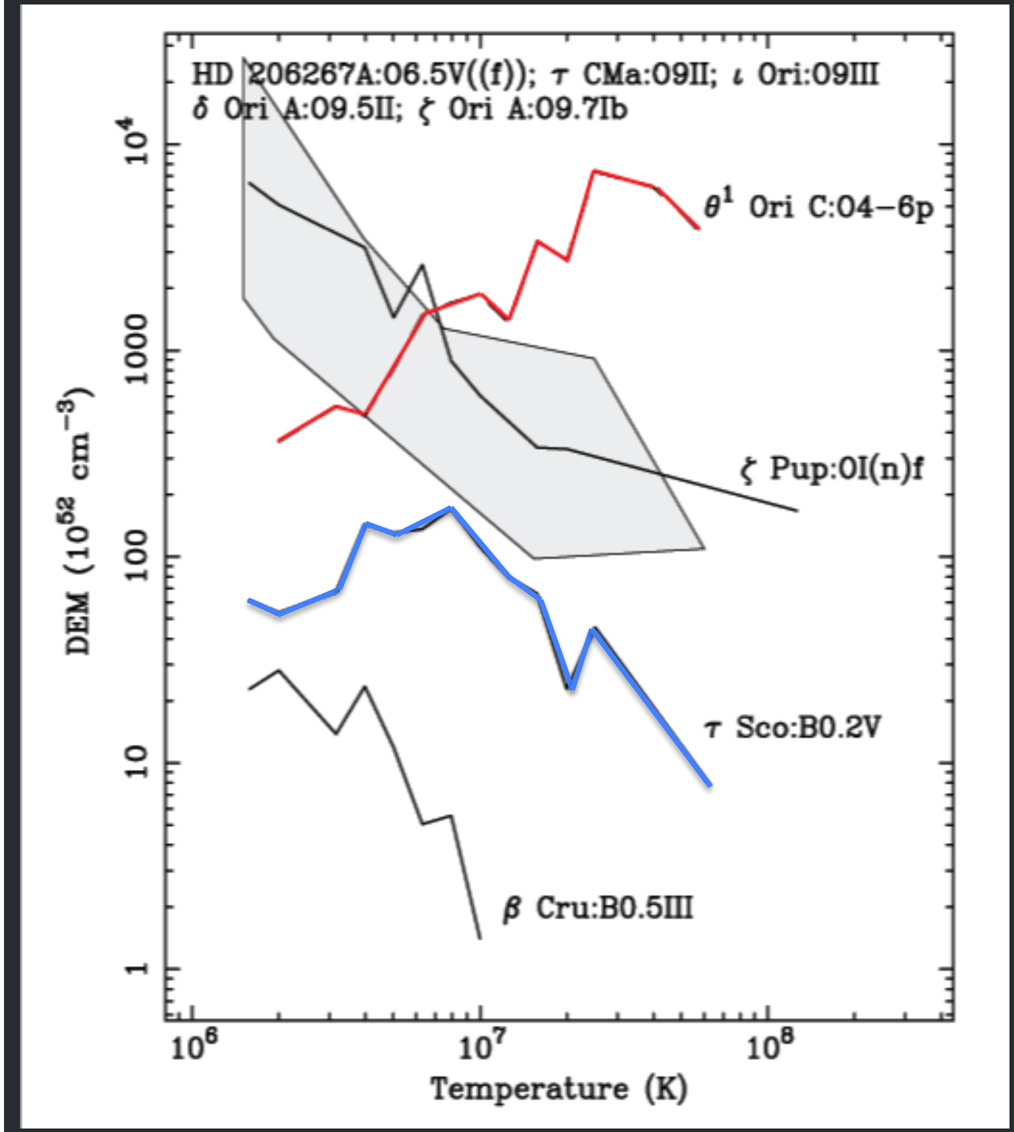

Wojdowski & Schulz (2005)

θ^1 Ori C:
peak near 30 million K

τ Sco:
peak near 10 million K

Non-magnetic O stars,
peak at 1 – 2 million K

X-ray emission lines are resolved, but narrower even than θ^1 Ori C

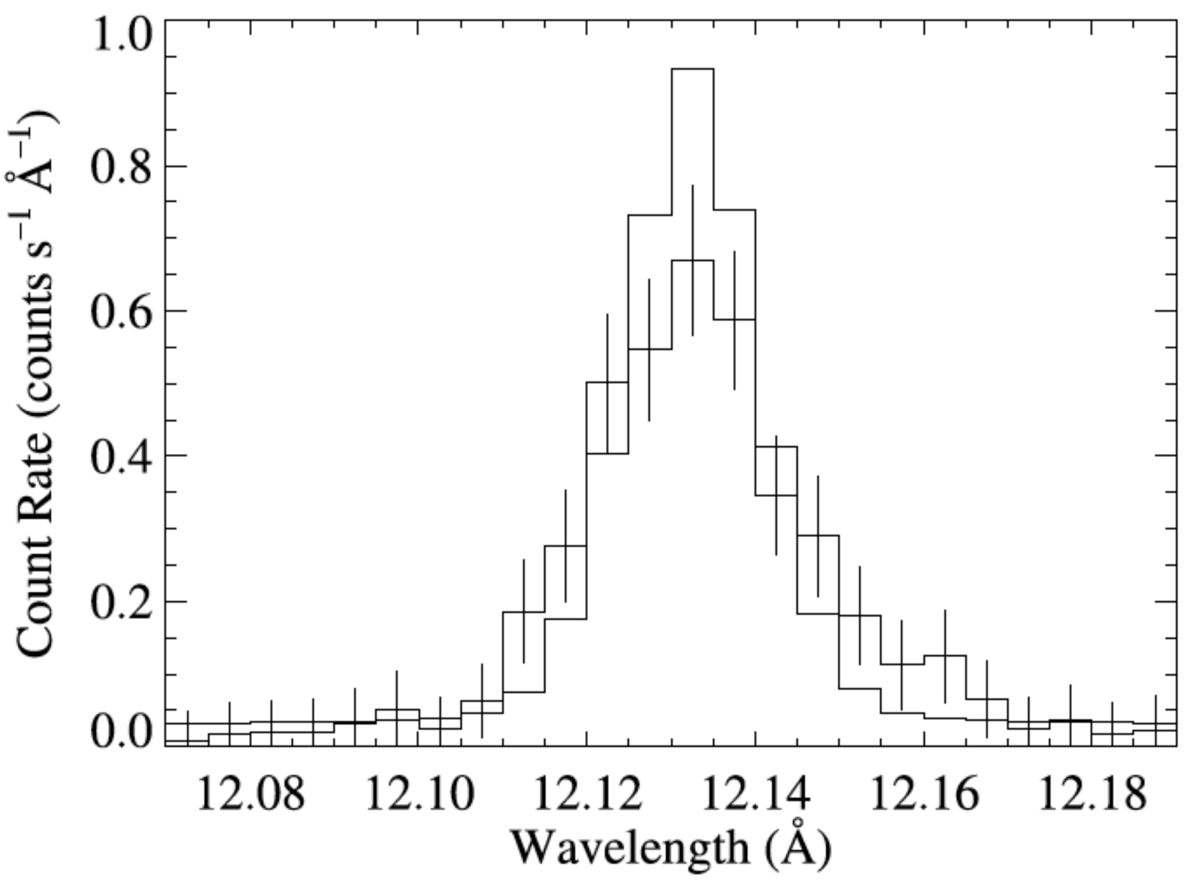

FIG. 5.—MEG +1 and −1 order observation of the neon Lyα line (*histogram*) with an intrinsically narrow model (convolved with the instrument response). The fit to the data shows a statistically significant line width.

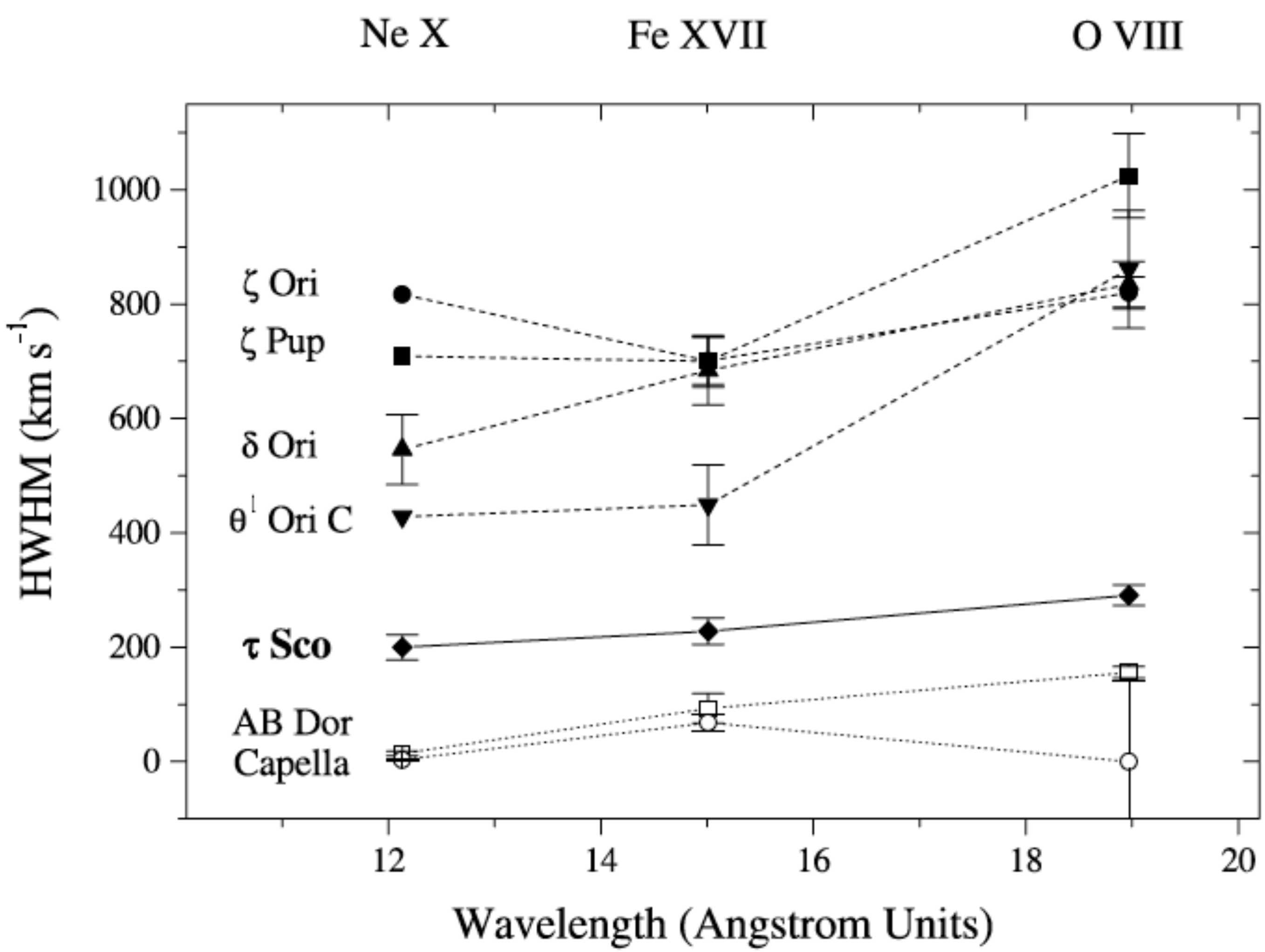

FIG. 6.—Derived line widths (HWHM) for three strong lines in seven stars: two stars representative of coronal sources (Capella and AB Dor: *open symbols connected by dotted lines*), τ Sco (*filled diamonds and solid line*), and four O stars (*filled symbols and dashed lines*), which are presumably wind X-ray sources.

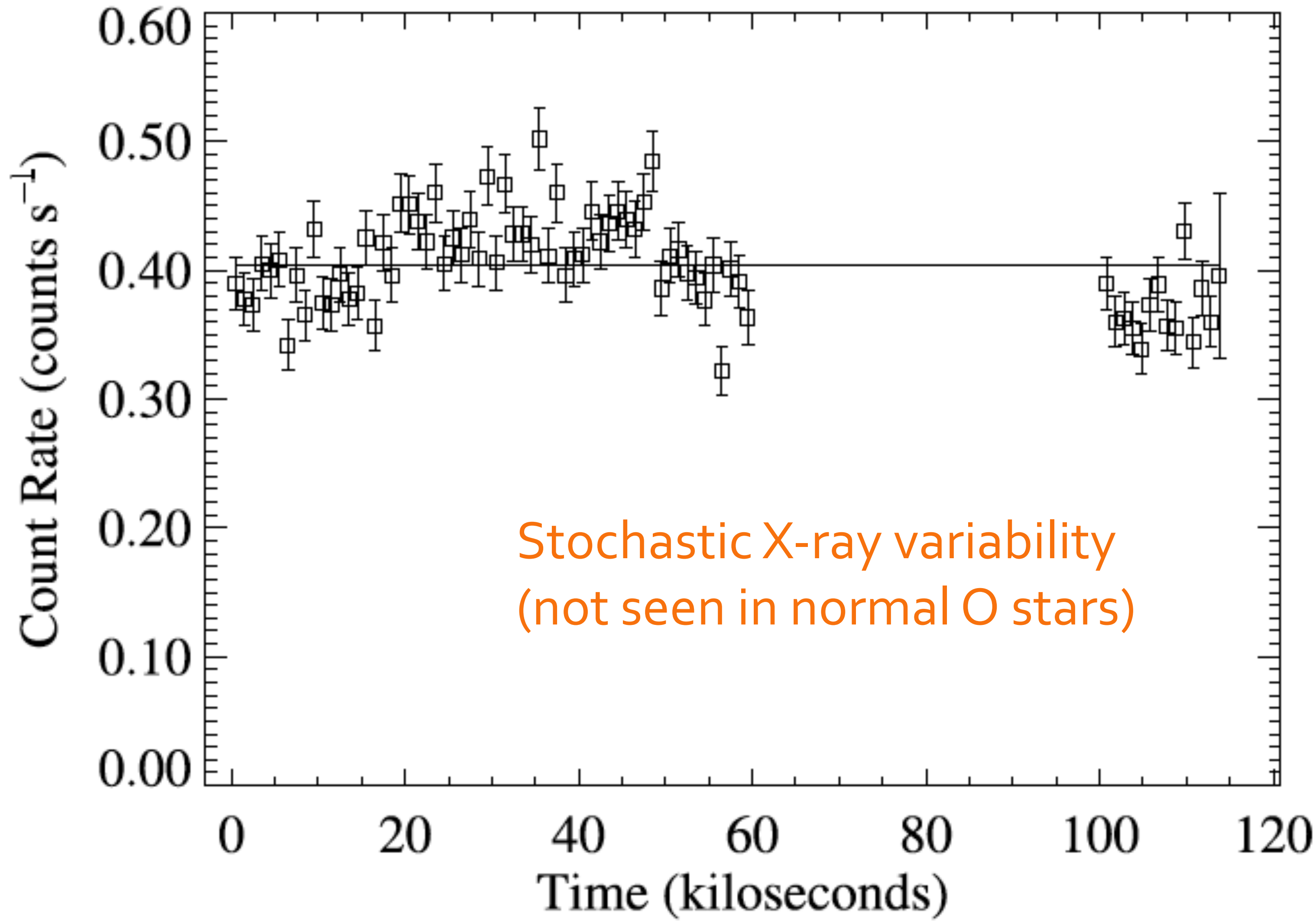

FIG. 3.—X-ray light curve formed from the combined MEG +1 and −1 order counts, with 1000 s bins. The mean count rate is indicated by the line. The hypothesis of a constant source can be rejected at a more than 99.99% confidence level.

The Astrophysical Journal, 721:1412–1420, 2010 October 1 doi:10.1088/0004-637X/721/2/1412

A MULTIPHASE *SUZAKU* STUDY OF X-RAYS FROM τ Sco

R. Ignace[1], L. M. Oskinova[2], M. Jardine[3], J. P. Cassinelli[4], D. H. Cohen[5], J.-F. Donati[6], R. H. D. Townsend[4], and A. ud-Doula[7]

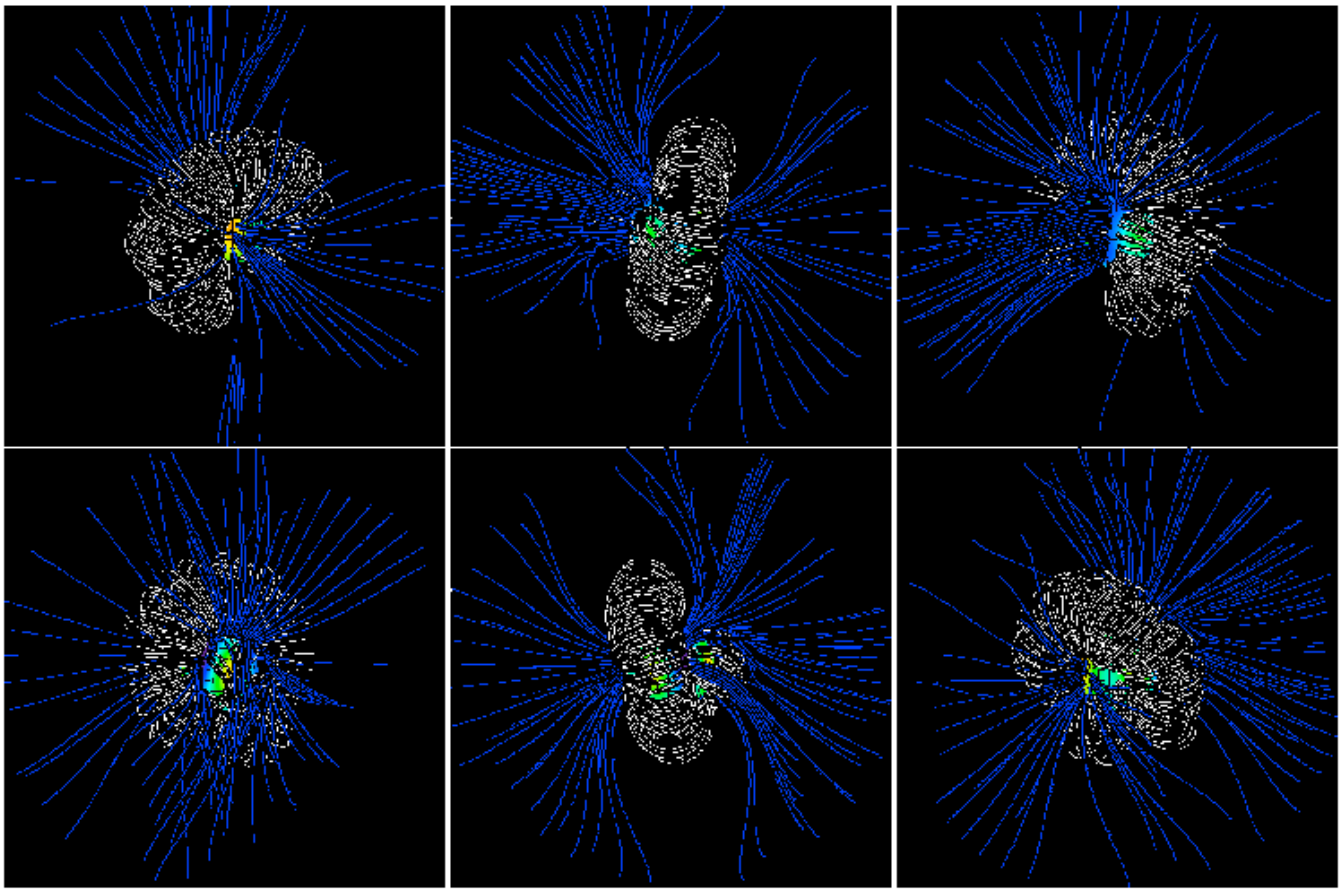

Fig. 7.— Structure of magnetic field lines at rotation phases 0.17, 0.34, and 0.50 (top, left to right) and 0.67, 0.83, and 0.97 (bottom, left to right). Closed field lines are shown white, while open field lines are shown blue.

No rotational modulation of the X-rays

X-ray plasma is *not* in the closed loops in the Donati/Jardine model

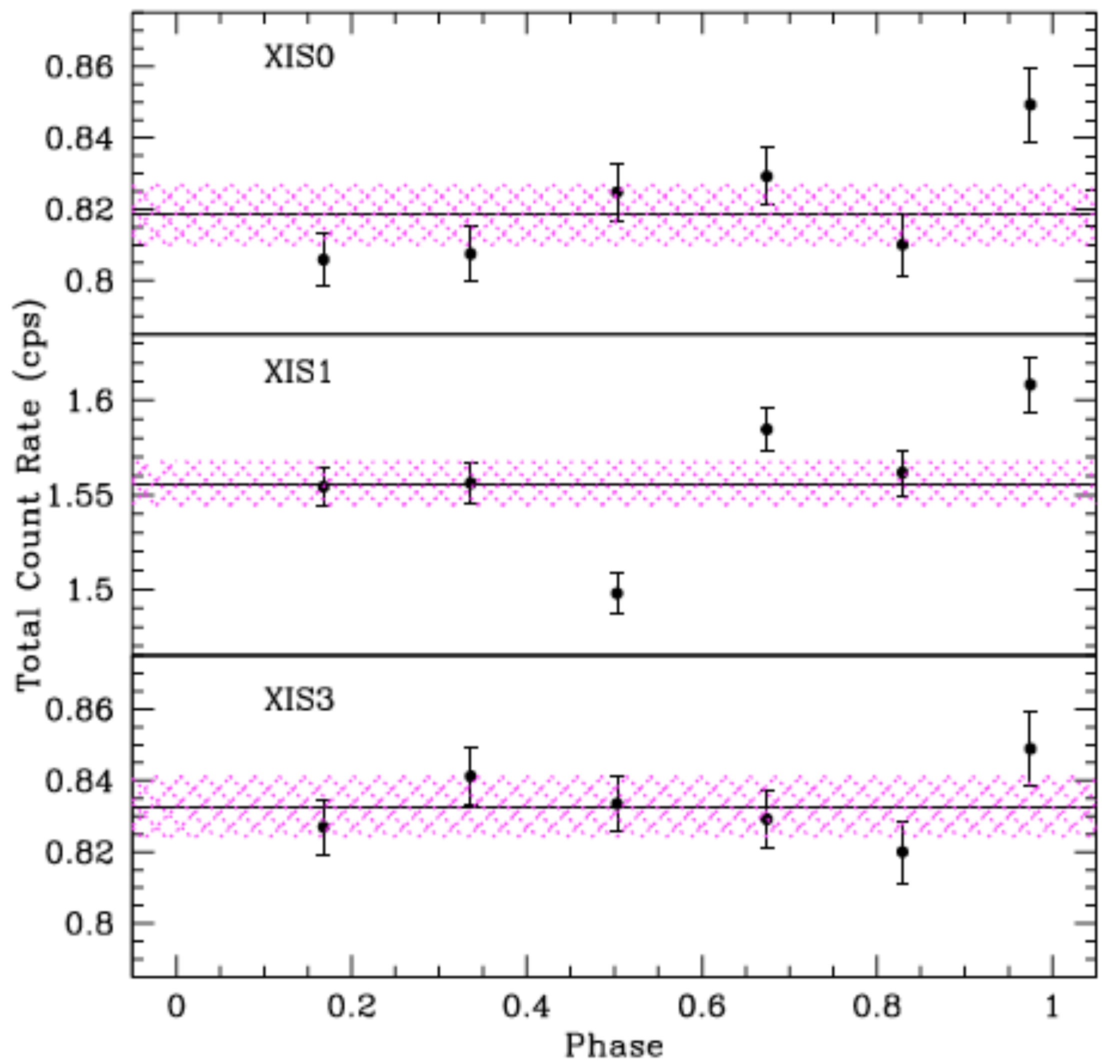

Fig. 2.— Total count rates from Table 1 plotted against rotational phase. The colored hashed region represents the rms error of the data, as described in the text.

The f/i ratio is thus a diagnostic of the strength of the local UV radiation field.

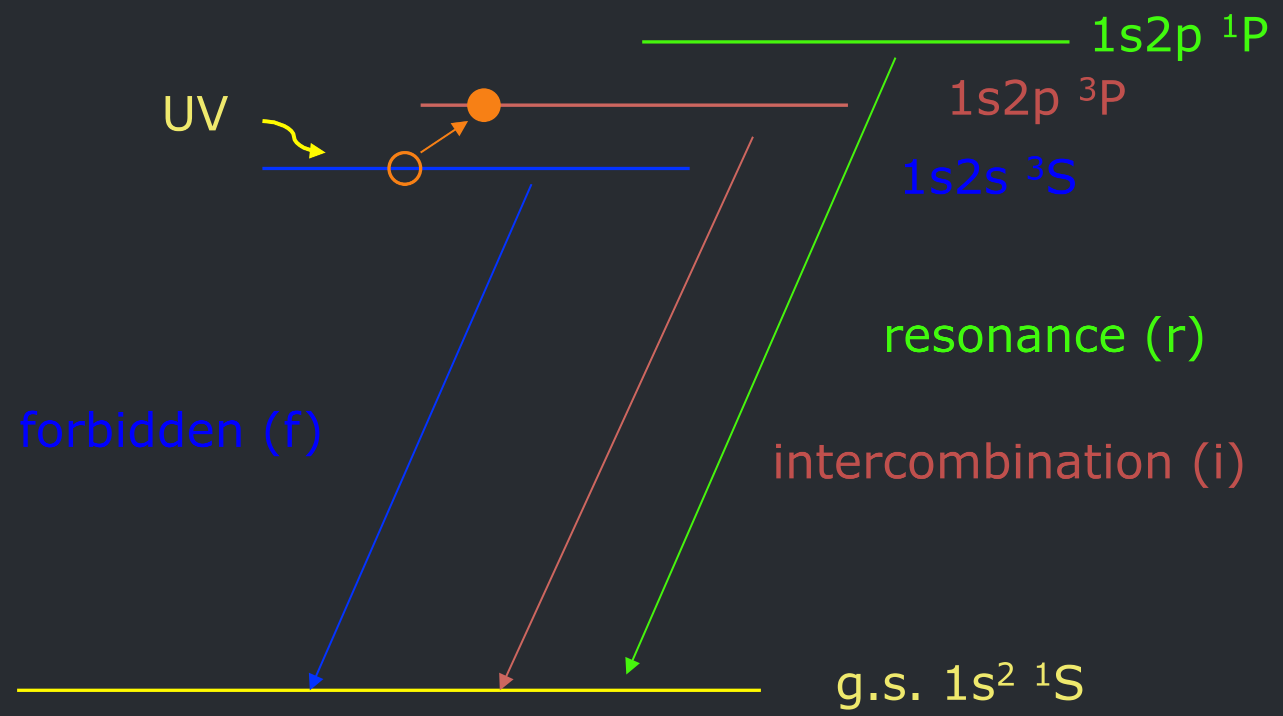

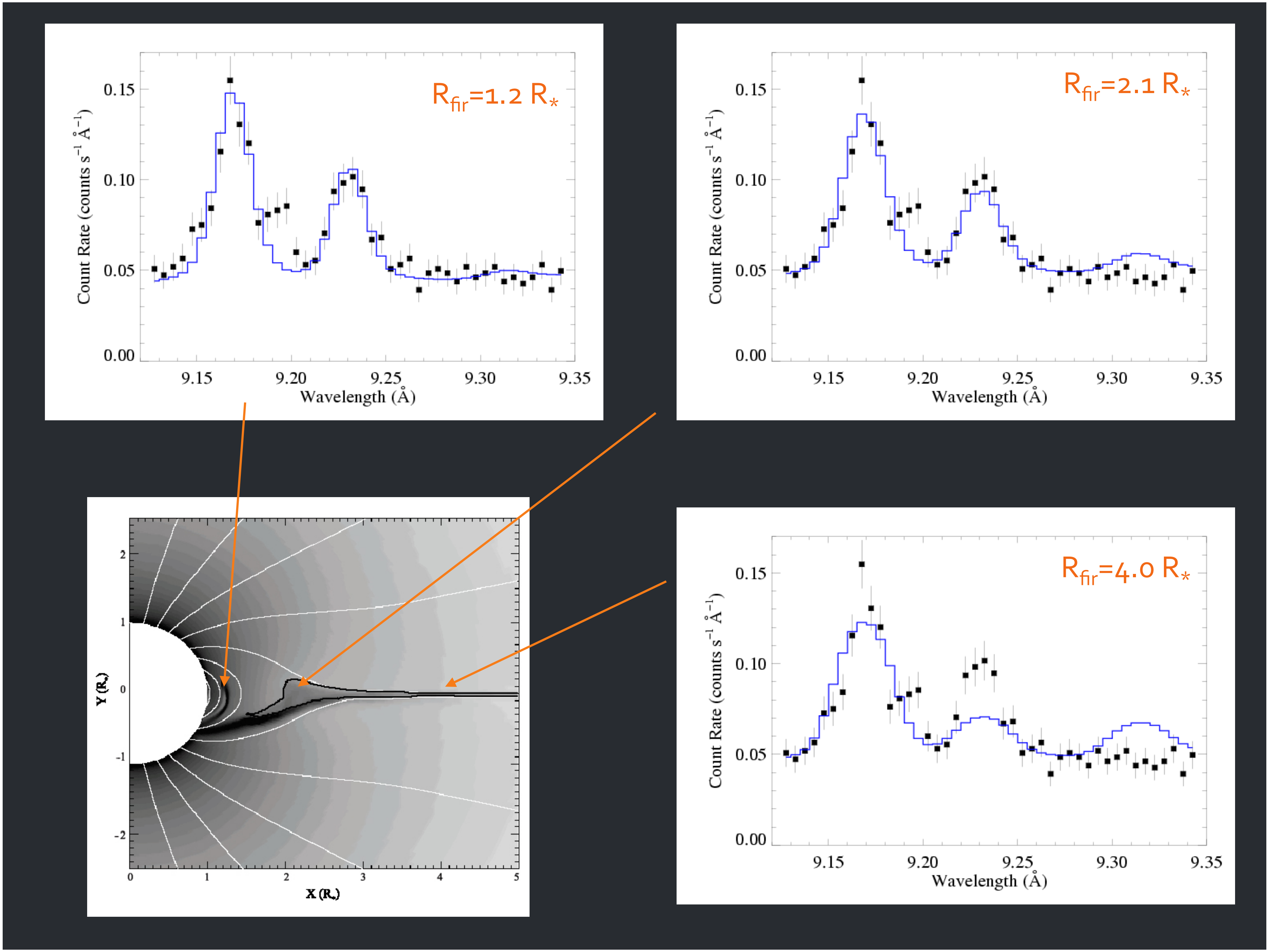

R_{fir}=1.2 R_*
R_{fir}=2.1 R_*
R_{fir}=4.0 R_*
Count Rate (counts s^{-1} Å^{-1})
Wavelength (Å)
0.00
0.05
0.10
0.15
9.15
9.20
9.25
9.30
9.35
Y (R_*)
X (R_*)

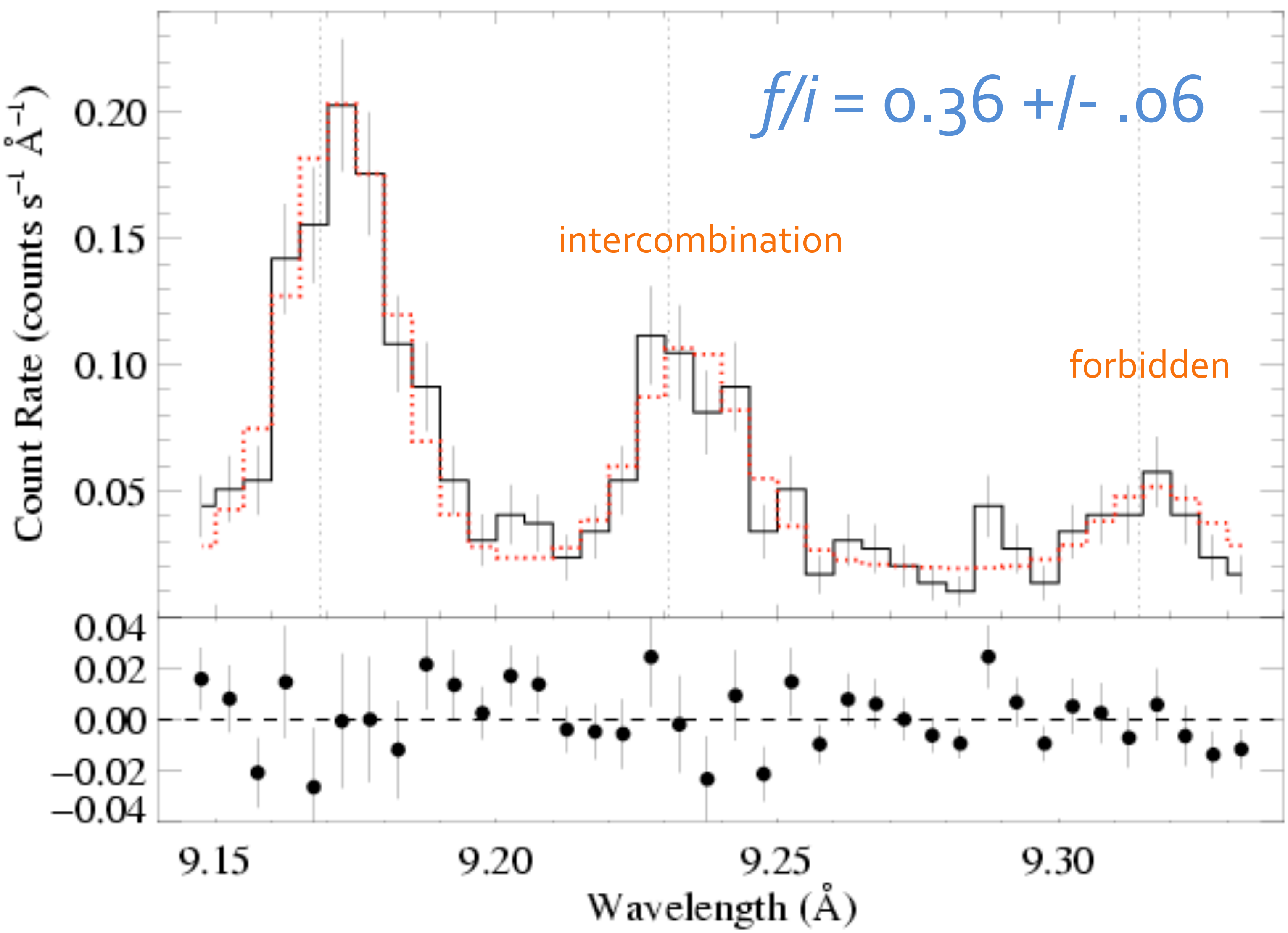

f/i = 0.36 +/- .06
intercombination
forbidden
Count Rate (counts s^{-1} Å^{-1})
0.20
0.15
0.10
0.05
0.04
0.02
0.00
−0.02
−0.04
9.15
9.20
9.25
9.30
Wavelength (Å)

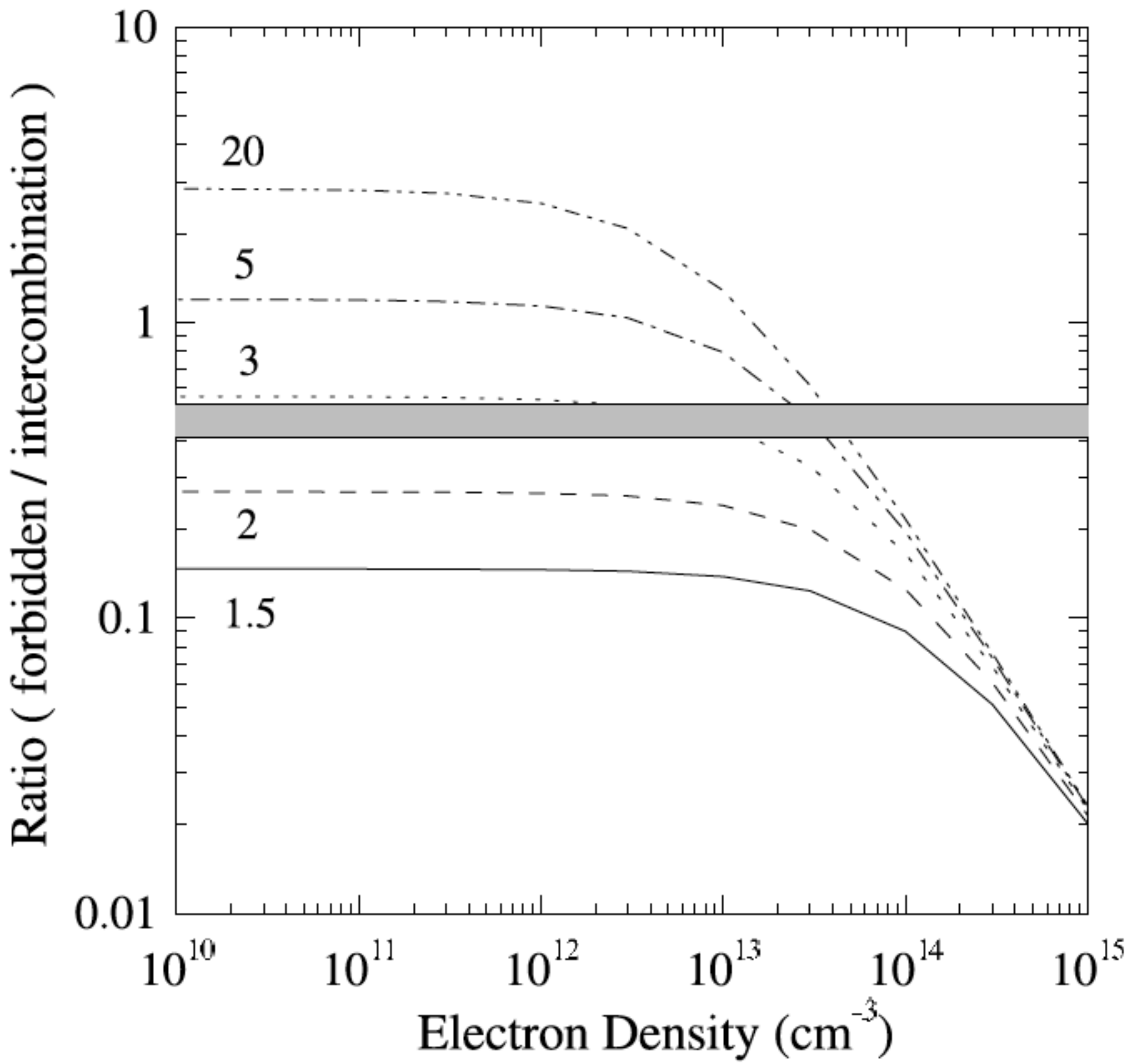

FIG. 9.—Calculation of the density and mean-intensity sensitivity of the f/i line ratio for Mg XI. Note that the sensitivity to the mean intensity enters via the distance from the photosphere. The distance of the plasma from the photosphere is indicated for each model in units of the stellar radius. The range from the data is indicated by the shaded area.

f/i ratios indicate
$r > 2R_*$

X-ray plasma is *not* in the closed loops in the Donati/Jardine model

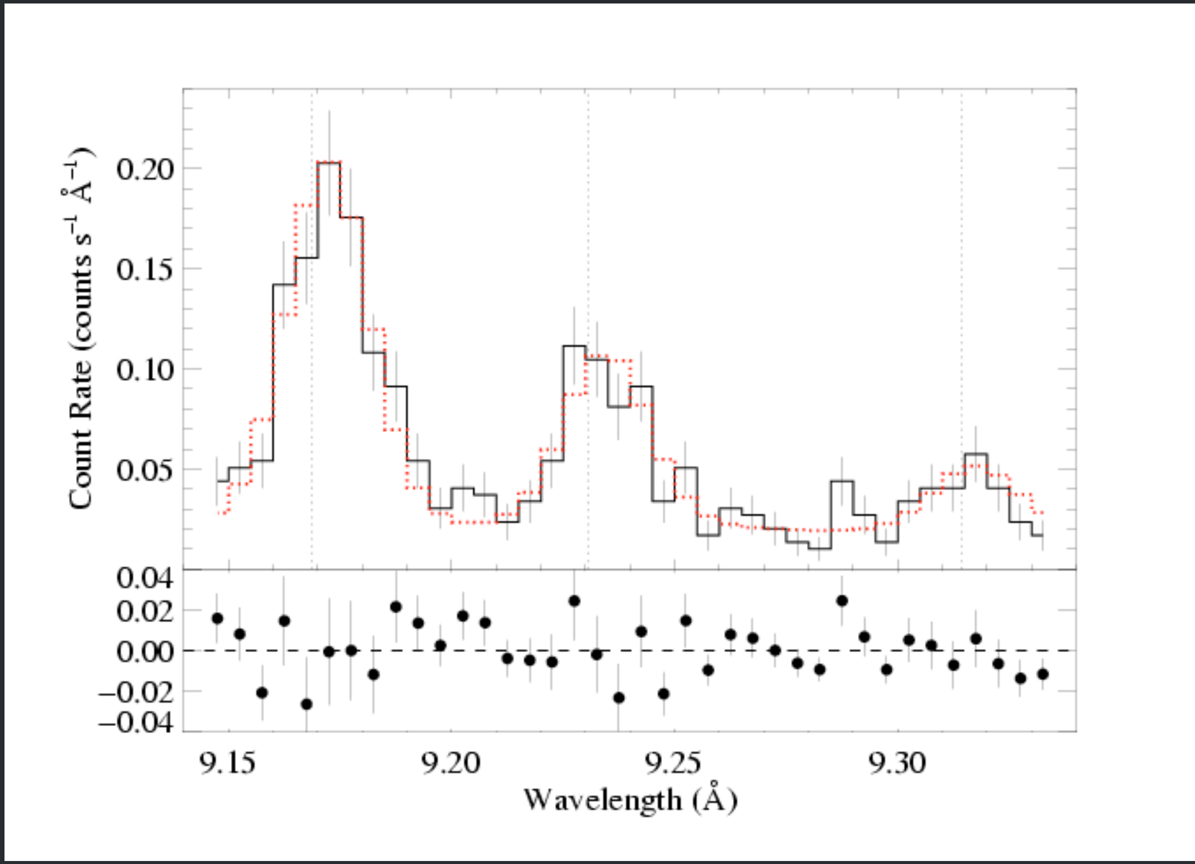

What needs to be done

What field configuration is consistent with the wind properties?

Can magnetically confined wind shocks heat a sufficient amount of plasma to the observed temperatures, and at distances above the photosphere to accommodate the *f/i* ratios and lack of rotational modulation?

HD 191612 physical and magnetic properties

Confirmation of the magnetic oblique rotator model for the Of?p star HD 191612⋆

G.A. Wade[1], I.D. Howarth[2], R.H.D. Townsend[3], J.H. Grunhut[1,4], M. Shultz[1,4], J.-C. Bouret[5,6], A. Fullerton[7], W. Marcolino[8], F. Martins[9], Y. Nazé[10], A. ud Doula[11], N.R. Walborn[7], J.-F. Donati[12] and the MiMeS Collaboration†

[1]Dept. of Physics, Royal Military College of Canada, PO Box 17000, Stn Forces, Kingston, Ontario K7K 7B4, Canada
[2]Dept. of Physics and Astronomy, UCL, Gower Place, London WC1E 6BT, United Kingdom
[3]Dept. of Astronomy, University of Wisconsin-Madison, 475 N. Charter Street, Madison WI 53706-1582, USA
[4]Dept. of Physics, Engineering Physics and Astronomy, Queen's University, 99 University Avenue, Kingston, Ontario K7L 3N6, Canada
[5]LAM-UMR 6110, CNRS & Universitde Provence, rue Frédéric Joliot-Curie, F-13388 Marseille Cedex 13, France
[6]NASA/GSFC, Code 665, Greenbelt, MD 20771, USA
[7]Space Telescope Science Institute, 3700 San Martin Drive, Baltimore, MD 21218, USA
[8]Observatório do Valongo, Universidade Federal do Rio de Janeiro, Rio de Janeiro, Brazil
[9]GRAAL-UMR5024, CNRS & Université Montpellier II, Place Eugène Bataillon, F-34095 Montpellier Cedex 05, France
[10]FNRS-Institut d'Astrophysique et de Géophysique, Université de Liège, Belgium
[11]Penn State Worthington Scranton, 120 Ridge View Drive, Dunmore, PA, USA 18512
[12]Observatoire Midi-Pyrén´ées, 14 avenue Édouard Belin, F-31400, Toulouse, France

Accepted . Received , in original form

ABSTRACT

This paper reports high-precision Stokes V spectra of HD 191612 acquired using the ESPaDOnS spectropolarimeter at the Canada-France-Hawaii Telescope, in the context of the Magnetism in Massive stars (MiMeS) Project. Using measurements of the equivalent width of the Hα line and radial velocities of various metallic lines, we have updated both the spectroscopic and orbital ephemerides of this star. We confirm the presence of a strong magnetic field in the photosphere of HD 191612, and detect its variability. We establish that the longitudinal field varies in a manner consistent with the spectroscopic period of 537.6 d, in an approximately sinusoidal fashion. The phases of minimum and maximum longitudinal field are respectively coincident with the phases of maximum and minimum Hα equivalent width and $H_{\rm p}$ magnitude. This demonstrates a firm connection between the magnetic field and the processes responsible for the line and continuum variability. Interpreting the variation of the longitudinal magnetic field within the context of the dipole oblique rotator model, and adopting an inclination $i = 30°$ obtained assuming alignment of the orbital and rotational angular momenta, we obtain a best-fit surface magnetic field model with obliquity $\beta = 67 \pm 5°$ and polar strength $B_{\rm d} = 2450 \pm 400$ G . The inferred magnetic field strength implies an equatorial wind magnetic confinement parameter $\eta_* \simeq 50$, supporting a picture in which the Hα emission and photometric variability have their origin in an oblique, rigidly rotating magnetospheric structure resulting from a magnetically channeled wind. This interpretation is supported by our successful Monte Carlo radiative transfer modeling of the photometric variation, which assumes the enhanced plasma densities in the magnetic equatorial plane above the star implied by such a picture, according to a geometry that is consistent with that derived from the magnetic field. Predictions of the continuum linear polarisation resulting from Thompson scattering from the magnetospheric material indicate that the Stokes Q and U variations are highly sensitive to the magnetospheric geometry, and that expected amplitudes are in the range of current instrumentation.

Key words: Stars : rotation – Stars: massive – Instrumentation : spectropolarimetry.

Stellar and field properties very similar to θ^1 Ori C

MHD MCWS simulations reproduce rotationally modulated H-alpha quite well (ud-Doula, Sundqvist)

To what extent is this star's magnetosphere like θ^1 Ori C's?

Table 1. Summary of stellar, wind, magnetic and magnetospheric properties of HD 191612.

Spectral type	O6f?p - O8fp	Walborn et al. (2010)
$T_{\rm eff}$ (K)	$35\,000 \pm 1000$	Howarth et al. (2007)
$\log g$ (cgs)	3.5 ± 0.1	Howarth et al. (2007)
$R_\star$ ($R_\odot$)	14.5	Howarth et al. (2007)
$v \sin i$ (km s^{-1})	$\lesssim 60$	Howarth et al. (2007)
$\log(L_\star/L_\odot)$	5.4	Howarth et al. (2007)
$M_\star$ ($M_\odot$)	~ 30	Howarth et al. (2007)
$\log \dot{M}$ ($M_\odot$ yr^{-1})	-5.8	Howarth et al. (2007)
v_∞ (km s^{-1})	2700	Howarth et al. (2007)
$B_{\rm d}$ (G)	2450 ± 400	This paper
β (°)	67 ± 5	This paper
η_*	50	This paper
W	2×10^{-3}	This paper
$\tau_{\rm spin}$	0.33 Myr	This paper

HD 191612 X-ray properties

Spectrum is somewhat harder than typical O stars, but not nearly as hard as θ^1 Ori C's

X-ray emission lines are broad, like ζ Pup's – highly incompatible with confined plasma

[redacted]

Mon. Not. R. Astron. Soc. **375,** 145–153 (2007) doi:10.1111/j.1365-2966.2006.11270.x

Towards an understanding of the Of ?p star HD 191612: phase-resolved multiwavelength observations⋆

Yaël Nazé,[1]†‡ Gregor Rauw,[1]§ A. M. T. Pollock,[2] Nolan R. Walborn,[3] and Ian D. Howarth[4]

[1]*Institut d'Astrophysique et de Géophysique, Université de Liège, Bât. B5c, Allée du VI Août 17, B-4000 Liège, Belgium*
[2]*European Space Agency, XMM–Newton Science Operations Centre, European Space Astronomy Centre, Apartado 50727, Villafranca del Castillo, 28080 Madrid, Spain*
[3]*Space Telescope Science Institute,¶ 3700 San Martin Drive, Baltimore, MD 21218, USA*
[4]*Department of Physics and Astronomy, University College London, Gower Street, London WC1E 6BT*

[redacted]

Differential emission measures from X-ray spectroscopy

HD 191612 : few million K

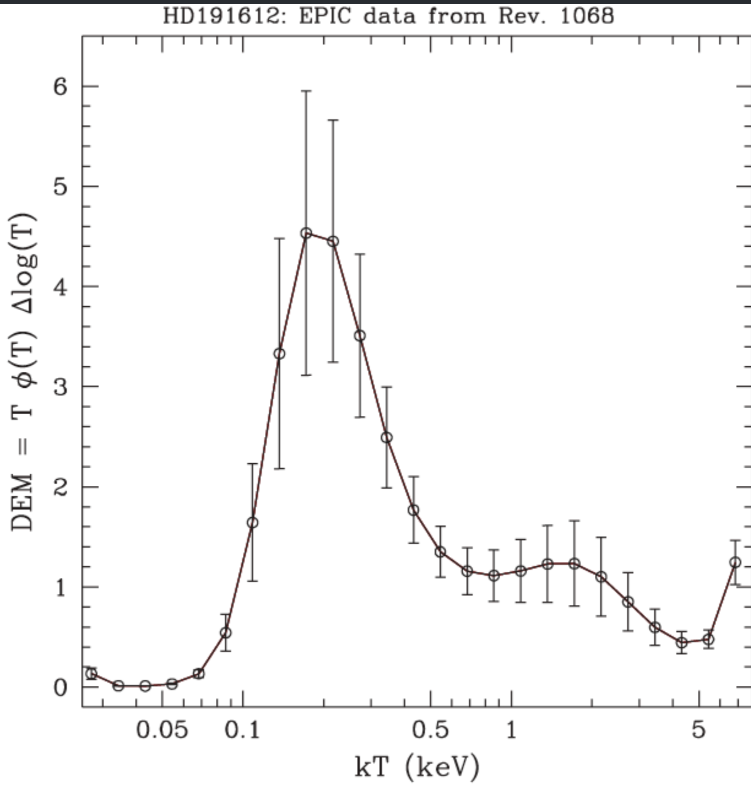

θ¹ Ori C : 30 million K

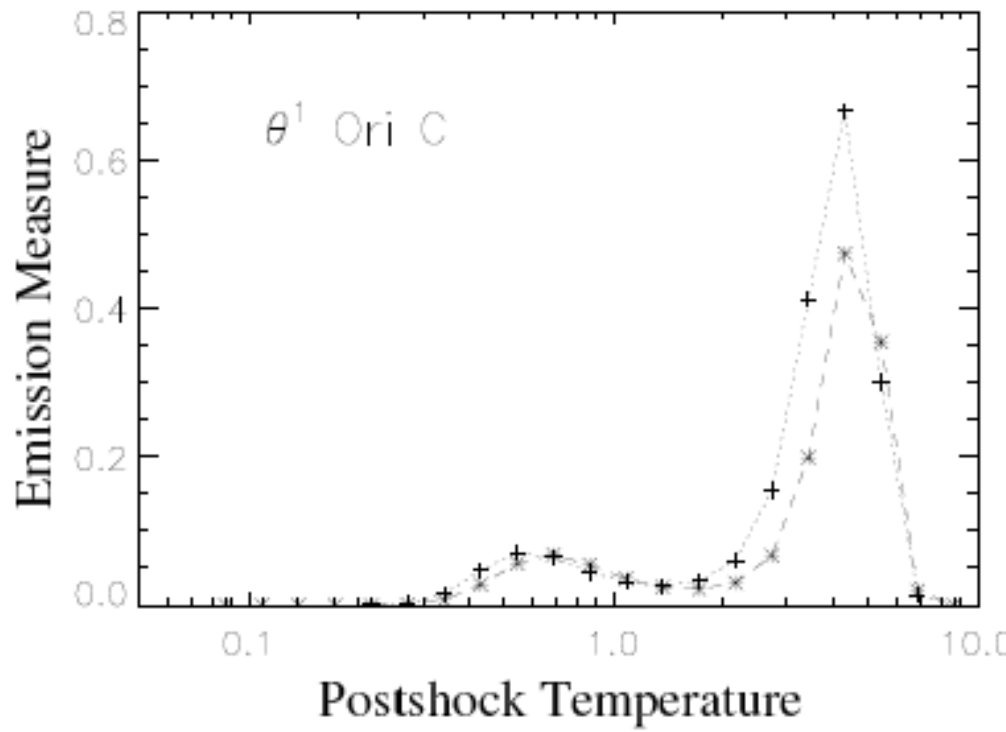

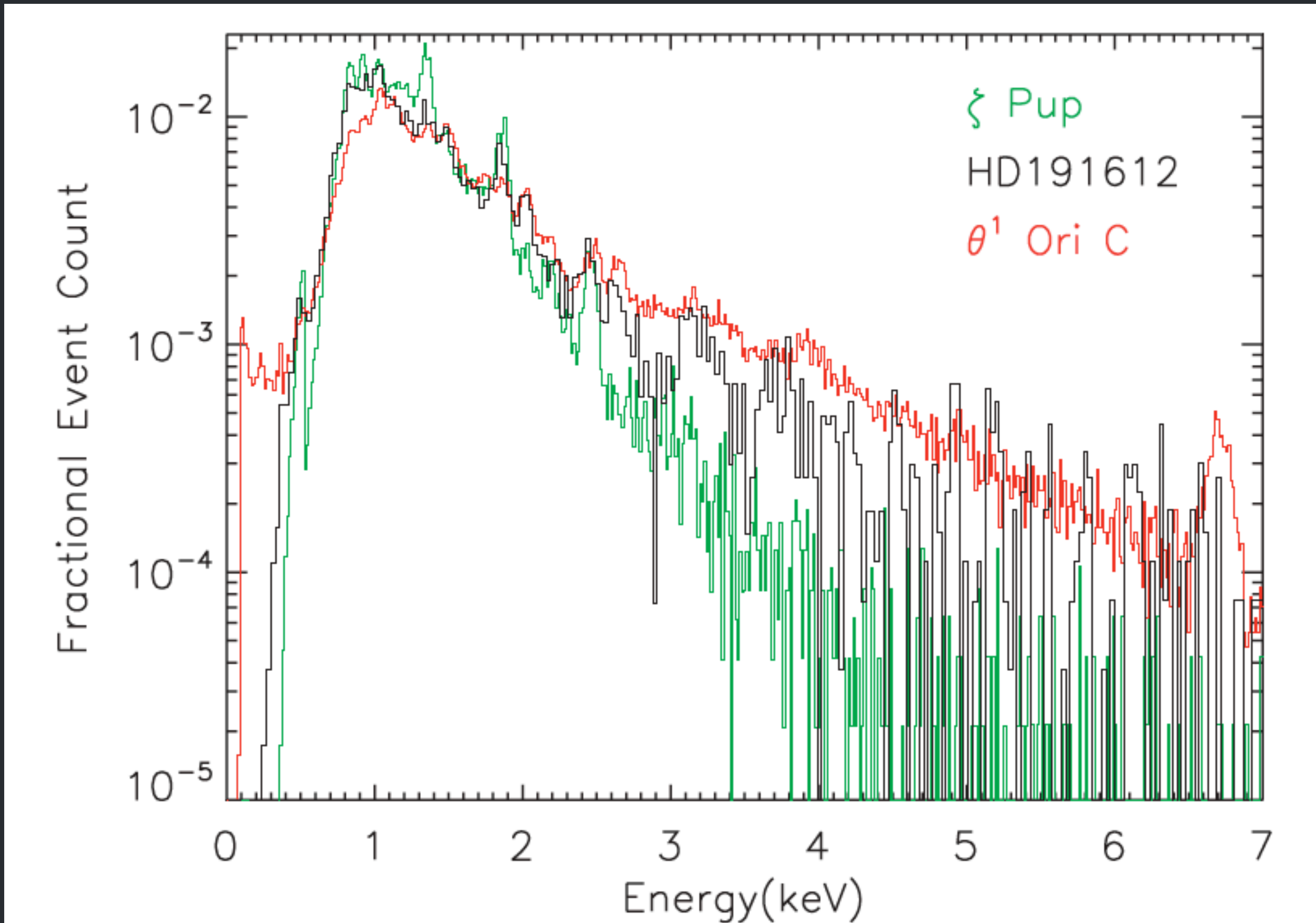

ζ Pup
HD191612
θ¹ Ori C
Fractional Event Count
10⁻²
10⁻³
10⁻⁴
10⁻⁵
0
1
2
3
4
5
6
7
Energy(keV)

X-ray plasma has a generally **low** temperature (with a bit of higher temperature plasma, too)

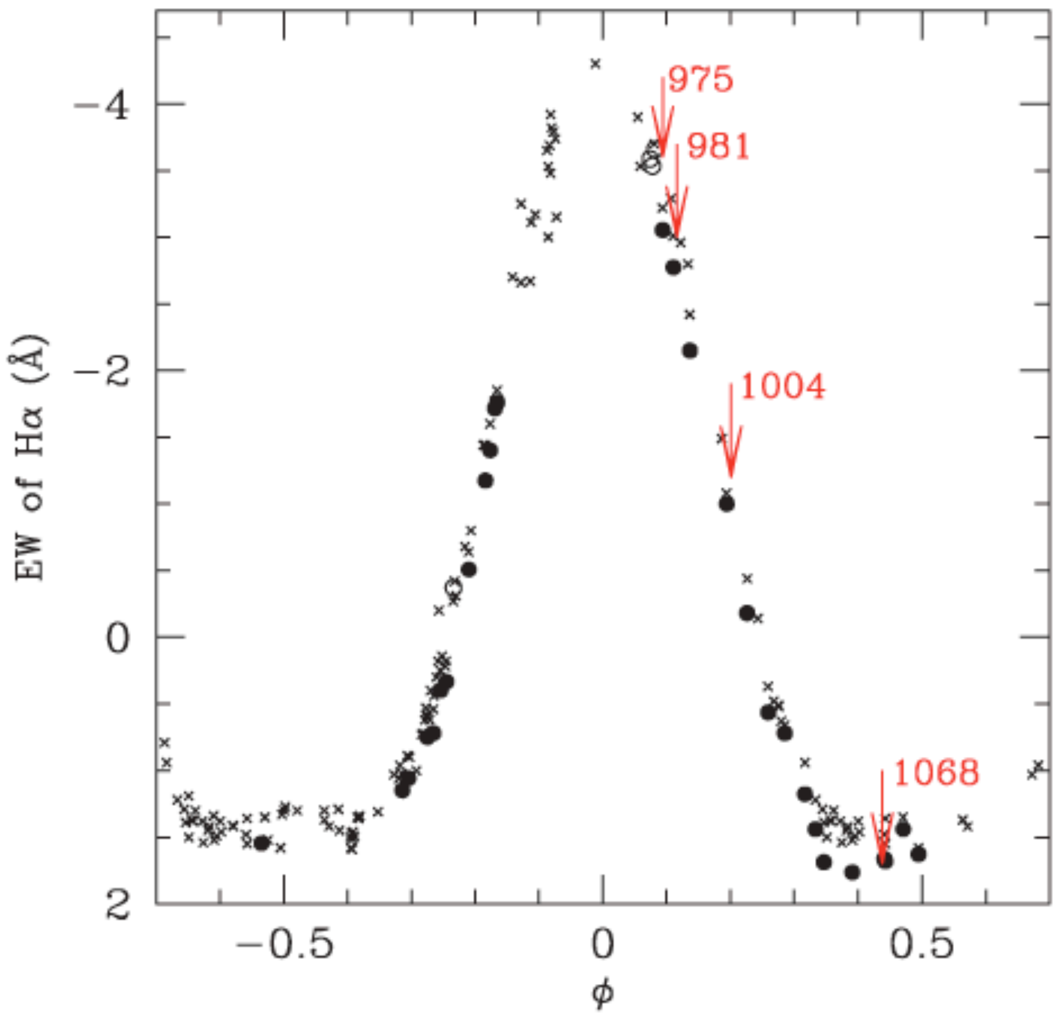

Figure 1. The phases of the *XMM–Newton* observations (between 2005 April and October) compared to the EW curve of the Hα line. Negative and positive EWs correspond to emission and absorption lines, respectively. The open circles indicate Aurélie data, filled symbols refer to Elodie observations, and crosses indicate other optical data (see Howarth et al., in preparation).

Rotational modulation? Same sense as θ^1 Ori C

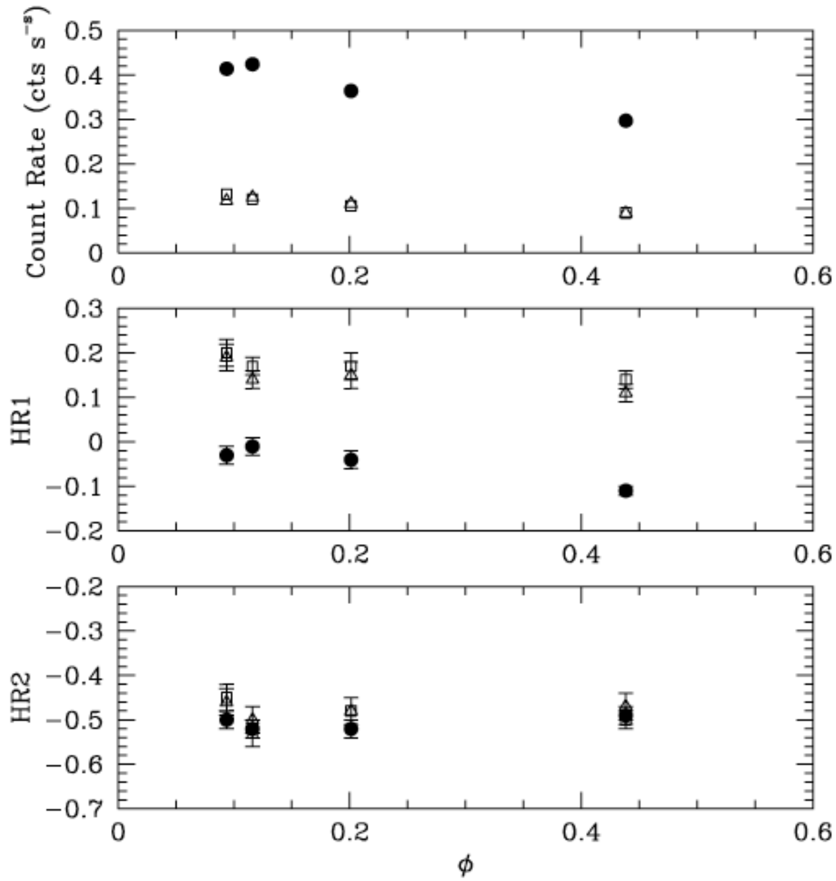

Figure 2. Variations with phase of the count rate in the 0.4–10.0 keV band (top panel) and of two hardness ratios (middle and bottom panels). Open symbols (triangles and squares) refer to EPIC MOS data, whereas filled circles represent EPIC pn observations. The hardness ratio HR_1 (respectively, HR_2) is defined as $(M - S)/(M + S)$ (respectively, $(H - M)/(H + M)$), where S is the count rate in the 0.4–1.0 keV band, M in 1–2 keV and H in 2–10 keV.

X-ray overluminous by a factor of ~5

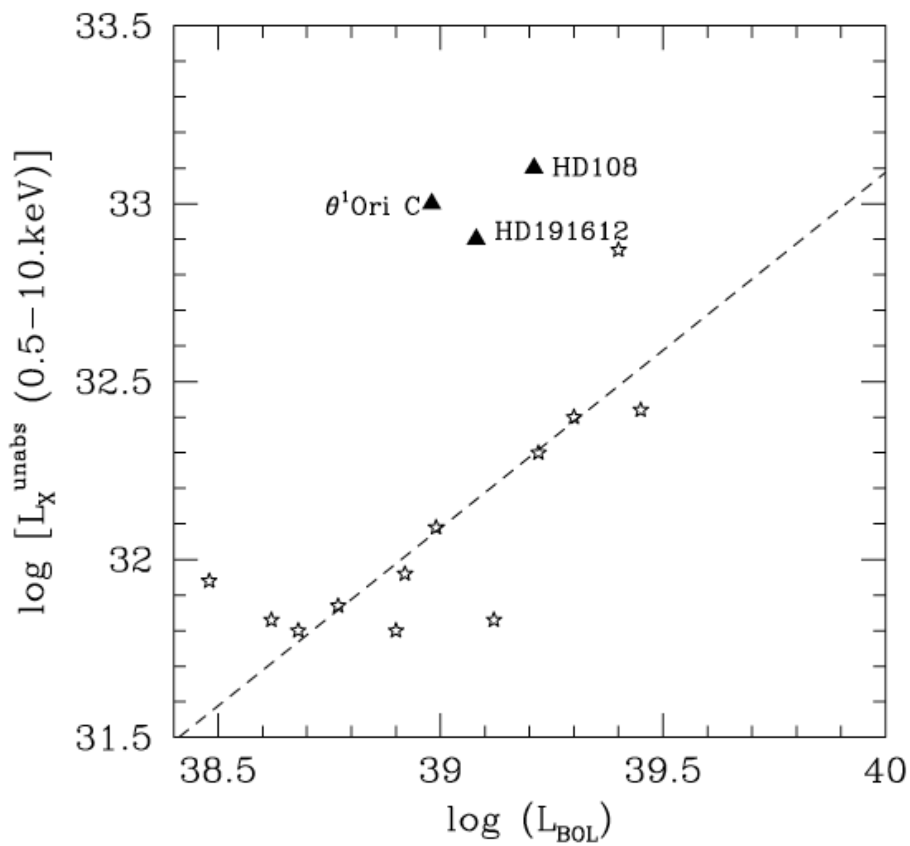

Figure 4. Diagram showing the X-ray luminosity (in erg s^{-1}) versus bolometric luminosity (in erg s^{-1}). The dashed line indicates the typical relation for O stars (from Sana et al. 2006); HD 108, HD 191612 and θ^1 Ori C all lie above it. Asterisks show the position of hot stars in NGC 6231 (Sana et al. 2006) with three outliers: the two objects lying above the line are CW binaries whereas the one lying below is a Wolf–Rayet binary.

X-ray line widths ~2000 km/s (FWHM)

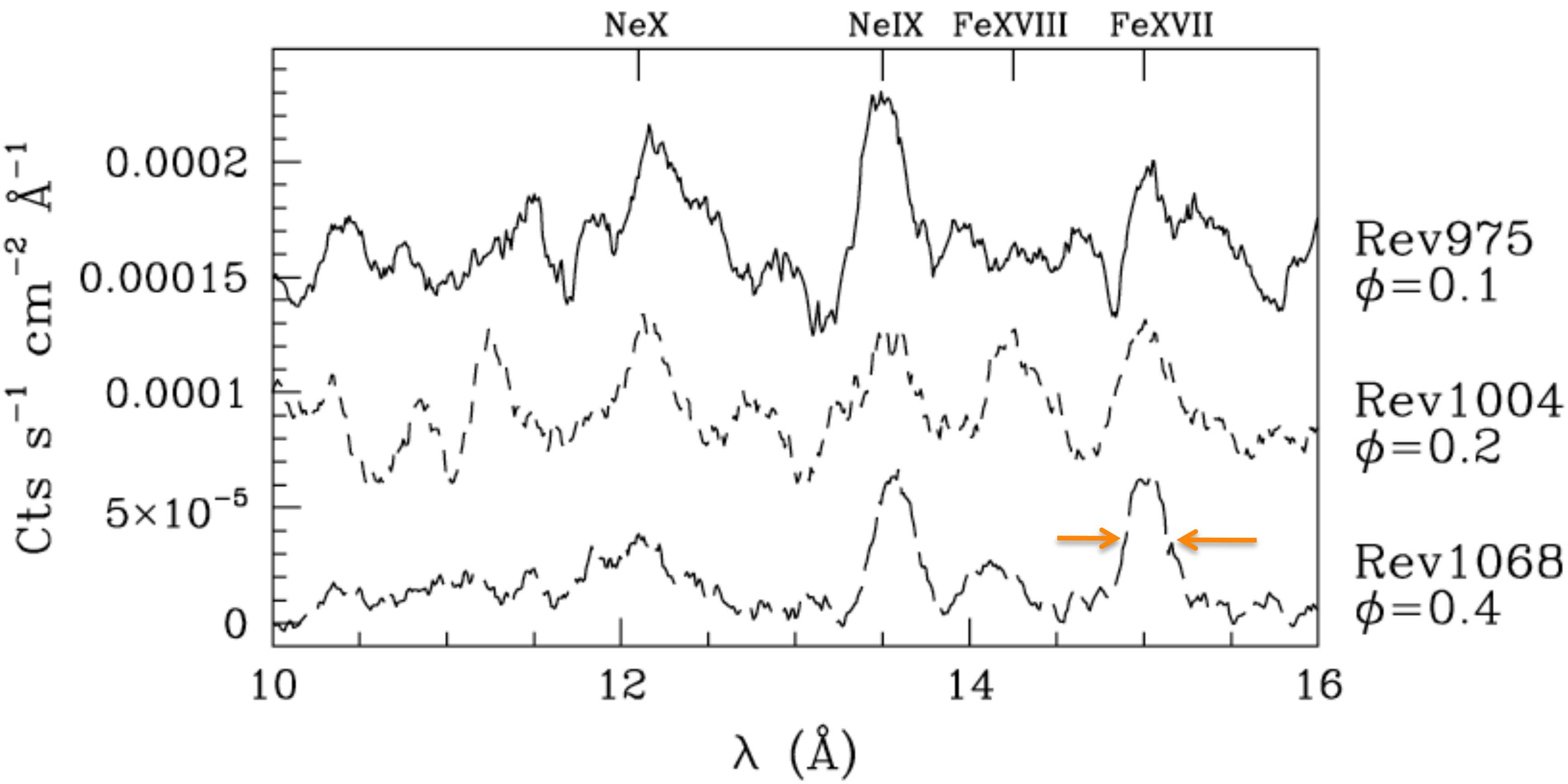

Puzzles

X-ray plasma temperature is low (shocks are weak)

X-ray emission lines are broad (not consistent with magnetic confinement)

But…L_x is high, & some evidence of rotational modulation

What needs to be done

Could the X-rays be primarily from EWS?

Could dynamical nature of MCWS plasma lead to broad lines (infall, outflow?)

Conclusions

X-ray properties of magnetic massive stars are diverse

X-ray properties within MCWS paradigm depend on field structure and wind properties (τ Sco)

Even where stellar and magnetic properties are similar to well-understood MCWS sources, X-ray emission is not the same (HD 191612)